CHARACTERISTICS OF NEAR SURFACE CRUSTAL DEFORMATION ASSOCIATED WITH SHIELD SEISMICITY: TWO EXAMPLES FROM PENINSULAR INDIA

Thesis submitted to the

Cochin Univeristy of Science and Technology

for the award of the degree of

Doctor of Philosophy

In the Faculty of Science

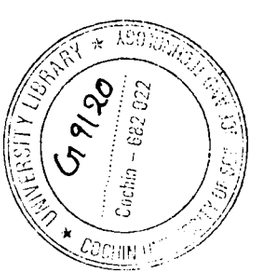

By

BIJU JOHN

Centre for Earth Science Studies
Thiruvananthapuram 695 031
Kerala, India

AUGUST 2003

C. P. Rajendran
Scientist

CENTRE FOR EARTH SCIENCE STUDIES
P.B.No.7250, Akkulam
Trivandrum 695 031
Tel. : +471 442451
Fax : +471 442280

SUPERVISOR'S CERTIFICATE

I, hereby certify that this thesis entitled, "Characteristics of near surface crustal deformation associated with shield seismicity: Two examples from Peninsular India", is a genuine research work done by Mr. Biju John under my guidance and supervision. I further certify that this thesis or part thereof has not been the basis for the award of any degree or diploma.

Dr. C.P. Rajendran

Place: Thiruvananthapuram
Date: August 11, 2003

Tel. (Home) : (+471) 360942; email: rajen@md3.vsnl.net.in; geo@giasmd01.vsnl.net.in

CONTENTS

List of figures

List of tables

		Page No
Chapter 1	**Introduction**	
1.1	Aim and scope of the present work	1
1.2	Paleoseismology as tool to reconstruct past seismicity	3
1.3	The 1993 Killari earthquake	5
1.4	The 1994 Wadakkancheri earthquake	6
Chapter 2	**Paleoseismology: A Brief Review of Concepts**	
2.1	Introduction	7
2.2.	Commonly observed earthquake-induced features	7
2.3	Evidence of faulting in crystalline rocks	8
2.4	Application of geomorphic indices	9
2.5	Developing earthquake chronology	9
Chapter 3	**The 1993 earthquake at Killari**	
3.1	Introduction	11
3.2	Earthquake parameters	11
3.2.1	Magnitude and Intensity	13
3.2.2	Aftershocks	14

3.3	Regional Geology and Tectonic Setting	16
3.4	Historic seismicity	19
3.5	Geomorphic analysis	20
3.6	The NW-oriented regional structure	22
Chapter 4	**Field investigations at Killari**	
4.1	Introduction	25
4.2	Surface rupture	27
4.2.1	Geometry and extent	27
4.2.2	Morphology	30
4.3	Trenching	32
4.3.1	Trenches in E-W segment	32
4.3.2	Trench close to the NW turn of the rupture	36
4.3.3	Well section	42
4.4	Regional Stratigraphy	44
4.5	Drilling near the surface rupture	46
4.5.1	Shallow drilling	46
4.5.2	Data from the deep bore hole	46
4.6	Style of deformation	47
Chapter 5	**The 1994 earthquake at Wadakkancheri**	
5.1	Introduction	51
5.2	Regional seismicity	52

5.3	The Wadakkancheri earthquake	52
5.3.1	Magnitude and intensity	54
5.3.2	Aftershocks	55
5.4	Geologic and tectonic Setting	55
5.4.1	Regional structure and lineament pattern	57
5.5.2	Morphometric analysis	59
5.6	Paleochannels and Neotectonism	65
5.7	Basement Structures	67

Chapter 6 **Field investigation at Wadakkancheri**

6.1	Introduction	70
6.2	Description of the fault zone	70
6.2.1	Terminology	74
6.2.2	Host rock (Protolith)	75
6.2.3	Damage zone	75
6.2.4	Fault core	76
6.3	Fault rocks	76
6.3.1	Fault gouge	78
6.3.2	Gouge fabric	81
6.4	Mineralogy of Fault rocks	82
6.4.1	Primary minerals	82
6.4.2	Secondary minerals	84
6.5	Fractures and fracture fillings	87
6.6	Sense of motion	89

6.7	Deformation mechanisms	90
6.8	Episodic nature of faulting	91
6.9	Presence of fluid	95
6.10	Dating the seismic events	96
Chapter 7	**Synthesis and conclusion**	
7.1	Introduction	97
7.2	Results from Killari	97
7.3	Results from Wadakkancheri	100
References		103
Annexure		112

LIST OF FIGURES

FIGURE NO	TITLE	PAGE
1.1.	Location map of the Killari earthquake	5
1.2.	Location of the Wadakkancheri earthquake	6
2.1.	Input from the paleoseismological studies	7
3.1.	Study area marked in the elevation map	12
3.2.	Locations of aftershocks and the main event at Killari	15
3.3.	Depth distribution of aftershocks at Killari	15
3.4.	Earthquake locations and Gravity data	19
3.5.	Historic seismicity in the Killari region	20
3.6a.	Digitally processed image of Killari area	21
3.6b.	Digitally processed image represented in FCC	23
3.7.	Location of fossil deformation zone	22
3.8a.	Photograph showing fossil faulting	23
3.8b.	Photograph showing close look of the fracture zone	23
4.1a.	Photograph showing rupture zone	26
4.1b.	Photograph showing two distinct zones	26
4.1c.	Photograph showing rupture zone and shallow drill holes	28
4.1d.	Helium anomaly map (modified after Reddy et al., 1994)	28
4.2.	Sketch of surface rupture	29
4.3.	Rupture zone and location of the dug well	29
4.4.	Digital elevation model of the Rupture zone	31
4.5.	Schematic diagram of the rupture zone	31

4.6.	Photograph of eastern wall of trench GSI-1	33
4.7a.	Sketch of western wall of trench GSI-2	33
4.7b.	Photograph of the trench in the northern side	35
4.8.	Shallow trench by in the E-W segment	35
4.9a.	Photograph of western wall of trench TR	37
4.9b.	Photograph of eastern wall of trench TR	38
4.10.	Sketch of western wall of trench TR	39
4.11.	The general observation of a red bole and clay layer	39
4.12.	Joint pattern in the epicentral area	42
4.13a.	Well section showing older thrust sheet	43
4.13b.	A further close look at the well section	43
4.13c.	Well section showing clay perturbation	43
4.14.	Regional stratigraphy based on bore well litho logs	45
4.15.	Logs of drilling across the surface rupture	45
4.16.	Simplified subsurface configuration	47
4.17.	Possible style of deformation in Killari area	48
4.18.	A synoptic model showing deformation at top level	48
5.1.	Study area in digital elevation map	51
5.2a.	Isoseismal map of 1994 Wadakkancheri earthquake	53
5.2b.	Wadakkancheri events and aftershocks of 1994 earthquake	53
5.3a.	Geological map of Wadakkancheri area	56
5.3b.	Profile along Western Ghats and Palghat Gap	58
5.4a.	Lineament map of the area derived	58

5.4b.	Image of the area band 4 of IRS-1C	60
5.5.	Drainage network of the Wadakkancheri area	62
5.6a.	Locations of suspected neotectonic activity	66
5.6b.	Profile along XYZ of 5.9a	66
5.7a.	Photograph showing systematic joints developed in the area	68
5.7b.	Photograph showing left lateral strike slip fault	68
5.7c.	Photograph showing fractures of multiple generation	68
6.1a.	Photograph showing waterfall created by the rock ridge	71
6.1b.	Photograph of natural dam and the quarry	71
6.2a.	Photograph showing the quarry in which the fault is traced	72
6.2b.	Photograph showing movement of the fault	72
6.3.	Schematic diagram representing the fault zone	73
6.4a.	Photograph showing fractures with the breccia	77
6.4b.	Photograph showing sub parallel fractures	77
6.4c.	Schematic diagram of a shear zone	78
6.5a.	Photograph showing shear bands	80
6.5b.	Photograph showing consolidated part of gouge	80
6.5c.	Photograph showing gouge injection	80
6.6a.	Photomicrograph of fractures (Fr1 and Fr2)	88
6.6b.	Photomicrograph of fractures (Fr2 and Fr3)	88
6.7.	Sequential development of fault rocks and time	92
6.8.	Sequential development of fault rocks	93,94

LIST OF TABLES

TABLE NO	TITLE	PAGE
3.1	Epicentral parameters of Killari Earthquakes	13
3.2	Teleseismic moment tensor solutions.	13
3.3	Stratigraphic classification of Deccan traps.	17
5.1	Seismic events from of Palghat Gap area.	54
5.2	Basin asymmetries calculated for five basins.	61
5.3	Mountain front sinuosity.	63
5.4	Ratio of valley-floor width to valley height.	65
6.1	Mineralogy of the host rock and gouges.	83
6.2	Mineralogy of intra-fracture materials.	89

CHAPTER 1

INTRODUCTION

1.1 AIM AND SCOPE OF THE PRESENT WORK

The Indian shield falls in the category of Stable Continental Regions (SCRs), characterized by low rate of deformation and low seismicity. Despite the stability assigned to such intracontinental regions, some SCRs are relatively active compared to others and the Indian SCR falls in that category (Johnston, 1989). Although a few moderate earthquakes have occurred in SCR-India, many seismogenic sources remain poorly understood. Thus, it is not surprising that most of the earthquakes in this region appear to occur in unexpected locations. Notable among such earthquakes is the, 1993 Killari earthquake (M 6.3), which occurred in a region with no record of seismic activity and no surface expression of any potential seismogenic structures.

It is generally well known that most intraplate earthquakes occur by the reactivation of pre-existing faults (Sykes, 1978; Talwani, 1999). The near N-S maximum horizontal stress, originating from the plate convergence in the Himalaya is the predominant stress field in the Indian SCR. Studies of the stress field as well as focal mechanism of many recent earthquakes testifies the role of this N-S compression (Goud, et al., 1992). Although some faults have the potential to be reactivated in the current stress regime, the fundamental issue in seismic hazard evaluation is to identify faults that are likely to be activated.

Mapping potentially active faults and extracting information on their past activities has become an essential part of seismic hazard assessment. This is particularly relevant where historic and recent data are available only for a short span of time, compared to the interseismic intervals. In the recent years, paleoseismology is being increasingly used for reconstructing the past activities associated with faults. While this tool may be applied more successfully in regions (such as plate boundaries) where earthquakes occur over shorter intervals (Sieh, 1978, for example) its application to SCR's is quite limited. Absence of

significant fault slip, poor development and preservation of secondary features and lack of morphological features that help in the identification of causative faults are a few factors that limit its application in SCRs. Thus very often, it becomes necessary to develop site-specific criteria to understand the nature of seismic sources in these regions.

The present study is an attempt to characterize active tectonic structures from two areas within peninsular India, namely, Killari and Wadakkancheri. An earthquake of magnitude 6.3 occurred at Killari (Latur) in 1993 and one of 4.3 occurred near Wadakkancheri in 1994. In one sense these earthquakes represent distinctly different types of settings. The Killari earthquake occurred in an area that is considered to be devoid of any neotectonic activity and historic seismicity. No active faults have been mapped here and the area is not known to have experienced any low-level earthquake activity, prior to 1993 (except a couple of isolated tremors). On the other hand, the 1994 Wadakkancheri earthquake occurred in an area that has experienced minor tremors in the past (M ~ 3); it was spatially associated with Palghat gap, the most conspicuous regional geomorphic feature within Western Ghats (Rajendran and Rajendran 1996).

There are more issues that set these two events apart. The association of the Killari earthquake with the preexisting fault is clearly demonstrated by the focal mechanisms, aftershock distribution and other data. The projected association of Wadakkancheri earthquake with the Palghat Gap is only inferred, based on its spatial association with the structure. The Killari earthquake occurred in a region, covered by basalt, which may deform differently from the Archaean basement below. The Killari earthquake generated a surface rupture providing some indications to search for previous faulting episodes. The Wadakkancheri earthquake occurred in the granulite terrain characterized by shear zones and faults that are exposed, but not currently active. Although the earthquake was not of alarming

size, its spatial association with a mapped structure makes it interesting, and we considered it would be useful to generate the past history of movements in this fault zone, based on deformational characteristics. Due to the differences in their respective geologic settings and nature of seismicity, paleoseismic indicators associated with these regions are also expected to be different from each other.

1.2 PALEOSEISMOLOGY AS TOOL TO RECONSTRUCT PAST SEISMICITY

Geological methods are being increasingly used to document past seismicity and to characterize earthquake zones and these are particularly useful in areas where data on past earthquake history are too scanty (e.g., McCalpin, 1996; Yeats et al.,1997 and references therein; Crone, et al., 1997). Due to the low strain buildup and longer recurrence periods, typical of continental region (SCR), evidence of past earthquakes is poorly preserved. Moreover, faults in some compressional settings may remain hidden; it may also develop complex geometries as they reach the surface. Such situations pose many difficulties in identifying the faults and estimating the slip associated with each event. A brief summary of the methodology and techniques followed in paleoseismology given in chapter 2, highlights some of these points.

In the backdrop of the global efforts to develop criteria to identify paleoearthquakes and active faults, this thesis summarizes the efforts at Killari and Wadakkancheri, to identify clues on past seismicity. At Killari, the work was centered on mapping of morphologic features using direct and indirect evidence, analysis of macro and micro-geologic features in the trenches and quarries; analysis of subsurface well logs from the vicinity of the causative fault, in addition to analysis of the recent earthquake sequence. At Wadakkancheri, the effort was to identify evidence for past movements and obtain the timing of the past movement.

Since the conventional paleoseismologic techniques (such as trenching) are hard to be applied in this region, we had to follow the approach of mapping fault zones and date the fault gouge (using ESR dating techniques) to obtain approximate estimates of past movement.

The flood basalts of the Killari region, which is one of our study areas, is not a typical area where the conventional approaches are readily applicable. The topography is rather featureless, with little or no surface expressions that could be related to faulting or fault-related morphology. With a poorly developed soil profile, combined with excessive erosion, this region cannot be considered as an ideal site for the development or preservation of liquefaction features. The other area of study, Wadakkancheri, is not known to have generated any known major earthquakes that had generated any seismically induced deformation features. However the prominent geomorphological features and associated shear zone provide some clues to location of the fault related structures. With the expected recurrence interval of tens of thousands of years as in most unrifted SCRs the relics of the past earthquakes are quite likely to have been lost to the erosional processes (see Rajendran and Rajendran, 2003).

In the following chapters of this thesis, results of investigations are presented. This thesis is arranged in seven chapters. Chapter one introduces the problem and study area. Chapter two is a review of the techniques employed in the study of active tectonics and paleoseismology. Chapter three describes the 1993 Killari (Latur) earthquake and the regional structures associated with it. Chapter four presents the salient features observed from the Killari rupture zone. The 1994 Wadakkancheri earthquake and the geomorphic anomalies within the epicentral area are presented in chapter 5. Chapter six describes the brittle exhumed fault zone at Wadakkancheri. Chapter seven presents a discussion on the observations made from both of the study areas.

1.3 THE 1993 KILLARI EARTHQUAKE

The Killari earthquake (m_b 6.3; Mw 6.1) occurred in the interior of the state of Maharashtra; its epicentre was located 40 km from Latur, the nearest district headquarters (Fig. 1.1). This event shares typical characteristics of intracratonic earthquakes, which include occurrence in a region of low background seismicity, lack of surface expressions of faulting, long recurrence intervals and poorly developed geomorphologic expressions.

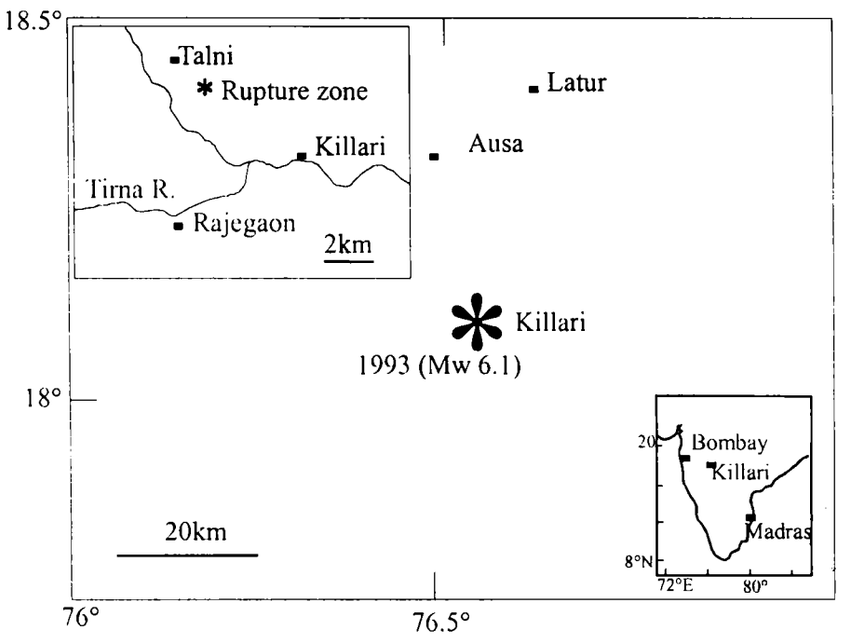

Fig. 1.1. Map showing locations of the Killari earthquake and the rupture zone.

Seismic history of this fault was considered as an important component that needs to be understood. In the absence of significant historic seismicity, the only way to reconstruct the seismic history of the region is through paleoseismological studies, which is described in chapter 4 of this thesis.

1.4 THE 1994 WADAKKANCHERI EARTHQUAKE

The Wadakkancheri earthquake (M_L4.3) of 2 December 1994 was felt around an area of 1000 km^2 in Talasseri-Desamangalam area, Kerala (Fig 1.2). Wadakkancheri (the taluk headquarters) and the adjoining regions have been experiencing microseismic activity during the last decade. Of these, four tremors fall within the present study area, which falls within the E-W trending geomorphic break, known as the Palghat gap. In the absence of a local network of stations, epicentres of these tremors were mostly located using primary field data. The 1900 Coimbatore earthquake (M >5.0) is the other significant earthquake reported from the vicinity of this structure. The data recorded by the Gauri Bidanur Seismic Array, operated by BARC also suggest occurrence of several microtremors originating from the gap region, but their locations are not well-constrained (see Fig. 1.2). Field investigations in the regions around the Wadakkancheri earthquake and results of laboratory studies carried out are presented in chapter 6.

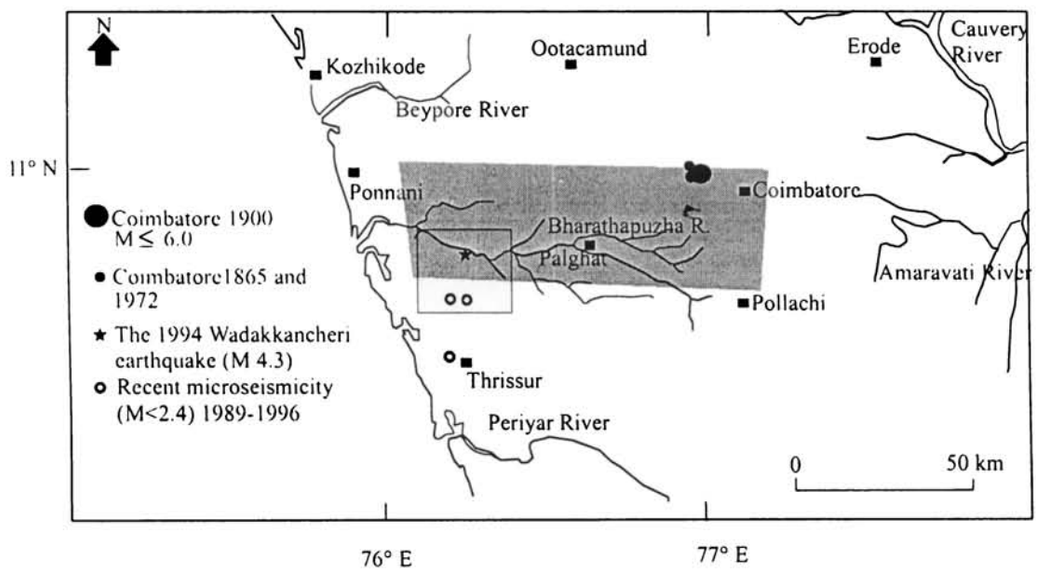

Fig. 1.2. Map showing the location of the Wadakkancheri earthquake. The shaded portion is Palghat Gap (from Rajendran and Rajendran 1996).

CHAPTER 2

PALEOSEISMOLOGY:

A BRIEF REVIEW OF CONCEPTS

2.1 INTRODUCTION

In the earthquake hazard evaluation, understanding the long-term activity of active faults is vital. In most cases the history of earthquakes associated with active faults are scanty. Thus, an assessment based on the historical data may not be sufficient or complete for long-term prediction. Paleoseismology, dealing with prehistoric earthquakes from the analyses of seismically induced structures preserved in the geological records, determines the interval between seismic events, their periodicity, timing, and the size of the past events (Fig.2.1).

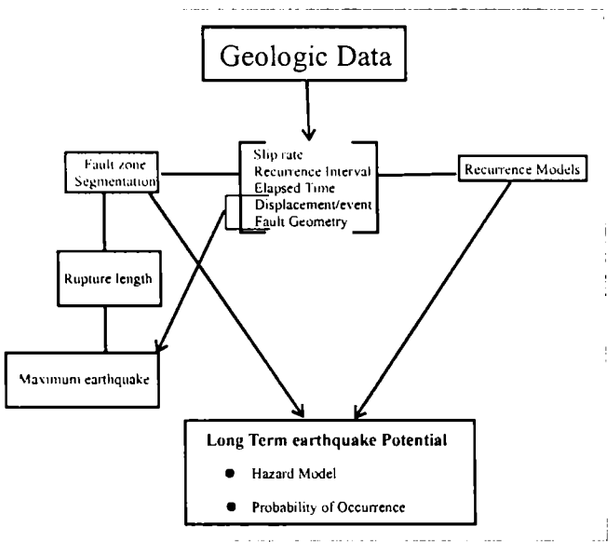

Fig. 2.1. Diagram showing inputs from paleoseismological studies for seismic hazard evaluation (from Schwartz and Coppersmith, 1986).

2.2. COMMONLY OBSERVED EARTHQUAKE-INDUCED FEATURES

A broad classification of earthquake-related structures into primary and secondary can be made based on their characteristics. For example, primary paleoseismic features are produced by tectonic deformation resulting from coseismic slip along a fault plane. Primary evidence can easily be associated with a faulting event. Fault scarps,

fissures and folds along the trace of a fault are typical examples of primary paleoseismic evidences. Secondary paleoseismic evidence consists of many diverse phenomena caused by earthquake shaking. Sand blows, sand dykes and other liquefaction features, damaged trees, landslides, rock falls, etc. are among the secondary effects. These features are either studied from the outcrops or from the specially made trenches.

Paleoseismic studies over the last decade have been tremendously successful in locating active faults and in identifying previous events. Micro-stratigraphic relations in the sedimentary sections; geomorphology of fault scarps; fault topography and offsets; regional geological relations including recognition of fluvial terraces and changes in the river courses related to uplift and faulting; and analyses of seismically induced sedimentary structures are some of the key inputs in paleoseismological studies. Each of these inputs will get priority in an area depending upon site-specific characteristics. McCalpin (1996) has reviewed these techniques in detail.

In the geologic set up of Killari, the top ~ 320 meters consist of basalt layers with poorly developed soil horizon, and one may not expect to see many traditionally described seismically induced features in such a medium. Furthermore, the soil and ground water conditions are not considered ideal for development of liquefaction features, another key proxy indicator of an earthquake. Our study, however, recorded many site-specific seismically induced structures in the rupture zone of the Killari earthquake, which will be described later in this thesis.

2.3 EVIDENCE OF FAULTING IN CRYSTALLINE ROCKS

In crystalline terrains, the study of fault rocks (breccia, cataclasite and gouge) in crystalline terrains could reveal the deformation mechanisms. At upper levels of the crust, the deformation is dominated by cataclasis, which involves the brittle fragmentation

of mineral grains with rotation of grain fragments accompanied by frictional grain boundary sliding and dilatancy. The fine-grained output of faulting is the gouge, which is essentially the rock powder formed during faulting. In many environments gouge is altered to clay obliterating the relation between chemical and mechanical processes, but in others the mineralogy of the source rock is preserved as such (e.g.: Anderson et al., 1983; Mawer and Williams, 1985) and offers the hope of distinguishing between the physical and chemical changes that gouge undergoes as it is produced. Our study in Wadakkancheri, described in this thesis is centered on identification of fault rocks and its application in recognizing the cycles of deformation.

2.4 APPLICATION OF GEOMORPHIC INDICES

In recent years, tectonic geomorphology increasingly has become one of the principle tools in identifying active tectonic features (e.g. Keller and Pinter, 1996 and references therein). Presence of active tectonic deformation will normally be reflected on the disposition of drainage pattern. Over the years, various workers have defined certain quantitative parameters. Commonly such analyses are useful in classifying areas as being very active, moderately active, or inactive. Such classification is useful in delineating areas where more detailed field studies could unravel active structures, and calculate rates of active tectonic process. In this thesis, we have attempted to use some of these principles to determine the nature of active tectonism around the fault zone in Desamangalam, near Wadakkancheri.

2.5 DEVELOPING EARTHQUAKE CHRONOLOGY

The primary objective of all paleoseismic studies is to determine the age of all paleoearthquakes as accurately as possible. Time of movement of an active fault is

important for tracing the history of earthquake. Absolute dating of fault movement is helpful in determining the neotectonic activity of a fault, and is an important technique in earthquake hazard assessment. The usual approach is to bracket the event using the youngest datable layer deformed by the earthquake (may be called as the 'event horizon') and the oldest layer that overlies the event horizon, which is particularly applicable in sedimentary environments.

Yeats et al. (1997) have discussed various techniques followed in dating and their limitations. Among these techniques, ^{14}C method is most widely used. Using this technique, the age of the soil cover can be used to bracket the age of the faulting event. Recent practice is that radiocarbon age obtained from the laboratory is calibrated with the calendric ages derived from the samples of wood of known age (Stuiver and Reimer, 1986). The major constraint in this regard is the nonavailability of required quantity of datable material. A major breakthrough in radiocarbon dating is the use of Accelerator Mass Spectrometry (AMS) for which the sample needs to be only a few milligrams. In our studies in Killari and Wadakkancheri, because of the site-specific characteristics, scope for age dating of the earthquake-induced structures using radiocarbon techniques was limited.

Fission track, K-Ar and Rb-Sr are the dating techniques conventionally used for determining age of intra-fault material. In recent years, electron spin resonance (ESR) and luminescence dating techniques are widely used to date intra fault materials (see Noller, et al. 1999 and reference therein). We have used ESR technique to date the fault gouge from Wadakkancheri. The basic principle of ESR spectroscopy is that the pressure and temperature generated during a faulting episode would reset the ESR signals from paramagnetic centers within the quartz crystal lattice, and the time of the last movement is determined by measuring the buildup of ESR signals within the quartz grains.

CHAPTER 3

THE 1993 EARTHQUAKE AT KILLARI

AND REGIONAL STRUCTURES

3.1 INTRODUCTION

The devastating earthquake of moderate size (Mw 6.1) occurred near Killari village in Maharashtra, central India. This earthquake occurred on September 29, 1993 at 22:25 UTC (see Table 3.1). One of the most damaging SCR earthquakes ever, this one caused about 8000 deaths and nearly wiped out settlements in about twenty villages (Gupta et al., 1995). The earthquake-affected area is the part of the Balaghat Plateau that gently slopes toward south and southeast (Narula et al., 1996). The Tirna River, which shows a E-W trend in the vicinity of the earthquake epicentre drains this area (Fig. 3.1). Focal mechanism of the main shock indicates reverse faulting on a NW-SE striking southwest dipping plane (Baumbach et al., 1994). Aftershocks are mainly confined to southwest block defined by tributary of the Tirna River. The distribution of historic earthquakes defines a northwest regional trend. The remote sensing studies also confirm the existence of a NW-SE trending regional structure.

3.2 EARTHQUAKE PARAMETERS

The source mechanism was of thrust type with the compression axis in the northeast direction (see Table 3.2). Epicentral parameters of the main event reported by various agencies are given in Table 3.1. Teleseismic moment tensor solutions by Harvard University (HRV) and the U.S. Geological Survey (USGS) indicate pure reverse faulting (Table 3.2).

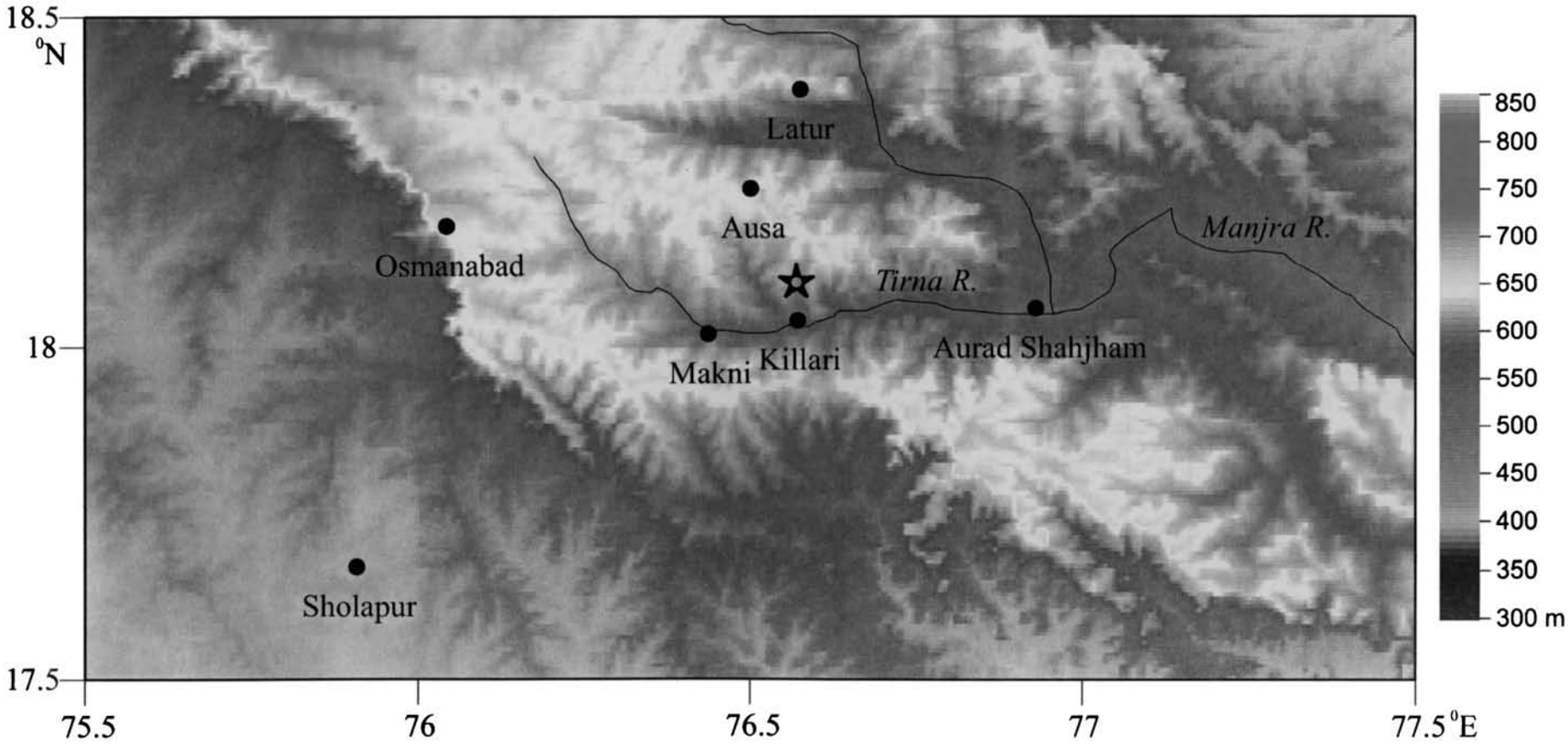

Fig. 3.1. Colour scaled location map of Latur and surrounding area, generated from Gtopo30 Digital Elevation Model (USGS, 1996).

Table 3.1 Epicentral parameters of the main event reported by different agencies

Origin Time (UTC)	Lat °N	Long °E	Depth (km)	Magnitude	Source
22:25:48.6	18.07	76.45	6.8	6.3	USGS
22:25:48.6	18.02	76.56	15	6.1	GEOSCOPE
22:25:48.6	18.01	76.56	6.0	6+	NGRI
22:25:52.0	18.11	76.55	15	-	HRV
22:25:47.5	18.07	76.62	6-17	6.3	IMD

Table 3.2 Teleseismic moment tensor solutions by the USGS and Harvard University

Agency	Moment (Mo)	Strike1	Dip1	Rake1	Strike2	Dip2	Rake2
USGS	1.7×10^{18}	123	41	92	299	49	88
HRV	2.2×10^{18}	134	47	112	284	47	68

3.2.1 Magnitude and intensity

Field studies of the damages were conducted by many agencies, including IMD, GSI, NGRI, IIT- Roorkee, and Maharashtra Engineering Research Institute (MERI). Although there is some discrepancy between the intensity maps produced by these agencies, there is a general agreement on the zone of maximum intensity. They assigned a maximum intensity of IX (MSK) in the meizoseismal area of 110 km^2. Gupta et al. (1995) suggested a NE trend of isoseismals, but they also noticed a large bulge towards NW. However, due to site amplification and concentration of damages in populated areas with settlements, the isoseismals may not be dependable in assessing the orientation of the fault. Gupta et al.

(1995; 1998) noticed a rapid decrease in intensity VI toward the north compared to the southwest and south of the hanging wall block of the fault. Site amplification was noticed at some locations. It is noted that more than two third of the intensity zones IX and VIII is located to the south west of the Tirna River. The NW-flowing branch of the river is considered to coincide with the likely location of the fault. This has been indicated by the digital imagery of the region, to be discussed in a later section.

3.2.2 Aftershocks

The Killari mainshock was followed by hundreds of aftershocks. Baumbach et al. (1994) located 187 aftershocks, using data from local stations. One hundred and thirty aftershocks recorded by IMD, GSI and NGRI stations were relocated. The aftershocks for which better locations could be obtained occurred between October 10, 1993 and February 26, 1994. Out of the 130 aftershocks that were relocated, only 69 were of A and B quality, and these are shown in Fig. 3.2. Rupture-area estimated on the basis of aftershock distribution is fairly small, 38.5 km^2, involving only a fault length of 5.5 km (Baumbach et al., 1994).

Spatially, the aftershocks define a rather tight cluster in an area less than 15X15 km. The relocated aftershocks also fall in the general zone of activity defined by earlier studies. Most of the seismicity is confined to a depth of 8 km, as suggested by Baumbach et al. (1994), and the maximum number of relocated earthquakes also occurred within 8 km (Fig.3.3).

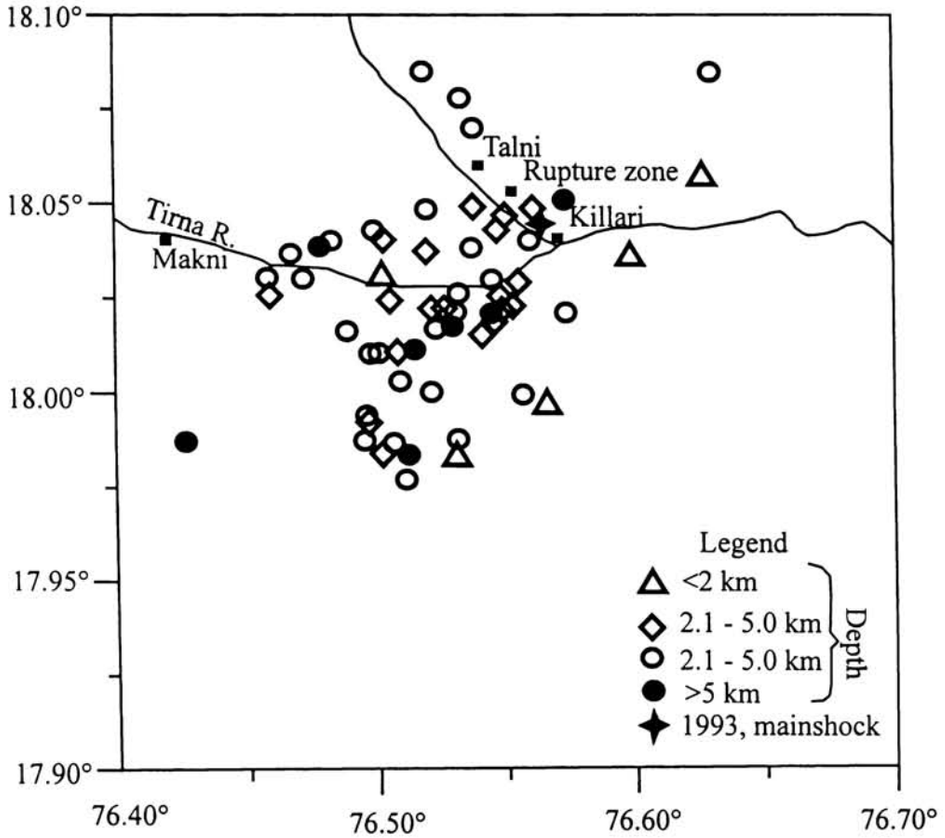

Fig. 3.2. Relocated aftershocks and the main event at Killari (after Rajendran et al., 1998).

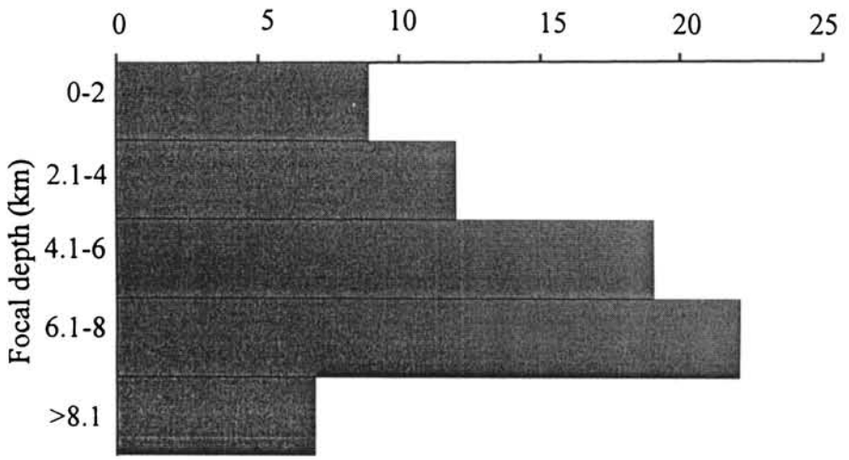

Fig. 3.3. Depth distribution of A and B quality locations of aftershocks at Killari (after Rajendran et al., 1998).

The distribution of aftershocks defines a tight cluster and it does not indicate any particular orientation. An important observation is that the deeper events were mostly confined to regions southwest of Killari. But, the main shock and a few aftershocks spatially coincide with the northwest tributary of the Tirna River (Fig. 3.2). Aftershock zone terminates along this trend, which also coincides with the rupture zone of the 1993 epicentre. If the regions south west of the NW flowing branch of the Tirna River is considered as part of the hanging wall block, it can be argued that the deeper events (>8 km) are spatially restricted to the hanging wall block. Among the seven earthquakes of depth >8 km, six of them fall in the hanging wall block.

3.3 REGIONAL GEOLOGY AND TECTONIC SETTING

The epicentral area of the Killari earthquake is situated in the Deccan Plateau. The Deccan Traps, which cover an area of more than 600,000 sq km of this region, consist of a number of flows ranging in thickness from a few meters up to about 100 m with the successive flows being separated by red bole or Intertrappean beds. The estimated cumulative thickness of the basalt flows varies from 60 m in Belgaum area to 1900 m in the Bombay coast. In the southwestern portion, the Deccan Traps overlie the Upper Proterozoic Bhima Group of rocks exposed in the Bhima and Krishna valleys. In the southern side, the Traps directly overlie the peninsular gneissic complex (Krishnan, 1968).

The Deccan trap sequence, in general, is classified into stratigraphic units on the basis of chemical composition of various flows (e.g. Mitchell and Widdowson, 1991) (Table 3.3). The southern part of Deccan volcanic province in the eastern Maharashtra is composed of Poladpur and Ambenali Formations of the Wai sub group (Mitchell and Widdowson,

1991; Bilgrami, 1999). However, the geochemical data for representative samples of different flows in the Killari region shows that they can be correlated to Poladpur and Ambenali Formations of Wai subgroup (Gupta et al., 2003).

Table 3.3 Stratigraphic classification of Deccan Traps after Mitchel and Widdowson (1991)

Group	Subgroup	Formation
Deccan Traps	Wai	Panhala
		Mahabaleshwar
		Ambenali
		Poladpur
	Lonavala	Bushe
	Kalsubai	Khandala
		Bhimshanker
		Thakurwadi
		Neral
		Igatpuri
		Jawhar

The thickness of traps varies from one location to another. Estimation through multi-level aeromagnetic survey around the 1993 epicentral area indicates a thickness of 330 m (Negi et al., 1996). Individual flows are generally several tens of meters thick and they are separated by relatively thin interflow material. These are actually the basalts that have been hydrothermally altered and reddened by succeeding flow commonly called as red bole. Red

boles are hard rocks in the subsurface but rapidly disintegrate into red clay upon exposure. Rapid accumulation of lava flows allows little time for weathering, resulting in insignificant development of intra-trapean sedimentary sequence (Snow, 1982). The attitude of the flow is essentially horizontal; some authors suggest a dip of 1 ° to 2° to the west. Layer of soil ranging from 1 to 3 m with isolated laterite caps have developed on the top of the basalts. Fairly large deposits of alluvium (maximum thickness: 10 m) are present along some of the river valleys.

Deep drilling in the epicentral area of the earthquake indicates a basalt thickness of 338 m (Gupta and Dwivedy, 1996). It comprises eight simple 'aa' type basaltic flows. Each characterized by a brecciated top and a chilled bottom. Apart from a persistent red bole layer between 173 and 178 m below surface, no other well-developed sequence of red bole beds is observed between the basalt flows. This may also be attributed to lack of retrieval due to washout of softer layers during the drilling operations. The shallow drilling and trenching (discussed in next chapter), however, indicate red bole layers occurring at upper levels.

The featureless terrain of Killari does not exhibit any prominent geomorphic features or lineaments. The evidence for the existence of a fault (prior to the earthquake) mainly came from the gravity data. Krishna Brahmam and Negi (1973) postulated a rift valley in the region, and called it 'Kurudwadi rift'. Although there is considerable debate about the Kurudwadi 'low' being called as a rift valley, the region appears to be marked by well defined zones of gravity highs and lows (Fig. 3.4). Kailasam (1993) suggested that the Killari earthquake occurred by the movement of the crustal blocks. More recent closely spaced gravity survey and modeling along two profiles (Mishra, et al., 1998) across the epicentral area suggest some high- and low-density bodies of shallow origin.

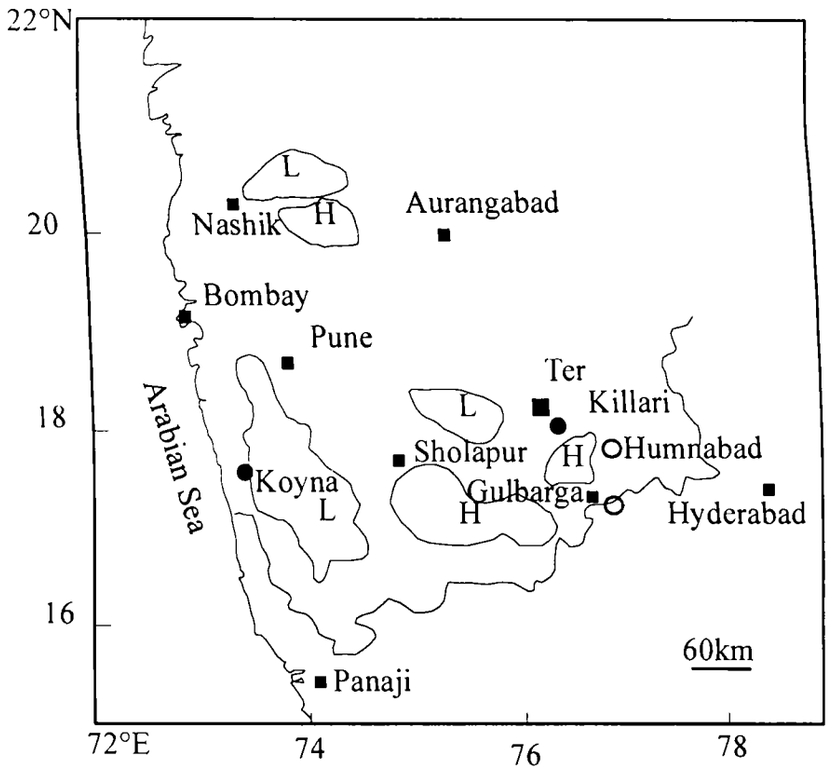

Fig. 3.4. Locations of M >6.0 events (solid circles); open circles show historical earthquakes; boundary of Deccan Traps is shown by solid line; gravity lows and highs are denoted by 'L' and 'H', respectively (Kailasam (1993).

3.4 HISTORIC SEISMICITY

The search for historic earthquakes in the vicinity of Killari shows occurrence of a few earthquakes, most of them of intensity III to IV (Fig. 3.6). Although the level of seismicity may be considered significant for a stable shield region, no large earthquakes of M >6.5 seem to have occurred in the epicentral area of the 1993 event, at least for the past 1000 yr. This assumption is based on the fact that the historical monuments dating back to A.D. 1000-1200 in the vicinity of Killari had remained intact until the recent earthquake. However, the distribution of historic earthquakes defines a regional trend that seems to

extend for more than 400 km to the north-west. At least five earthquakes of intensity IV or more have occurred in this corridor during the past 150 years (Fig. 3.5).

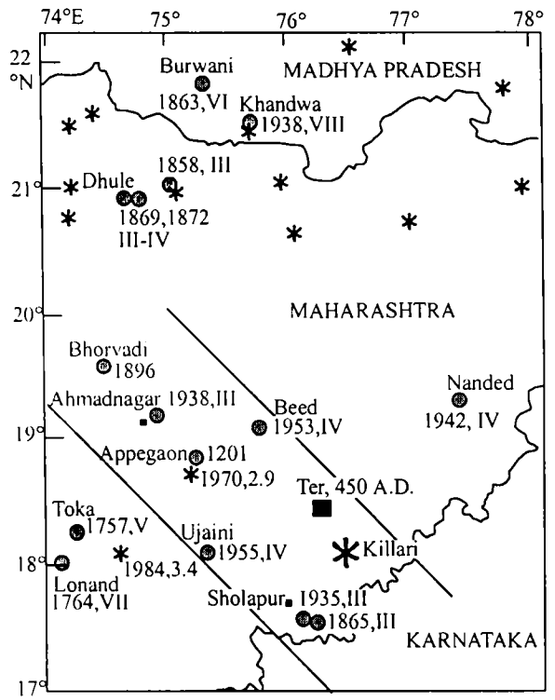

Fig. 3.5. Historic seismicity in the region adjoining Killari. Filled circles are historic events and stars are instrumentally recorded events. Location of Ter, the site of an ancient earthquake, is shown by filled square. The seismicity north of N20° is coincident with Narmada rift (after Rajendran and Rajendran, 1999).

3.5 GEOMORPHIC ANALYSIS

We used the digital image of the Killari area (Landsat TM) as a first step in the geomorphic analysis of the area. The digital image was enhanced by applying multi spectral ratio techniques. Accordingly, the ratio between 6 and 7 (spectral width: 2.08-2.35 μm) and band 4 (spectral width: 0.76-0.90 μm) was used to enhance the differences in the vegetative

and soil cover. Band 7 detects the exposed rock and the soil cover, and band 4 delineates the vegetation. The data were used to identify contrasts in the area in terms of vegetation stress, soil cover, and moisture content. The panchromatic view shows two contrasting blocks, viz., (Figs. 3.6a and 3.6b) to the northeast and southwest, recognized on the basis of tonal difference. A northwest-oriented tributary of Tirna River also flows along the contact between these blocks.

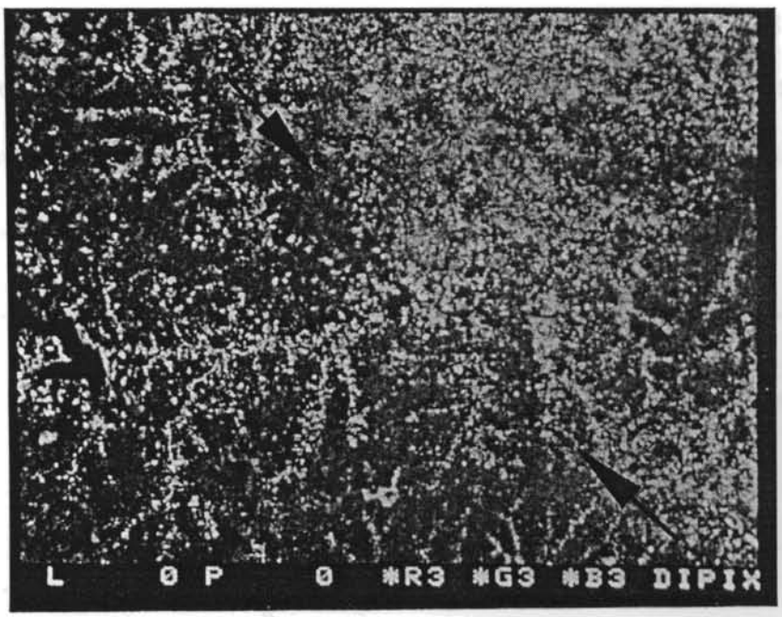

Fig. 3.6a Digitally processed image (Landsat TM) of Killari area.

Lighter tone of the southwest block is indicative of sparse vegetation and soil cover. On the other hand, the darker tone of the northwest block reflects a thicker soil profile, supporting denser vegetation. A northwest trending lineament passing through the epicentral regional defines the contact between the two blocks. The fault plane solution (Baumbach et al., 1994) indicates reverse faulting on a northwest striking nodal plane with the southwest block thrusting over the northeast block. All these observations suggest that the northwest trending lineament represents the fault that generated the Killari earthquake.

3.6 THE NW-ORIENTED REGIONAL STRUCTURE

As mentioned earlier, the focal mechanism of the main shock indicates reverse faulting on a NW-SE striking southwest dipping plane, and spatially, the aftershock zone is mainly confined to southwest block defined by a tributary of the Tirna River. The distribution of historic earthquakes also defines a northwest regional trend. Remote sensing data confirms this observation and shows a distinct separation between two blocks, defined by difference in surface characteristics on either side of the southeast flowing tributary of the Tirna River. It must also be mentioned that the field studies revealed an older shear zone further southwest of the epicenter of this earthquake, indicating much older tectonic activities (Fig. 3.7).

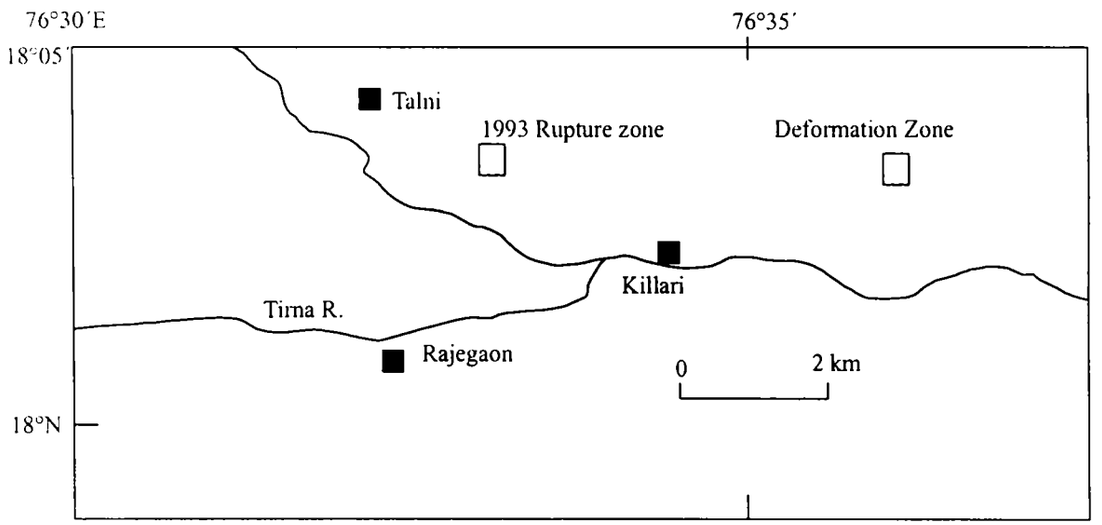

Fig. 3.7. Location of an older deformation zone and the 1993 rupture zone.

The above mentioned 100-m-wide zone of an older deformation is apparently associated with intense fracturing and mineralization, which was exposed on the walls of an irrigation canal about 3 km east of Killari (Figs. 3.8a and b). This zone consists of a south-dipping shear zone containing fractures with breccia. Clear signs of displacement, however,

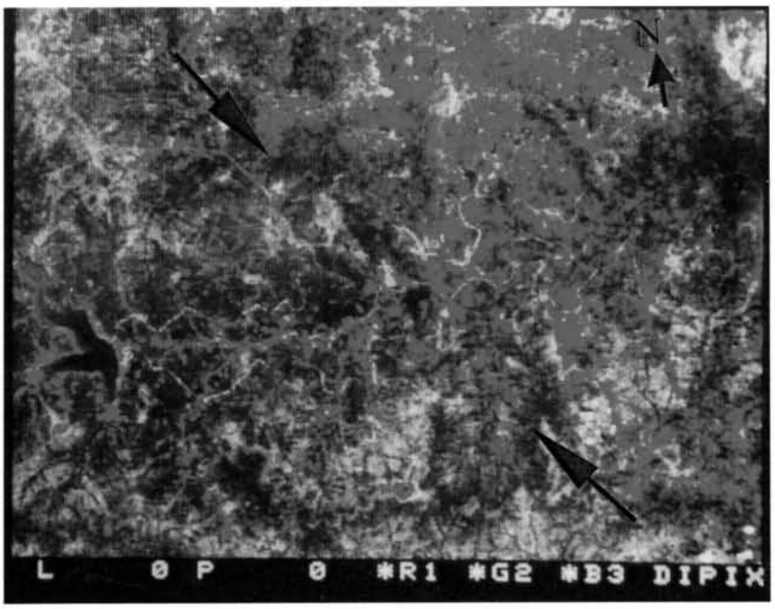

Fig. 3.6b. Digitally processed FCC (Landsat TM) of the Killari area. Arrow shows the trend of the inferred fault.

Fig. 3.8a. Photograph showing a fracture zone probably representing old shear zone (see the elevation difference). The location is 5 km east of the epicentre (Fig. 3.7). The fracture zone (indicated by arrow) is marked by mineralization. The change in elevation can be attributed to the erosion aided by fracturing at the top of the fracture zone. Orientation of this fracture zone is approximately E-W (view facing south).

Fig. 3.8b. Photograph showing a close look of the fracture zone shown in Fig. 5.8a. Orientation of this fracture zone (indicated by arrow) is approximately E-W (view facing northeast).

could not be identified in the exposure, but corrugated surfaces of some fractures suggest intense shearing or repeated movements. The central part of the deformation zone, composed of three major parallel bands of fractures, contains mostly angular basalt pieces embedded in fine-grained matrix. The cemented matrix is composed of calcite and zeolite minerals. The fractures close to this zone are also filled with these secondary minerals. Since gouge was not found along the deformation zone, it could be surmised that the deformation occurred close to the surface that was mainly controlled by the processes related to dilation.

CHAPTER 4

FIELD INVESTIGATIONS AT KILLARI

4.1 INTRODUCTION

The epicentral tract of the Killari earthquake lies within the Manjra River basin in a gentle depression carved out by an easterly flowing Tirna River, which has its confluence with the Manjra River near Aurad Shahjham, located 40 km east of Killari (Fig. 3.1). A zone of ground deformation features, which will be discussed here, was identified along the north bank of Tirna River between Killari and Talni. This surface rupture, coseismically produced during the 1993 earthquake, is a rare phenomenon as far as an SCR event is concerned. Only ten stable continental region earthquakes are known to have ruptured the surface prior to Killari earthquake (Johnston and Kanter 1990; Adams, et al., 1991). The surface deformation zone, located near Talni village, extends over a strike length of about 3 km in NW-SE direction with a width of about 300 m (e.g. Seeber et. al., 1996). This chapter presents the salient observations obtained during the field investigations in and around the rupture zone. Field studies at Killari included mapping of the scarp morphology, trenching and shallow boring in the rupture zone. Details of mapping of the scarp, trenching, and shallow drilling are discussed. Features related to a previous deformation episode deciphered from the trench sections are also described here. Several agencies worked in the rupture zone to study the nature and characteristics of earthquake faulting (Chetty and Rao, 1994; Pande et al., 1995; Rajendran et al., 1996; Seeber et al., 1996). These studies are reviewed in this chapter, which help in crosschecking our data and interpretation. The studies conclude that the trap rocks in the Killari area have indeed been affected by previous seismic event/s, and are characterized by a unique pattern of deformation.

Fig. 4.1a. Photograph showing rupture zone developed consequent to the 1993 Killari earthquake. Note the barren field north of the rupture zone indicating low vegetation (see Fig. 4.2 for location of the photograph).

Fig. 4.1b. Photograph showing two distinct zones on either side of the rupture (view to north). This distinction was observed after a heavy rainfall in the area. The area south of the scarp shows more soil moisture compared to the north of the scarp.

4.2 SURFACE RUPTURE

As mentioned earlier, the Killari event is one of the rare events in SCRs that produced a surface rupture (Fig 4.1a, 4.1b and 4.1c). The deformation zone showed discontinuous and arcuate rupture trends. Many subdued extensions of the rupture zone were visible further east and west of this zone where a thick soil cover has developed. The height and morphology of the scarps varied considerably over short distance. Thus the pattern of deformation was complex and discontinuous. The best-developed part, initially mapped by Seeber et al. (1994; 1996) was marked by opposite verging scarps (Fig. 4.2). This zone was located near Talni, about 4 km northwest of Killari, which measured about 500 m in length and 100 m in width. The dominant south-facing scarp had a height of about 80 cm. An ~ 70 cm- horizontal shortening was also evident from the strike-slip movement on one end of the rupture zone (Fig. 4.2).

4.2.1 Geometry and extent

Besides the main segment exposed near Talni, the trace of surface rupture extended discontinuously for a distance of 3 km. The various agencies that surveyed in the epicentral zone also found that the surface deformation extending up to 3 km (Fig. 4.3) (eg. Chetty and Rao, 1994; Gupta, 1994). Furthermore, Reddy et al., (1994) recorded highly elevated soil-gas helium over the surface rupture near Talni (Fig. 4.1d), which indicates that the surface rupture is connected to the fault at deeper level (e.g. Jones and Dorzd, 1983). Apart from the main rupture (shown in Fig. 4. 1d), the other surface cracks identified elsewhere in the region are not marked by helium highs (Reddy, et al., 1994). Thus it is evident that the surface rupture at Talni is indeed a manifestation of the movement at depth. However, it is likely that the observed discrepancy of the orientation of the rupture zone (in WNW direction) with that of the fault plane solution

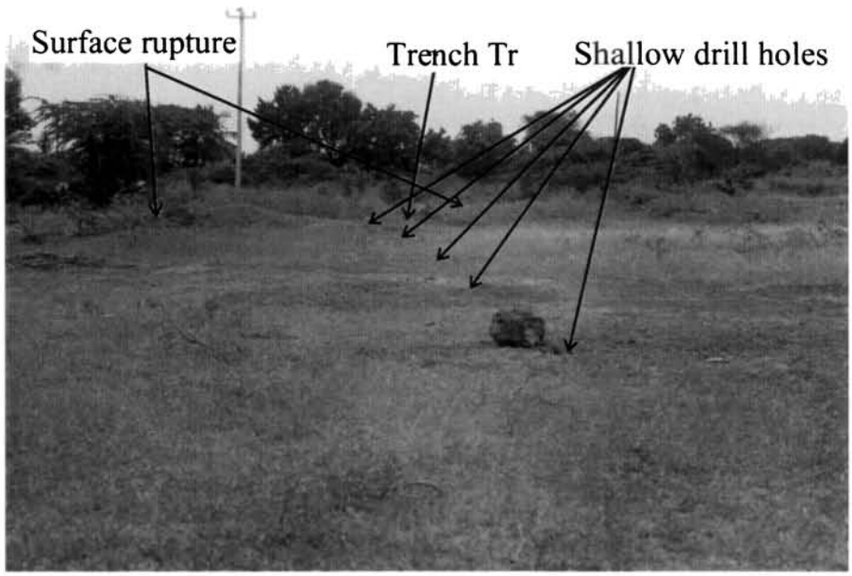

Fig. 4.1c. Photograph showing rupture zone and shallow drill holes (see Fig. 4.2 for location of the photograph).

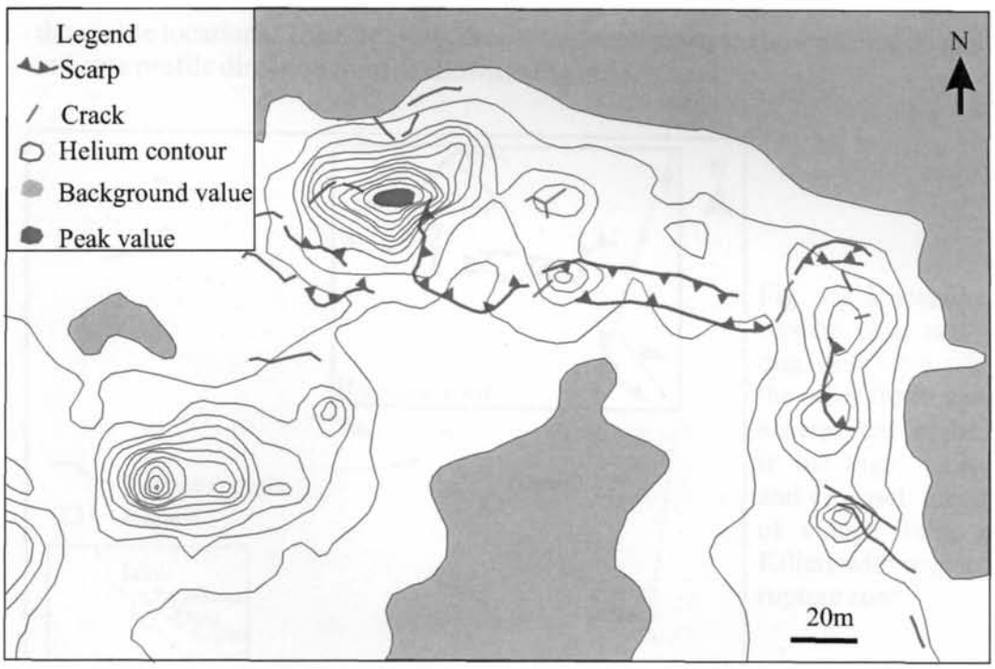

Fig. 4.1d. Helium anomaly map superimposed on rupture zone (modified after Reddy et al., 1994)

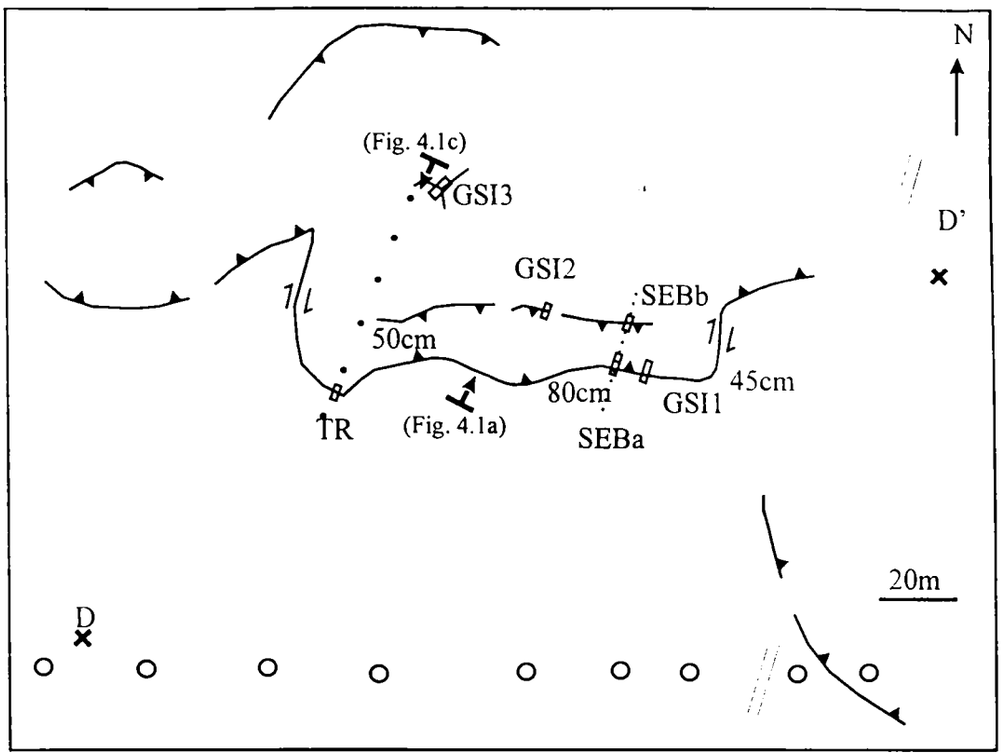

Fig. 4.2. Sketch of surface rupture; TR is the location of our trench discussed in the text; GSI-1 GSI-2 and GSI-3: trenches excavated by Pande et al., 1995; SEBa and SEBb: trenches excavated by Seeber et al., (1996). The open circles denote the theodolite locations. The black dots denote the locations of shallow drilling. D and D' indicate profile direction (profile shown in Fig. 4.5).

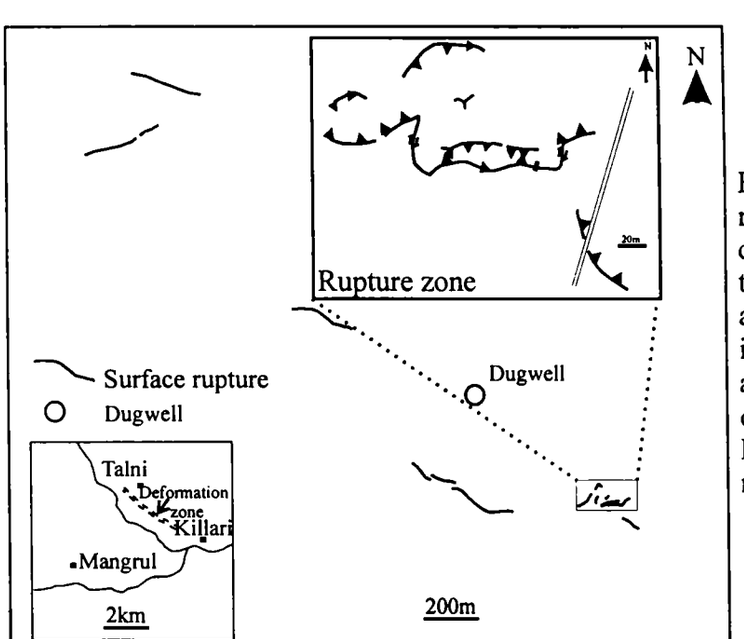

Fig. 4.3. Locations of rupture zone and the dug well from where the older thrust sheets are reported (as shown in the Figs. 4.13a, b and c). Inset: location of village Talni and Killari with respect to rupture zone

(fault oriented in NW direction) may be due to the heterogeneities along the rupture propagation path. The weathering characteristics and layered cake structure of the basalt flows contribute to this complexity (e.g. Seeber et al., 1996; Gahalaut et al., 2003). The studies elsewhere also support the precept that the ruptures developed in the cratonic hinterlands tend to develop complex geometries as it reaches the surface. The relevant global examples include the ruptures associated with the 1989 Ungava (Ms 6.3), Quebec (Adams et al., 1992), and the 1986 Marryat Creek (Ms 5.8), Australia (Machette et al., 1993) earthquakes.

4.2.2 Morphology

In order to constrain the topographical characteristics of the area, a number of elevation profiles were taken across the rupture zone, using digital theodolite and electronic distance meter. The locations of the theodolite points are shown in Figure 4.2. A digital elevation model is prepared on the basis of the theodolite survey (Fig 4.4). A notable morphological feature of these profiles is that the hanging wall occurs at a lower elevation, in spite of it being thrust onto the footwall block. For cross verification, another profile was taken diagonally across the rupture (Fig 4.5), which again confirms the same. A generally expected faulting scenario results in an elevated hanging wall block because of the accumulated upward slip and repeated thrusting. But, here the topography indicates a hanging wall block occurring at a lower elevation, and can be qualified as an inverted topography. This situation can be explained as due to the repeated thrusting from the south, which must have left this block highly crushed and fragmented, facilitating erosion, in contrast to the footwall, which is more compact and massive. These observations suggest, somewhat tangentially, that during the periods of long interseismic quiescence, most geomorphologic expressions got washed away,

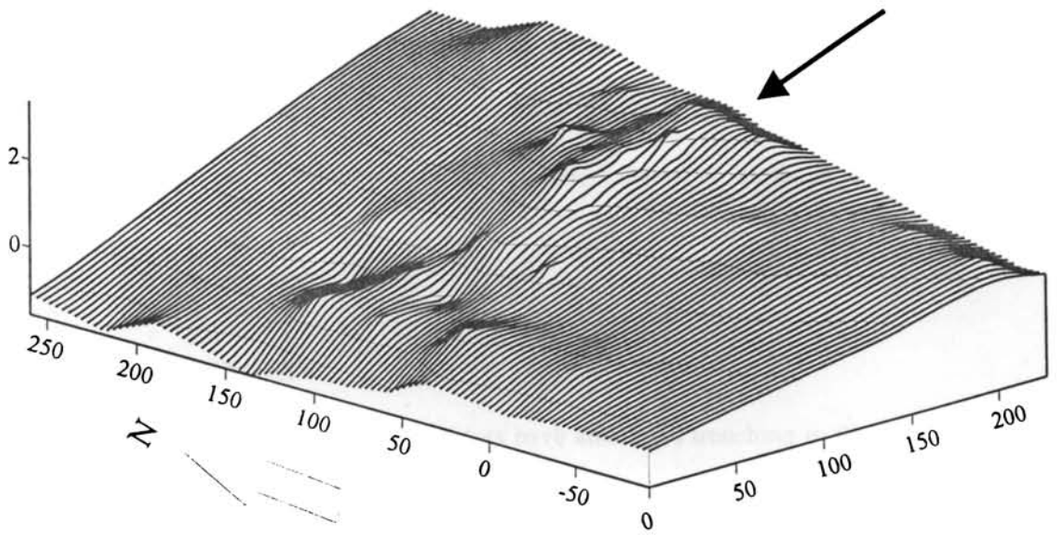

Fig.4.4. Digital Elevation Model generated for the rupture zone of the 1993 earthquake (shown by an arrow) using elevation data (see Fig.4.2 for location). The southern block (hanging wall) occurs at lower elevation.

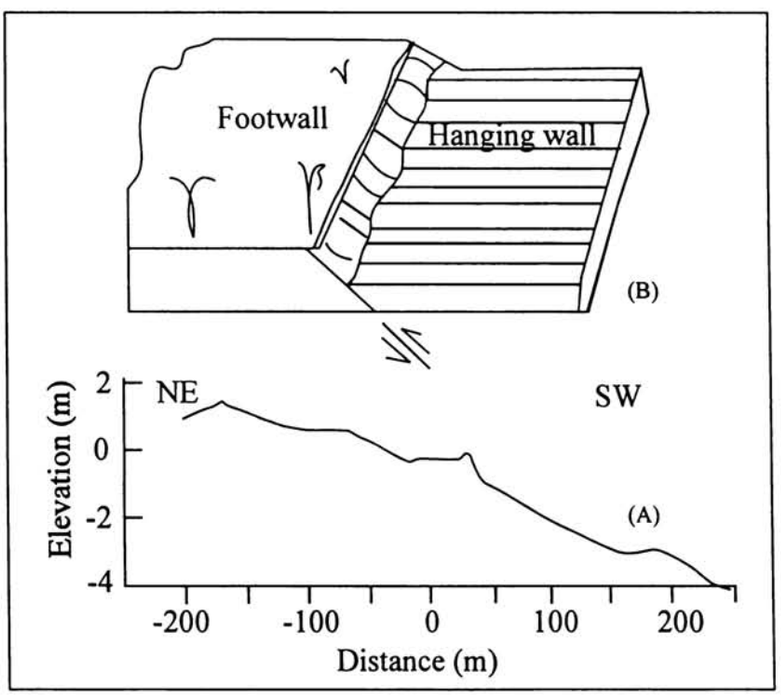

Fig. 4.5. Schematic diagram of the area based on the digital elevation model; the diagonal profile across D-D' as shown in Fig. 4.2.

leaving little evidence of any previous activity. This aspect of tectonically produced landscape, out-stripped by more vigorous erosional processes is a major factor that inhibits proper development of geomorphic expression of faults in the intracratonic settings.

4.3 TRENCHING

Several teams of investigators have attempted trenching in the rupture zone, and all of these attempts were restricted to a depth of 1 m. Locations of trenches excavated by Pande et al (1995) and Seeber, et al (1996) are shown in Figure 4.2.

4.3.1 Trenches in E-W segment

Trenches excavated by GSI (Pande et al., 1995) and by Seeber et al. (1996) in the Killari rupture zone are discussed here. Locations of the trenches marked as GSI-1, GSI-2 and GSI-3 are shown in Figure 4.2. Trench GSI-1 oriented in N15°E- S15°W direction was located in the southern scarp of the E-W segment where the soil cover varies from 10 to 45 cm (Pande et al., 1995). Although no fault plane is visible in the eastern wall of the trench GSI-1 (Fig.4.6), a yellow clayey material was found at the bottom of the trench wall. This yellow material was later identified as clay rich in montmorellonite, which was also found in a deeper trench TR that we made across the rupture zone (discussed later). Random distribution of clay lenses near the fault interface appears to be an important characteristic associated with near surface deformation associated with the 1993 Killari earthquake. This point is amplified later in the discussion.

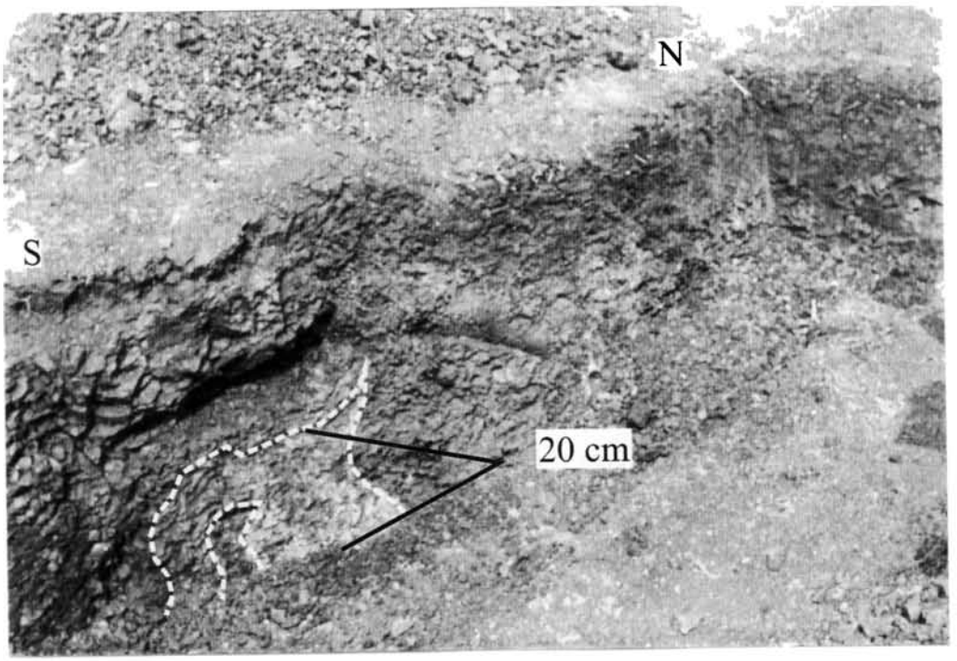

Fig. 4.6. Photograph of eastern wall of trench GSI-1 (courtesy: Pande. P) shows a distinct highly weathered southern block and a much more compact northern block. Note the yellow coloured clay injection at the bottom.

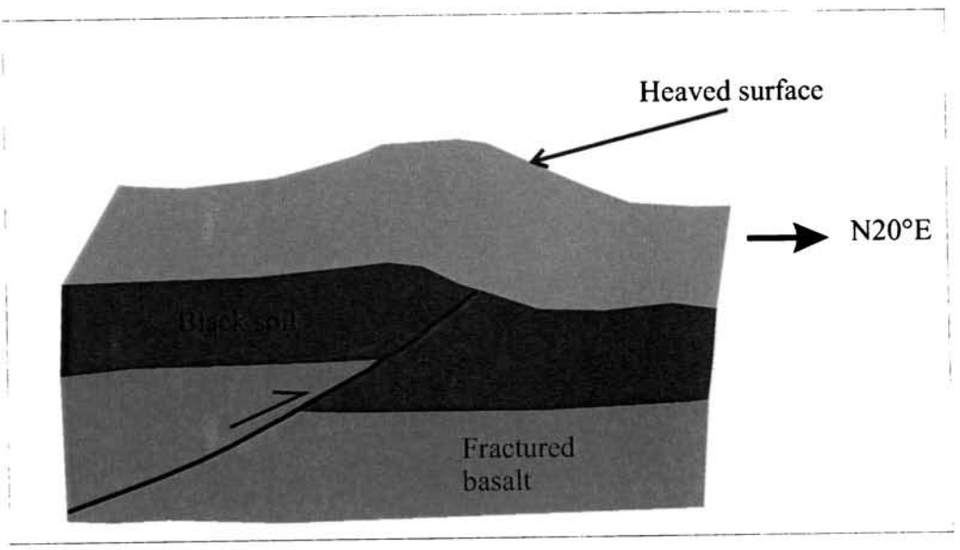

Fig. 4.7a. Sketch of western wall of trench GSI-2 (Pande et al., 1995); see Fig. 4.2 for location.

The trench GSI-2 (orientated in N20°E- S20°W) is located in the northern fringe of the E-W segment of the surface rupture (see Fig. 4.2). Both walls of the trench show a low angled south-dipping fault (Fig. 4.7a). Another trench dug on open fissures in the northern side of the surface rupture (Fig 4.2) revealed vertical extensional crack, and it seemed to have been developed as a cooling crack (Fig. 4.7b). A significant observation worth mentioning here is that the basaltic flow in the northern side was of compact type, in contrast to the trap rocks on the south of the rupture zone.

The shallow trench excavatd by Seeber et al. in the E-W segment of the rupture exposed a reverse sense of throw and a south dipping fault (Fig. 4.8). According to Seeber et al. (1996), the mode of faulting observed in these trenches was influenced by the geometry of the preexisting exfoliation fractures. They observed two kinds of fractures: the larger vertical ones in the north-northeast direction in the direction of shortening, which were interpreted by them as extension fractures, parallel to the direction of maximum compressive stress, and the second group was interpreted by them to be weathering related exfoliation fractures, parallel to the rock-soil interface. The sense and amount of rotation of the fragments from their original position in the exfoliation structure seems to align with the 1993 deformation (Fig. 4.8). Seeber et al. (1996) did not record any evidence of pre-1993 deformation along any of the 1993 fault, as in the form of slickenslides, concentrated zones of weathering or mineralization, and they concluded that the 1993 rupture developed on a new fault or a fault with no substantial neotectonic displacement.

Fig. 4.7b. Photograph of the trench on the northern side of the surface rupture (courtesy: Pande, P). Not the compactness of the top layer of basalt compared to the the rupture zone and its southern side.

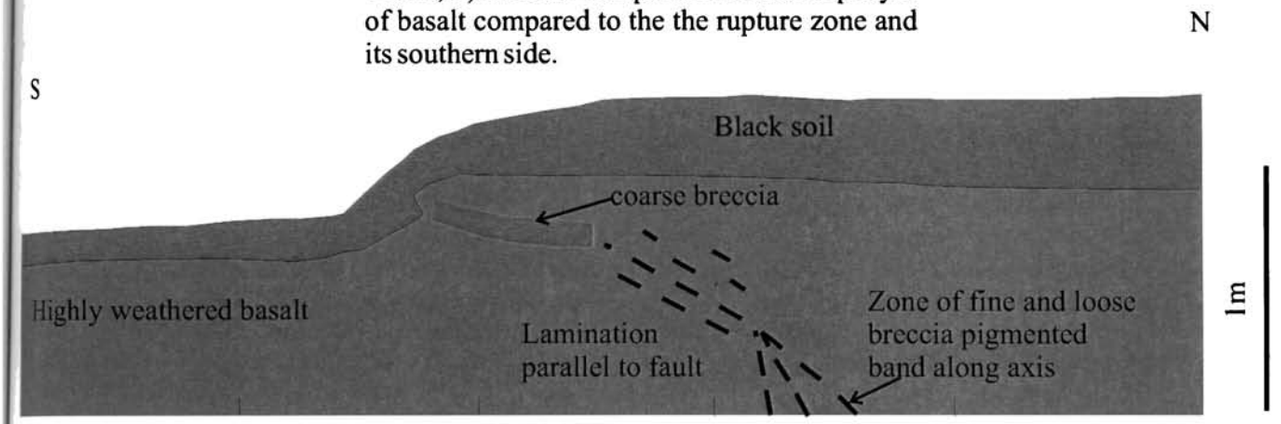

Fig. 4.8 Shallow trench showing the 1993 fault (Seeber et al., 1996); see Fig. 4.2 for location, denoted as SEB.

4.3.2 Trench close to the NW turn of the rupture

A trench measuring 5 m long, 2 m wide and 2 m deep was dug across the rupture zone (N20°E) close to the western end of the rupture zone (TR in Fig. 4.2). This trench exposed the top basalt flow, and showed a highly complex picture (Figs. 4.9a and 4.9b). At 1.9 m the trench exposed a red bole layer. Several structures, including a low angle (~ 15°) northeast dipping thrust fault were exposed on the eastern wall (Fig 4.9b). The shear planes and the rock layers showed the same angle of dip (~15°). From the dip of the structures, it is clear that the southern block had been thrust onto the northern block, which resulted in overriding of northern block.

In contrast, the northern block, although highly compressed and buckled, consisted of northeast dipping layers of basalt. Presence of both vertical and south-dipping mineralized veins was also observed. The rock fragments exposed on the northern wall were larger (> 8 cm), in comparison to the highly crushed basalt in the southern block. In addition to the multiple thrust sheets, a layer of highly flexured and fragmented reddish basalt, which did not show any offsets, was also exposed at the base of the trench (Fig 4.9a and 4.10).

Here, it is also worth mentioning that high values of helium concentration have been observed in the western terminus and southern portion of the main rupture zone, which implies the presence of deep fracture network. It is significant that 'TR' is the only trench that was excavated in the region of elevated helium values (Fig. 4.2).

This trench (TR) walls showed a wide impact zone at the interface of a block of fragmented basalt on the south and more compact basalt on the north. The impact zone comprised minute fragments of basalt embedded in yellowish and whitish clay (Fig. 4.9b). The XRD studies show that these yellow materials are composed of

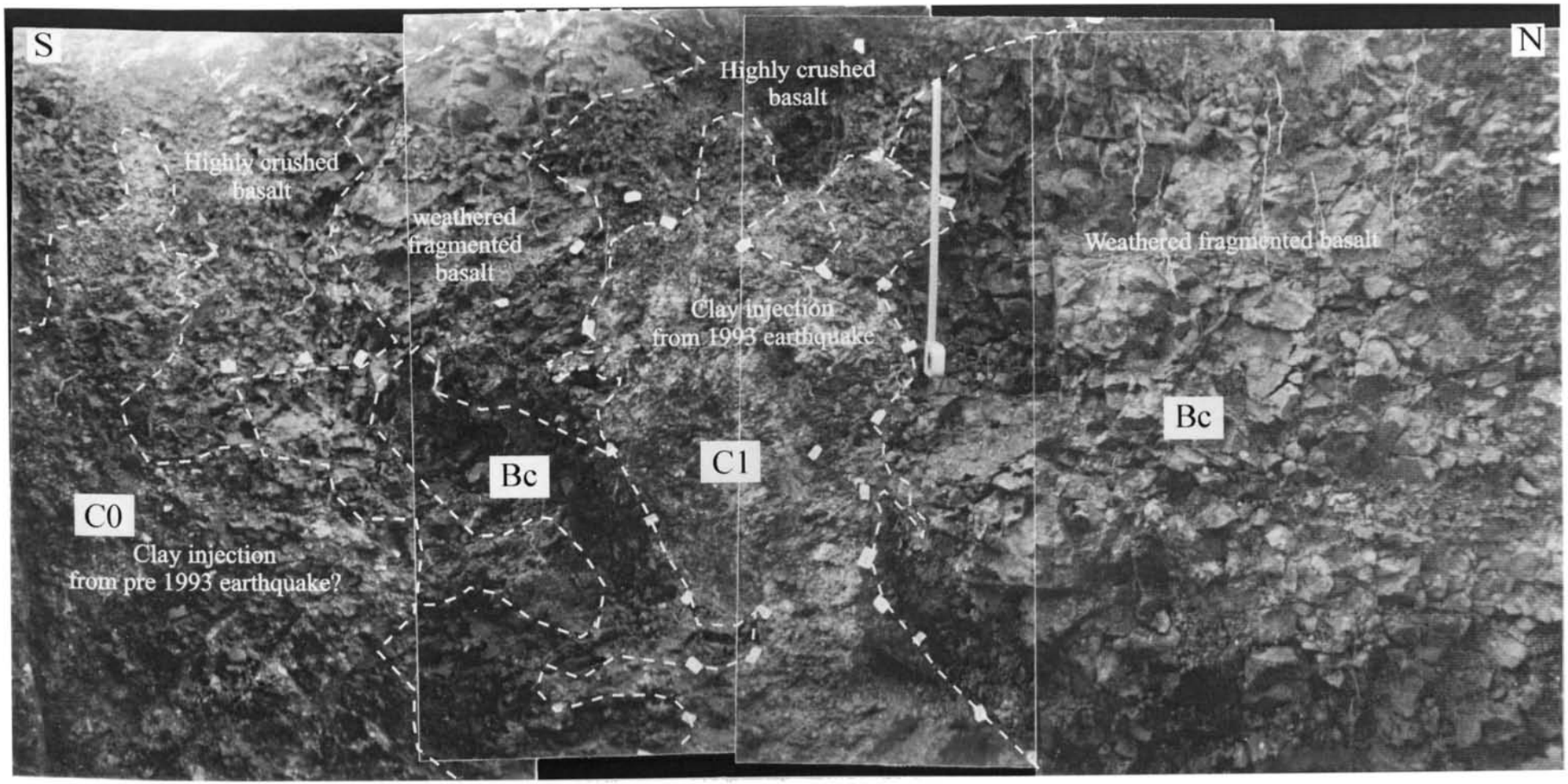

Fig. 4.9a. Photograph of western wall of trench TR. Bc: relatively compact rock; C1: clay injection due to the present event. Note that the clay C1 has split the Bc during the injection; C0 shows clay enrichment possibly during an earlier event. A distinct compact northern block can be easily distinguished from a crushed and/or shattered southern block. The clay injection (C1) associated with 1993 event shows an intense yellow colour, which seems to break through the interface of crushed basalt and the northern massive basalt (Bc). A zone of crushed basalt-clay mixture can also be seen on this wall, which may be indicative of a pre 1993 event.

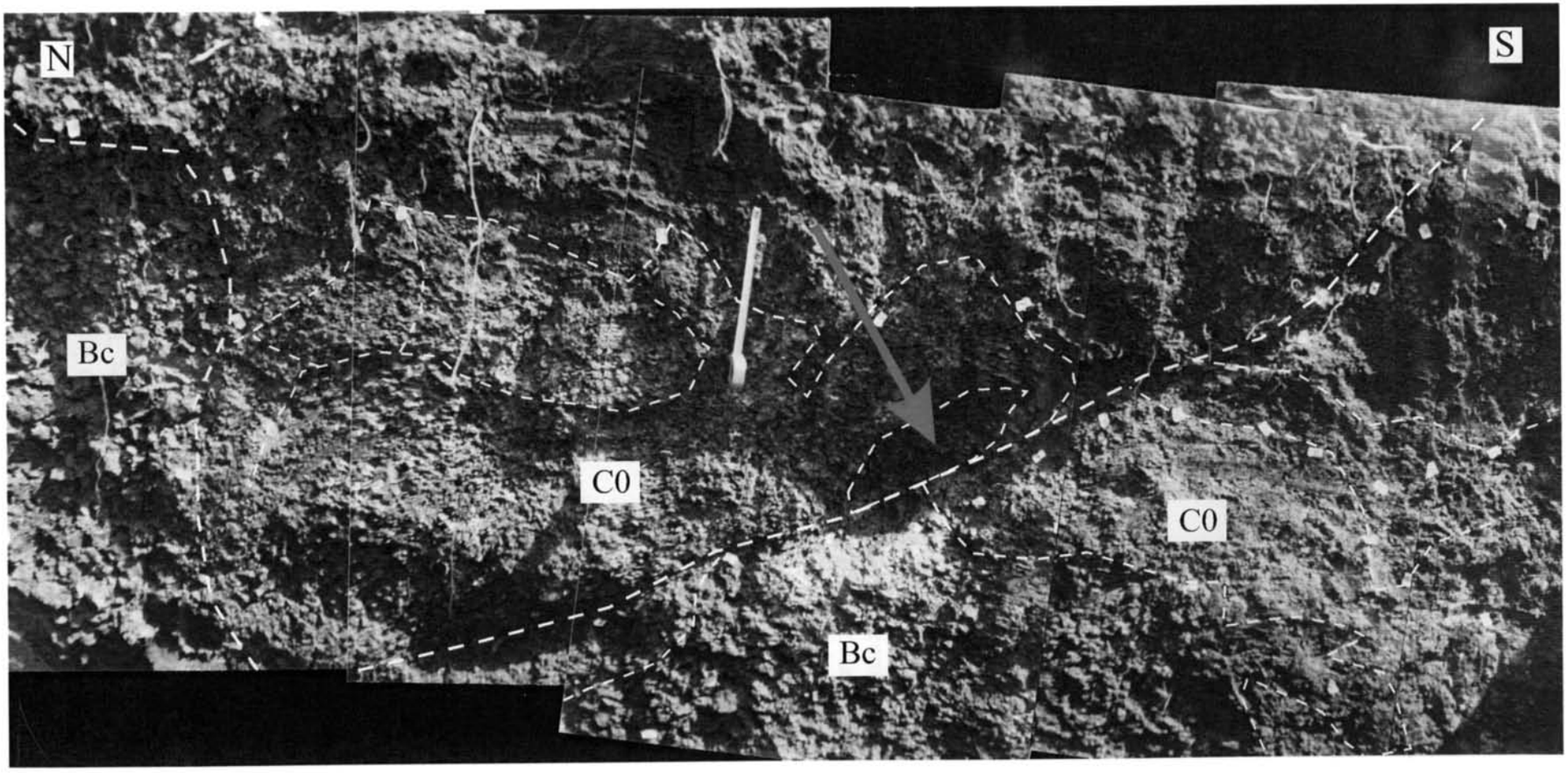

Fig. 4.9b. Photograph of eastern wall of trench TR (location shown in Fig. 4.2). The distinct compact northern block can be easily distinguished from a crushed and/or shattered basaltic layer. Rotated fragments of basalt together with yellow material (clay rich in montmorellonite) can be easily distinguished from overlying soil and relatively compact basalt. A north dipping slip plane can be clearly seen in this wall. Arrow shows a piece of relatively compact basalt entrapped in the clay-basalt mixture. Notations are same as in Fig.4.9a.

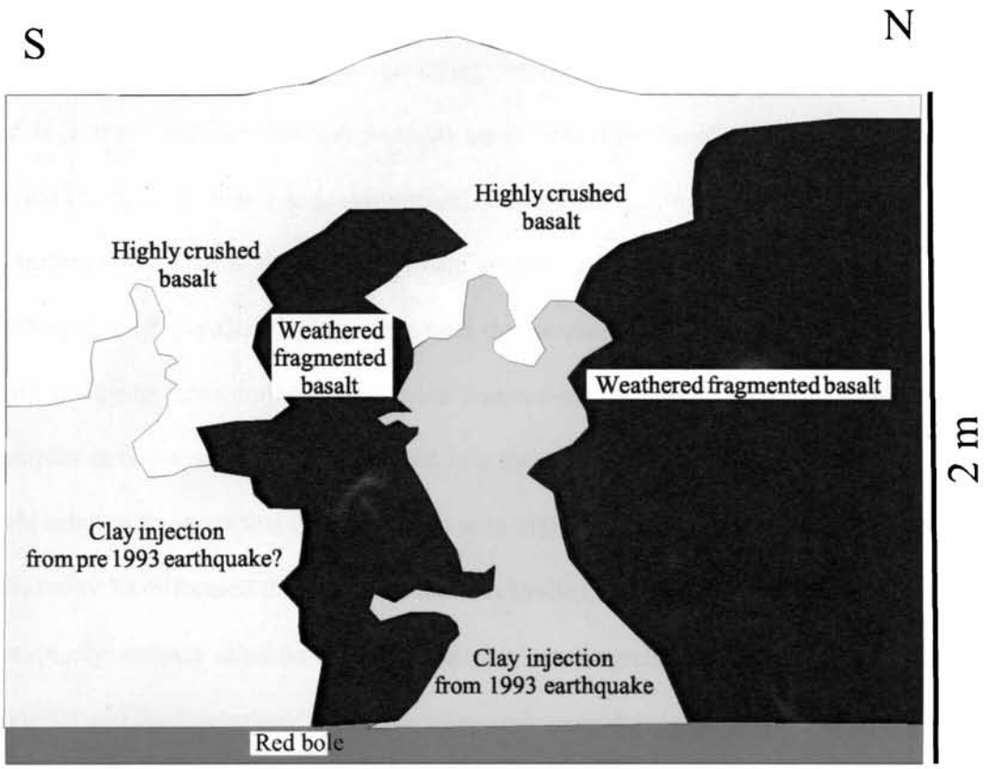

Fig. 4.10. Sketch of western wall of trench TR showing coseismic clay injection due to 1993 faulting and a probable clay injections associated with the pre 1993 faulting.

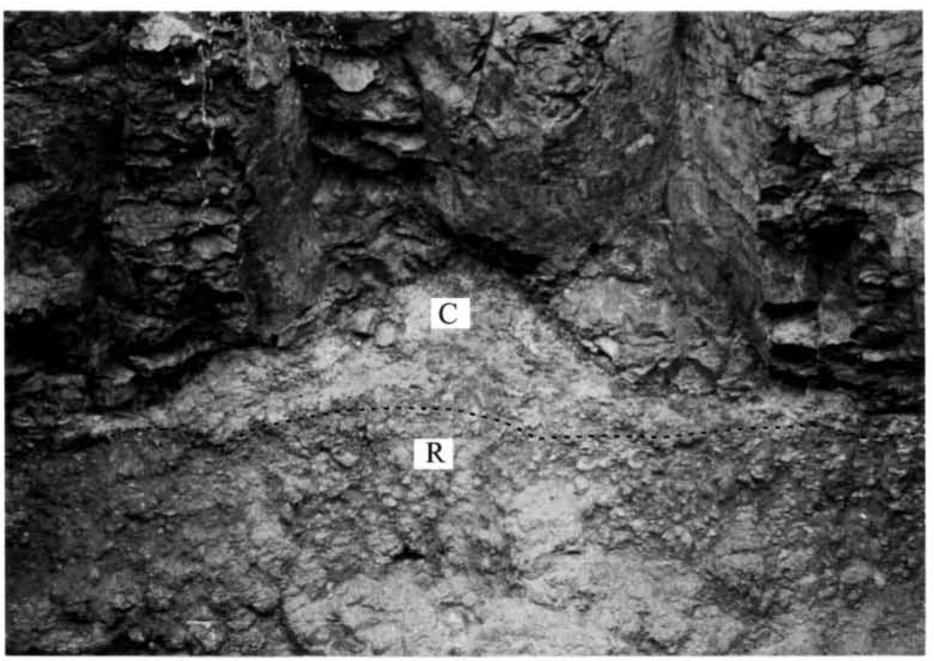

Fig. 4.11.A section showing interface between a red bole and a basalt flow layer near the epicentral area. Note the layer of clay material as 'C', which is yellowish and can be easily distinguished from underlying red bole. The dotted line represents the boundary between 'C' and 'R'.

montmorillonite-rich clay. This clay at the impact zone had a 'dome shape' and its continuity could be traced to the underlying redbole layer. Relation with the underlying red bole layer indicate that this material could have been emplaced to a higher level, during the faulting episodes. In this context, it may be noted that there are a few geologic examples of somewhat similar type of emplacement associated with seismic faulting: the melting-related pseudotachylyte veins and the pore-pressure related liquefaction veins formed during large earthquakes. These features are associated with both simple and complex network veins that are injected into the wall rocks or overlying sediments. The field relation suggests that the clay lumps seen in the trench (as shown in Figures 4.6 and 4.9a) may have formed through a similar mechanism. These mechanisms imply that the previously formed montmorillonite- rich clay was injected into the crushed basaltic material and the fractures of the surrounding rock mass during the faulting episodes. This point is further discussed in the following sections.

As mentioned earlier, a red bole clay layer was found between two lava flows in the epicentral area (Fig 4.11). A thin layer of montmorillonite-rich clay (yellowish in colour) was also found distributed at many locations above the red bole layer. Three possibilities could be accounted for the formation of montmorillonite: one, by hydrothermal action of volcanic fumaroles; two, by transformation of volcanic ash and tuff within the aqueous environment of sedimentary basins; and three, by weathering of volcanic ash and tuff (Millot, 1970). Pyroclastic materials such as ash and tuff are particularly vulnerable to weathering. For example, Sudo (1954) showed in Japan that moderate weathering is sufficient for the conversion of ash into montmorillonite.

We assume that the impact zone as revealed in many trenches, especially the trench TR (Fig. 4.9a), is made up of montmorillonite-rich clay, which was squeezed up during the 1993 event. But, in the trench TR one could also observe a mixture of clay

and crushed basalt, which we believe was formed due to recycling of a clay injection possibly formed from a pre-1993 event. Even though the older injected material appeared to have been recycled, resulting in a mixed zone, we infer at least one older event in this trench. The eastern wall of this trench also shows an older clay injection (Fig. 4.9b).

The recent movement had crushed the rocks further and accentuated the shear planes that must have formed during the previous events. The thrust sheets had obviously propagated along the layer of underlying reddish basalt, which probably acted as a detachment surface (dècollement). An analogy may be made here to fault-bend or fault propagation folds where the thrust sheets move over the weaker rock layers. These thrusts generally propagate along the detachment surfaces, which define the bedding planes, and these can also be called as bedding thrusts.

Fractures and joints in the epicentral zone of Killari are also mapped (Fig. 4.12). They are moderate to steeply dipping (30°-45°) and show different trends, in the NNE-SSW as well as in the NW-SE directions. Away from the fault zone, the trend changes to E-W. It is noted that fracture pattern in the regions to the northeast of the Tirna River (footwall block) is predominantly NW-SE to E-W. Contrary to this, in the regions to the southwest (hanging wall block), the NNE-SSW oriented fractures predominate. Consistent orientation of fractures and distinct changes across the fault zone therefore suggests a tectonic control. Average dip of beds also indicates changes across the fault zone. It is noted that in the close vicinity of the epicentral zone the beds show steeper (25°-30°) dips, whereas away from this region (to the northeast as well as the south west), they tend to be shallower. Thus, fracture pattern and disposition of beds in the vicinity of the fault zone show variations across the fault zone. They also indicate that even within the highly heterogeneous zone with overprints of weathering, the tectonic control is persistent.

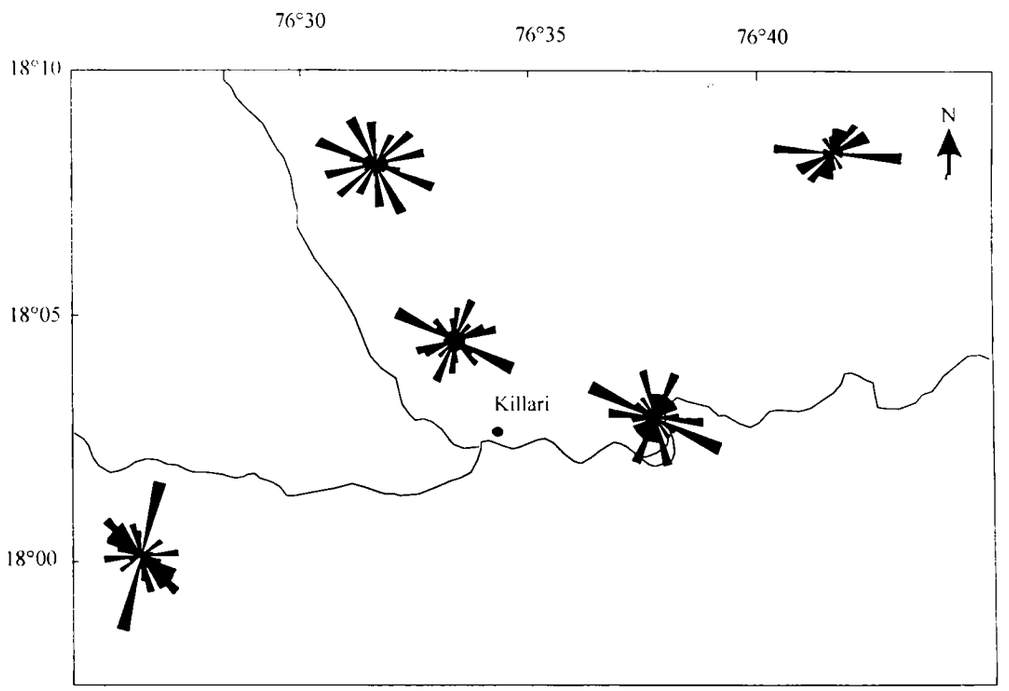

Fig. 4.12. Joint pattern in the epicentral area

4.3.3 Well section

Further evidence for the pattern of near-surface deformation was obtained from a dug well (Figs. 4.13a, b and c), located ~500m northwest of main surface rupture (see Fig. 4.3 for location). The well section essentially shows what appeared to be older thrust sheets, interlayered with red bole material. Thickness of the remnant top flow is only 6 m (see Figs. 4.13a and 4.13b, which show the southeastern wall and the Fig. 4.13c for the opposite wall). Apparently the thrust sheets formed in basalt layers had propagated along the slipping surface provided by incompetent beds (red bole layers), capped with a thin layer of clay enriched in montmorillonite (Fig 4.3d). One important point to be noticed here is that the absence of red bole at the top of the thrust sheet. The footwall block appears to have been crushed and affected by secondary mineralization. If the pattern of deformation observed here is any indication, then much of the near surface deformation

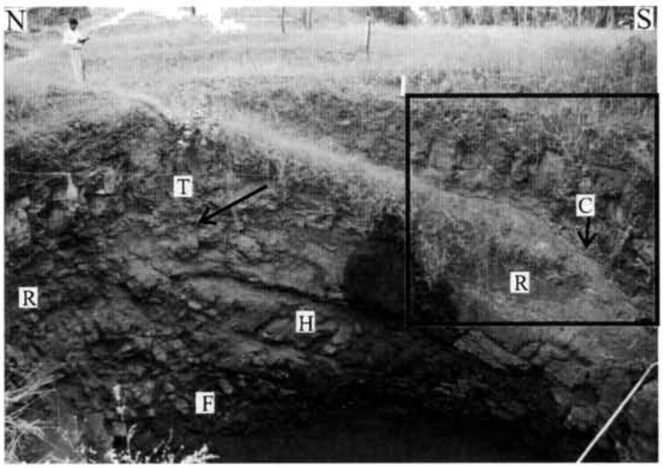

Fig. 4.13a. Well section near the rupture zone (see Fig. 4.3 for location). R: red bole; T: undisturbed top layer; H: thrust sheet; F: footwall; C: clay perturbation into the top flow. Note the absence of red bole at the top of H, indicated by an arrow. Area marked in the rectangle is further shown in Fig. 4.13c.

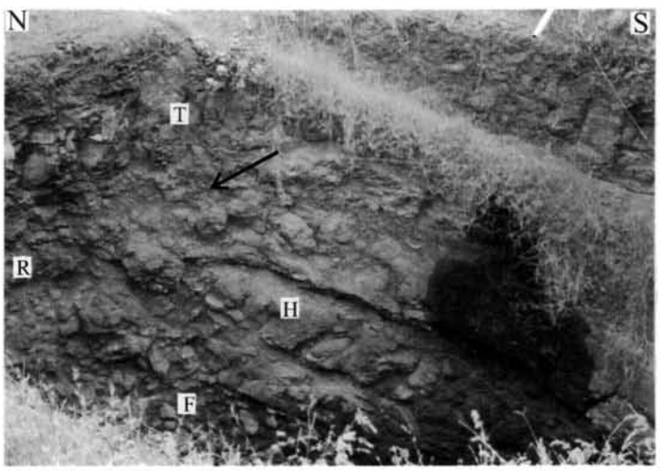

Fig. 4.13b. A closer look of the section shown in the previous photograph. R: red bole; T: undisturbed top layer; H: thrust sheet; F: footwall; Note the absence of red bole at the top of H, indicated by an arrow.

Fig. 4.13c. A close look at the area marked in rectangle in Fig. 4.13a. C: clay perturbation within the top flow.

in the area is in the form of bedding plane thrusts and parallel folding, typical of contractile regions. Just like in the rupture zone, a clay perturbation is also observed in the bottom of the top flow (Fig. 4.13c).

The presence of thrust sheets from earlier deformation below the 1993 event horizon suggests repeated activity on a preexisting fault. The minimum age of the penultimate faulting cannot be estimated by direct methods, as no suitable materials for dating were present in the trenches. The subdued topography and the erosional scarp in the rupture zone are suggestive of erosion of the previously formed fault ramp and long recurrence interval (of the order of hundreds of thousands of years) of slip events. A preliminary TL date from the clay sample from the trench indicate >20,000 years (Rajendran and Rajendran, 1999) for the older deformation in the trench.

4.4 REGIONAL STRATIGRAPHY

The lithologic data from about 50 bore wells in the region around Killari collected from the Maharashtra Groundwater Development Agency were analysed. Locations of selected wells across the rupture zone and their respective well logs are shown in Fig. 4.14. The litho logs indicate that there is considerable change in stratigraphy on both sides of the fault zone. For example, the absence of soil profile is visible in wells 21a and 18a. The poor development of soil in this area may be interpreted as due to the increased erosion in the hanging wall block, as it is more crushed, compared to the footwall.

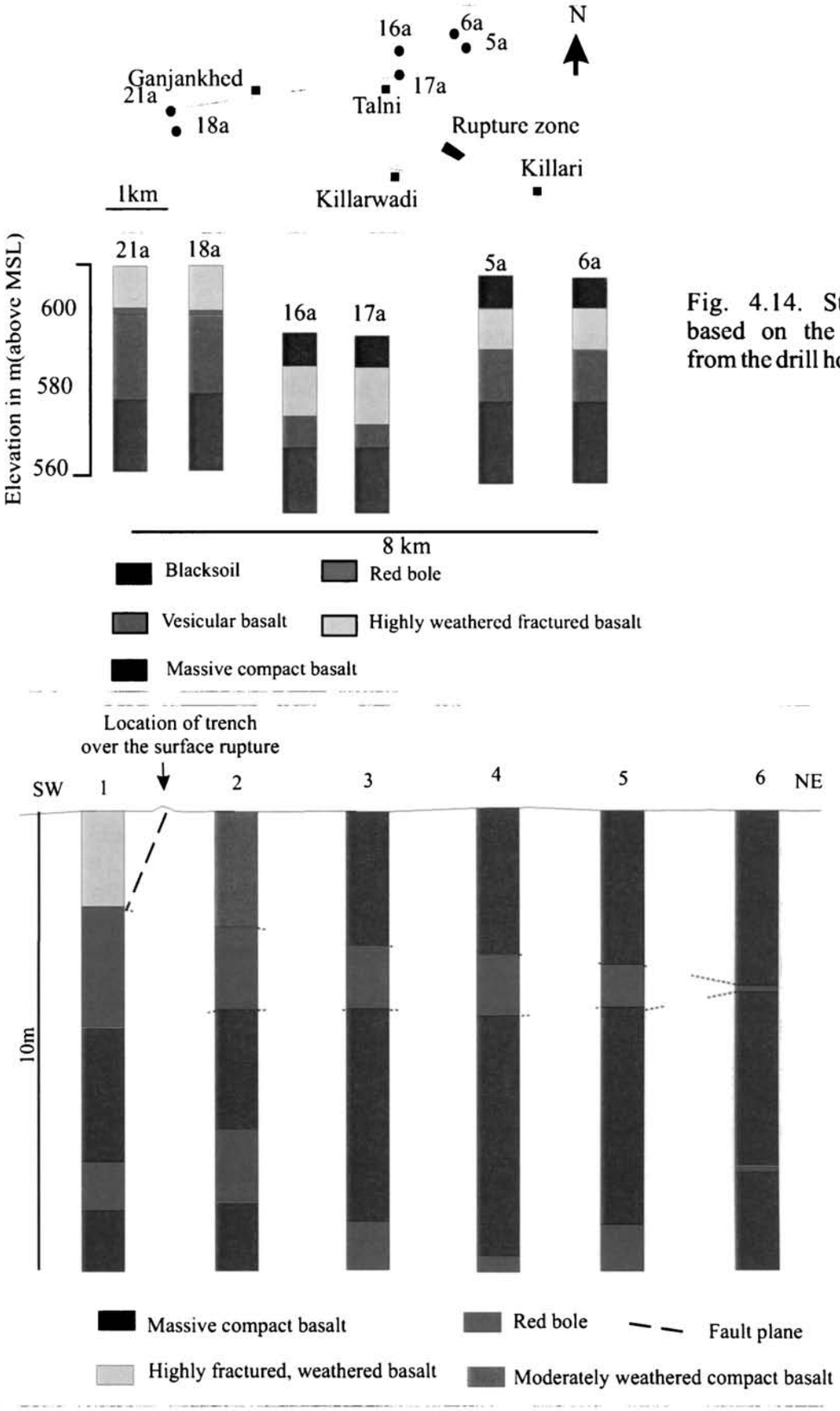

Fig. 4.14. Stratigraphy based on the litho logs from the drill holes.

Fig. 4.15a. Logs prepared from shallow drilling across the surface rupture and trench TR (location shown in Fig. 4.2).

4.5 DRILLING NEAR THE SURFACE RUPTURE

4.5.1 Shallow drilling

Shallow drilling was carried out at an interval of 20 m in the N20E direction across the rupture zone (Fig. 4.1c and 4.15). The litho log revealed the presence of red bole at shallow depth, further confirming the observation from the trench TR (Fig. 4.15a). The drill data provides an important constraint on the nature of the near-surface deformation at Killari, and for the role of red bole being a slipping interface. The Fig. 4.1c shows the locations of drill holes, and thick vegetation south of the rupture zone where the area has developed a thicker soil cover compared to the northern block (Fig. 4.1a and 4.1b), indicating an inverted topography.

4.5.2 Data from the deep bore hole

The data obtained from a deep bore hole near the rupture zone help in corroborating some of the assumptions on the style of deformation that we made on the basis of near-surface observations. Borehole data (Gupta and Dwivedi, 1996) revealed a 338 m-thick trap and 6-8-m-thick sedimentary cover over a granite-gneiss basement (Fig. 4.16). The Deccan Trap sequence consists of eight simple 'aa' type basaltic flows. The fault plane appears to be steep with an angle of ~50° toward SSW (Gupta et al., 1999). The shattered basalts occasionally displayed slickensides. Although a persistent red bole was observed at 173–178 m below surface (Gupta, et al., 2003), no red boles were reported at shallow depth in this bore hole.

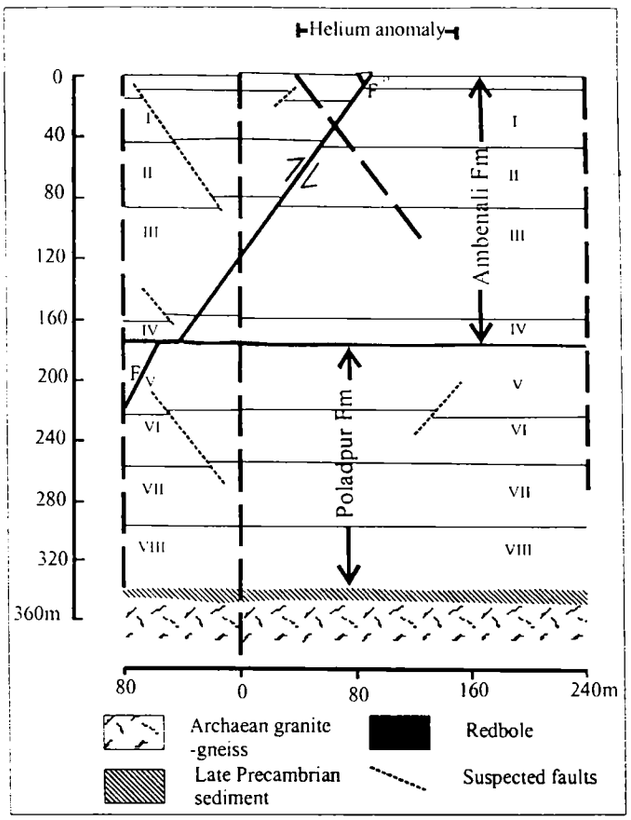

Fig.4.16 Simplified subsurface stratigraphy based on the data from deep drilling in the area of 1993 surface rupture (after Gupta et al., 1999)

4.6 STYLE OF DEFORMATION

It was Seeber et al (1996), who originally discovered the double vergence and complex pattern of surface rupture near Talni. Their trenches made in the northern rupture shows a clearly visible slip planes along which the movement took place (Fig. 4.8). Although the basalt on either side of these planes looked somewhat identical, those on the southern scarp showed a sharp variation in weathering and compaction. But at many other places, no distinct slip plane could be observed (e.g. GSI-1; Fig. 4.6). In other words, the variation in deformation style changed from one site to the other. This

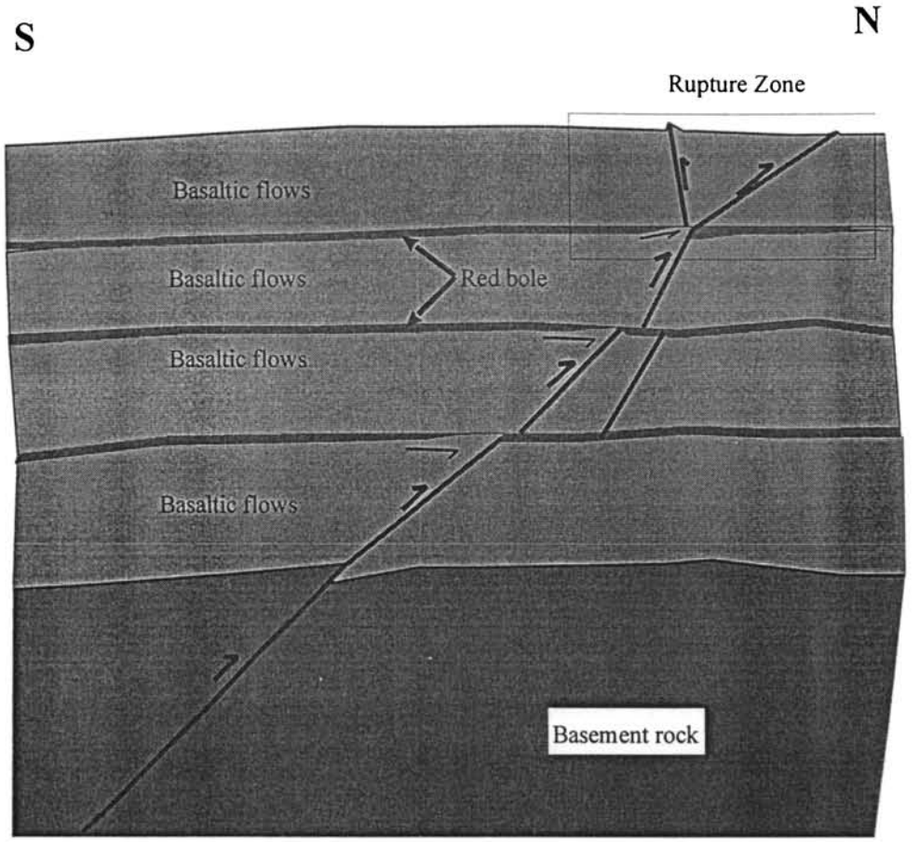

Fig. 4.17. A synoptic model showing a possible style of deformation at Killari. (not to scale)

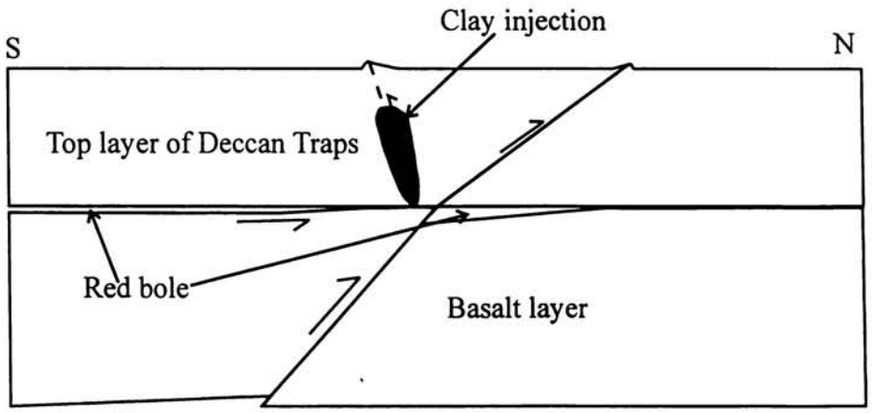

Fig. 4.18. A synoptic model showing deformation at the top level of the rupture zone at Killari. Note that the clay injection is observed only in the discrete slip plane-dipping north, antithetic to the main south-dipping plane.(not to scale)

observation suggests non-uniform slip as the rupture propagated to the surface. The occurrence of a red bole layer within the vicinity of rupture zone at around 2 m (see Figs. 4.10 and 4.15 - section from the trench TR and shallow drill hole data) is another significant observation. Gradual thinning of the red bole layer and evidence of ramping are also noted from shallow drilling.

The non-uniform surface slip and ramping – two significant characteristics of the surface deformation- may have been influenced by the layered structure of basalts. This situation is compounded by the presence of incompetent layers of low strength, i.e., reddish basalt, sandwiched between more competent rocks. The red bole, together with clay rich in montmorellonite, probably acted as a detachment surface (dècollement), which promoted horizontal movement. Nature of exposures observed in this study indicates that much of the shortening in this region is accommodated by co-seismic folding and thrusting. In fact, this is not surprising because deformation in the layered basalts under horizontal compression may follow the least resistant paths, assuming the form of bedding plane thrusts. Therefore, when stack of competent beds, interlayered with incompetent layers are end loaded, competent beds tend to buckle up by slip on the mechanically weaker surfaces.

Several scenarios of fault propagation models can be built based on the above discussion. One, as the fault propagates to the surface, it may develop many splays and flower structures, which will also accommodate some component of displacement. Two, layers of rocks, separated by interlayer materials may stack up forming multiple thrust sheets. In a sequence of highly weathered and fractured basalt layers that are not visibly separated by interlayer material, the mode of deformation is hard to identify. Only where red boles are present, multiple layers can be identified. The process of near surface thrust propagation aided by low strength interlayer material is illustrated in Figures 4.17 and

4.18. In the Killari region, this process has eventually led to a highly deformed hanging wall block, characterized by series of thrust events as against a relatively intact footwall block.

CHAPTER 5

THE 1994 EARTHQUAKE AT WADAKKANCHERI AND GEOMORPHIC ANOMALIES

5.2 REGIONAL SEISMICITY

Among the historic and the recent earthquakes of the region, the December 2000 Kottayam (M 5.0), the June 1988 Idukki (M 4.5) and the December 1994 Wadakkancheri (M 4.3) (Bhattacharya and Dattatrayam, 2002; Rastogi et al., 1995; Rajendran and Rajendran 1995) are the three significant events in Kerala. Historic and recent data suggest occurrence of a few earthquakes in the vicinity of Palghat Gap between 1865 and 1996, including a moderate event near Coimbatore in 1900 (Table 5.1). During 1989, 1993 and 1994, events of magnitude between 3 and 4.3 occurred near Wadakkancheri. Epicentres of these three events were mostly located using primary field data. Rajendran and Rajendran (1996) suggested a possible association of these earthquakes with the Palghat Gap on the basis of structural and tectonic characteristics.

5.3 THE WADAKKANCHERI EARTHQUAKE

Epicentre of the 1994 Wadakkancheri earthquake (M_L 4.3) has been located at 10.75°N and 76.25°E (Rajendran and Rajendran 1995; IMD, 1995). The epicentre falls on the left bank of Bharathapuzha. This tremor was felt on 2 December 1994 in an area of about 1000km^2 around Talasseri-Desamangalam, near Wadakkancheri, Thrissur District in Kerala, and the maximum effects were reported from areas around Talasseri, Desamangalam, Varavur, Arangottukara and Chittanda (Fig 5.2a).

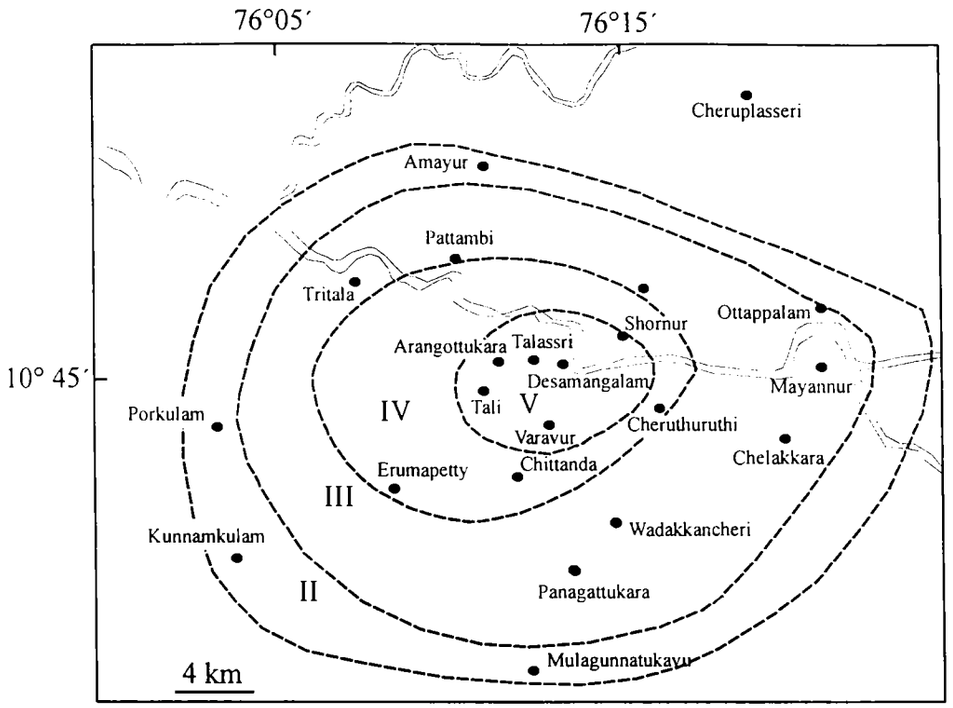

Fig. 5.2a. Isoseismal map of the 1994 Wadakkancheri earthquake.

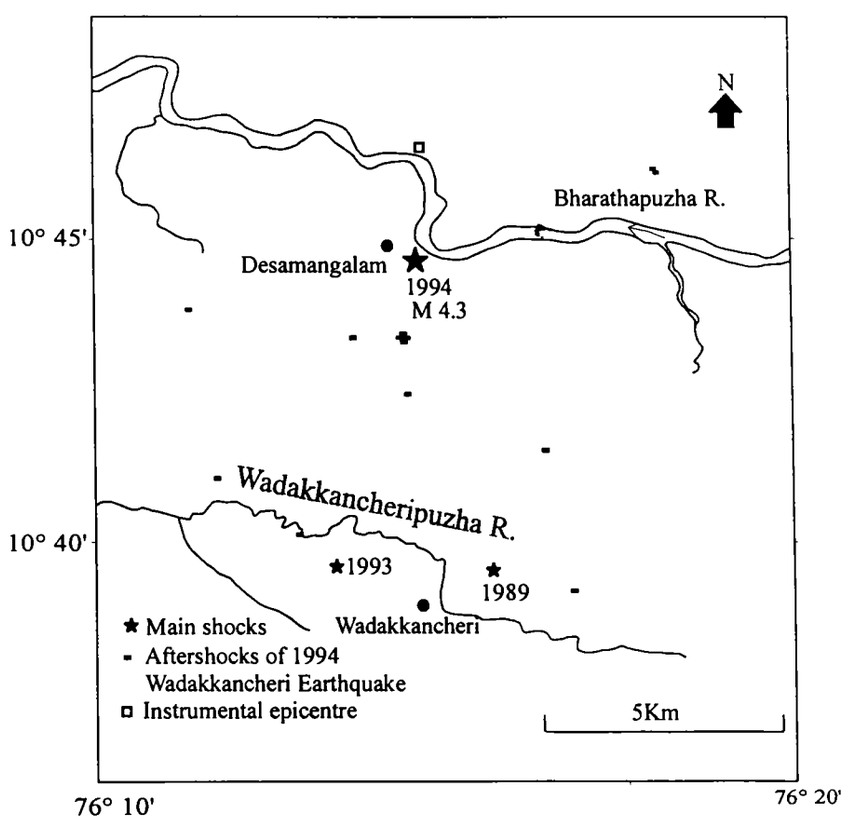

Fig.5.2b. Location of the Wadakkancheri events (1989, 1993 and 1994) and the aftershocks of 1994 earthquake.

Table 5.1 Seismic events reported within the vicinity of Palghat Gap area (modified after Rajendran and Rajendran, 1996).

Date	Location	Magnitude/ Intensity	Source
24-06-1865	Near Coimbatore	IV	Chandra (1977)
28-02-1900	Near Coimbatore	VII	Basu (1964)
29-07-1972	Near Coimbatore	VI	Chandra (1977)
1981-1993 (40 microtremors)	Central Part of the Gap South of 11°N and West of 77°E	1-2	GBA records.
15-03-1989	Near Wadakkanchari 10.64°N 76.26°E	3.0	Singh and Raghavan (1989)
25/26-02-1993	Near Wadakkanchari 10.64°N 76.20°E	3.6	Singh and Santosh (1993)
02-12-1994	Near Wadakkanchari 10.75°N 76.25°E	4.3	Rajendran and Rajendran (1995)
06-09-1996	Trichur 10.52° N 76.22°E	III-IV	CESS report (1996)

5.3.1 MAGNITUDE AND INTENSITY

The 1994 tremor was felt by every one in Talasseri-Desamangalam area. Unplastered/poorly plastered housed were affected most. Nearly 1500 buildings have

been reportedly damaged. Most of the damages occurred in the areas south of WNW-ESE flowing Bharathapuzha River. The smaller 1989 and 1993 Wadakkancheri tremors are also located on the same side of the river. Based on the damage/felt report, a maximum intensity of V was assigned to the epicentral area of 1994 earthquake (Rajendran and Rajendran, 1995). The epicentre derived from the isoseismal map is given in Fig. 5.2a. The magnitude of the earthquake is estimated to be 4.3, based on the maximum intensity.

5.3.2 AFTERSHOCKS

Over a 100 tremors were reported by the residents of the epicentral area. Most of these were very small, but accompanied by loud thundering sound. Later, portable stations operated by the India Meteorology Department in the epicentral area recorded 20 of them (IMD, 1995). Most of them are located to the south of WNW-ESE flowing Bharathapuzha River (Fig. 5.2b).

5.4 GEOLOGIC AND TECTONIC SETTING

The south Indian craton can be divided into a number of large Archaean/ Precambrian blocks separated by major shear belts (Drury et al., 1984). The Palghat-Cauvery shear zone is considered as an important tectonic boundary (Ramachandran, 1992; Yoshida and Santosh, 1996; Harris et al., 1994).

The region of ongoing microseismic activity falls in the southern flank of the Palghat Gap, a conspicuous geomorphic feature associated with Palghat-Cauvery shear-zone, in the Western Ghats, marked by a variety of rock types (Fig. 5.3a). The hill ranges of Western Ghats, extending in a NNW direction from the southern tip of Indian peninsula are marked by a number of peaks of altitude over 2000 m above MSL. The

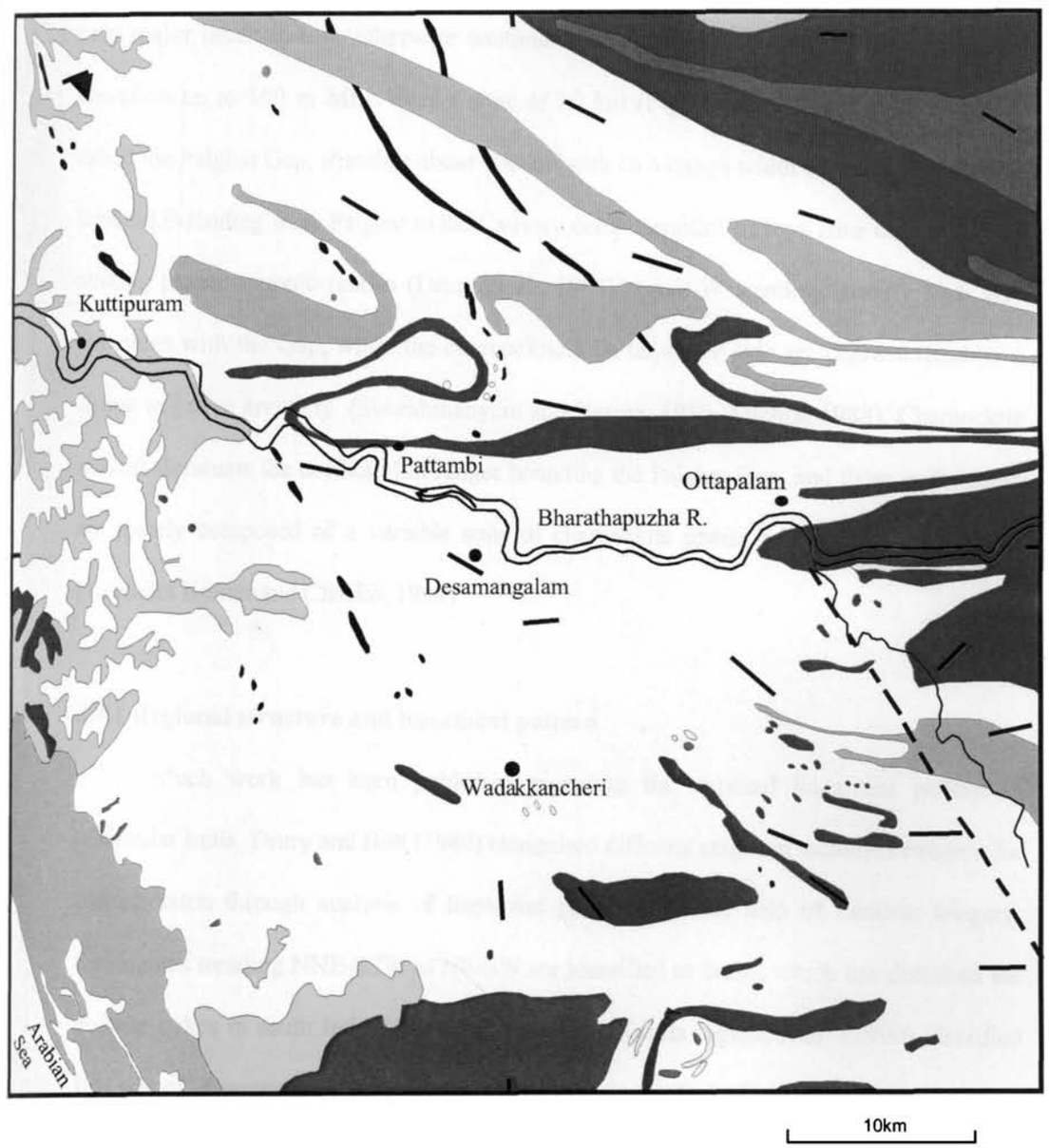

Pyroxene granulite
Biotite gneiss
Warkalli
Alluvium
Pink granite
Quartzo feldspathic gneiss
Hornblende biotite gneiss
Amphibolite
Gabbro
Dolerite
White sand
Charnockite
Regional lineaments

Fig. 5.3a. Geological map of the Wadakkancheri area (GSI, 1992)

only major break in this, otherwise continuous chain, is manifested by a sharp drop of elevation up to 100 m MSL over a zone of 30 km (Fig. 5.3b). This geomorphic break, called the Palghat Gap, stretches about 100 km with an average width of about 50 km. This lowland extending from Palghat to the Cauvery delta is controlled by a zone of strong E-W striking planar tectonic fabrics (Drury et al., 1984). An E-W trending gravity high also coincides with the Gap, while the charnockite hills on either side are characterized by a strong negative anomaly (Subrahmanyam and Verma, 1980; Mishra, 1988). Charnockite massifs dominate the northern hill ranges bounding the Palghat Gap, and those in the south are mostly composed of a variable suite of charnockite gneiss and pink granitic gneiss (Ravindra Kumar and Chacko, 1994).

5.4.1 Regional structure and lineament pattern

Much work has been published regarding the regional lineament pattern of peninsular India. Drury and Holt (1980) recognised different stages of tectonic evolution for Indian craton through analysis of lineament pattern with the help of Landsat imagery. Lineaments trending NNE-SSW to NE-SW are identified as faults, which has disturbed the dolerite dykes in south India (Grady, 1971). In the Kerala region, Nair (1990) identified five sets of lineaments: 1) WNW-ESE, 2) NW-SE, 3) NNW-SSE, 4) NNE-SSW and ENE-WSW. In another study, three major directions of fracture zones have been identified in the Palghat region based on the magnetic and electrical resistivity surveys; these zones trend in E-W, NW-SE and NE-SW directions (Kesavamoni and Bose, 1979).

We have looked at the principal lineament pattern of the area independently. Lineament patterns detected with the help of remote sensing, geomorphological features and drainage network for the study area are shown in Fig. 5.4a. Multispectral data is also

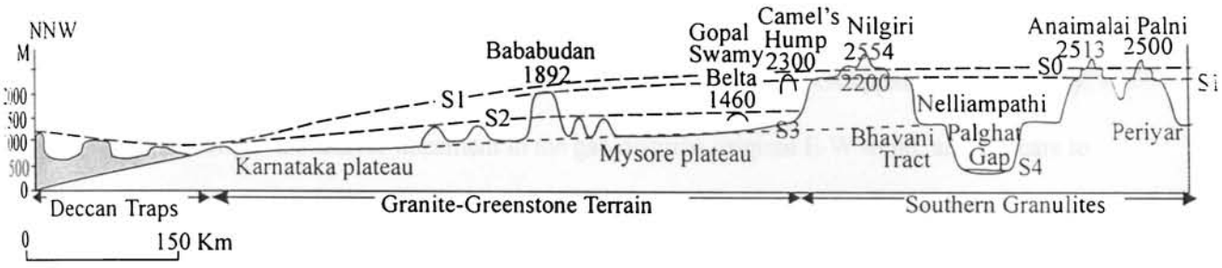

Fig. 5.3b. Profile across Western Ghats and Palghat Gap after Gunnel and Fleitout, (1998).

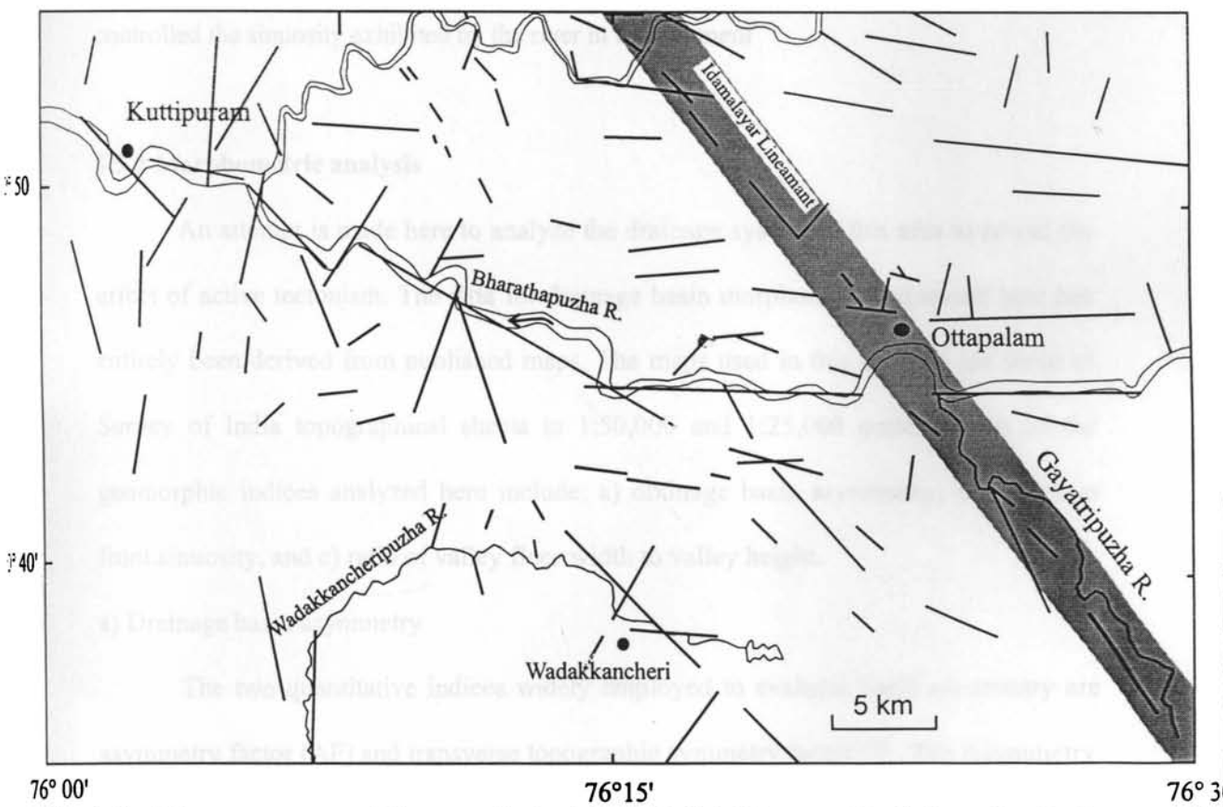

Fig. 5.4a. Lineament map of the area derived from IRS-1C image. Shaded portion is the zone of Idamalayar lineament.

used here to pick up subtle difference in spectral characters of surface features such as those due to vegetation, soil, moisture, slope etc. The E-W lineaments are found be regionally the most pervasive features within the Palghat Gap. The E-W flowing segment of Bharathapuzha River follows one such lineament. The NNW-SSE Idamalayar lineament is also prominent here, as it has disturbed the river course at Ottappalam (Fig. 5.4a). Continuation of Idamalayar lineament in the gap disturbs original E-W trend, and appears to have been overprinted on it (Fig. 5.4a). These lineament patterns with marked kinks in the NW-SE direction is probably controlled by emplacement of basic dykes connected with Deccan volcanism (Krishnaswamy, 1981; Nair, 1990). The Bharathapuzha River takes a deviation from E-W to WNW-ESE from Desamangalam after taking an abrupt turn along NNE-SSW (Figs. 5.4a & 5.4b). It appears that the WNW-ESE lineament may have controlled the sinuosity exhibited by the river in this segment

5.5.2 Morphometric analysis

An attempt is made here to analyze the drainage system of this area to reveal the effect of active tectonism. The data for drainage basin morphometry presented here has entirely been derived from published maps. The maps used in this analysis are those of Survey of India topographical sheets in 1:50,000 and 1:25,000 scales. Some of the geomorphic indices analyzed here include: a) drainage basin asymmetry, b) mountain front sinuosity, and c) ratio of valley floor width to valley height.

a) Drainage basin asymmetry

The two quantitative indices widely employed to evaluate basin asymmetry are asymmetry factor (AF) and transverse topographic symmetry factor (T). The Asymmetry

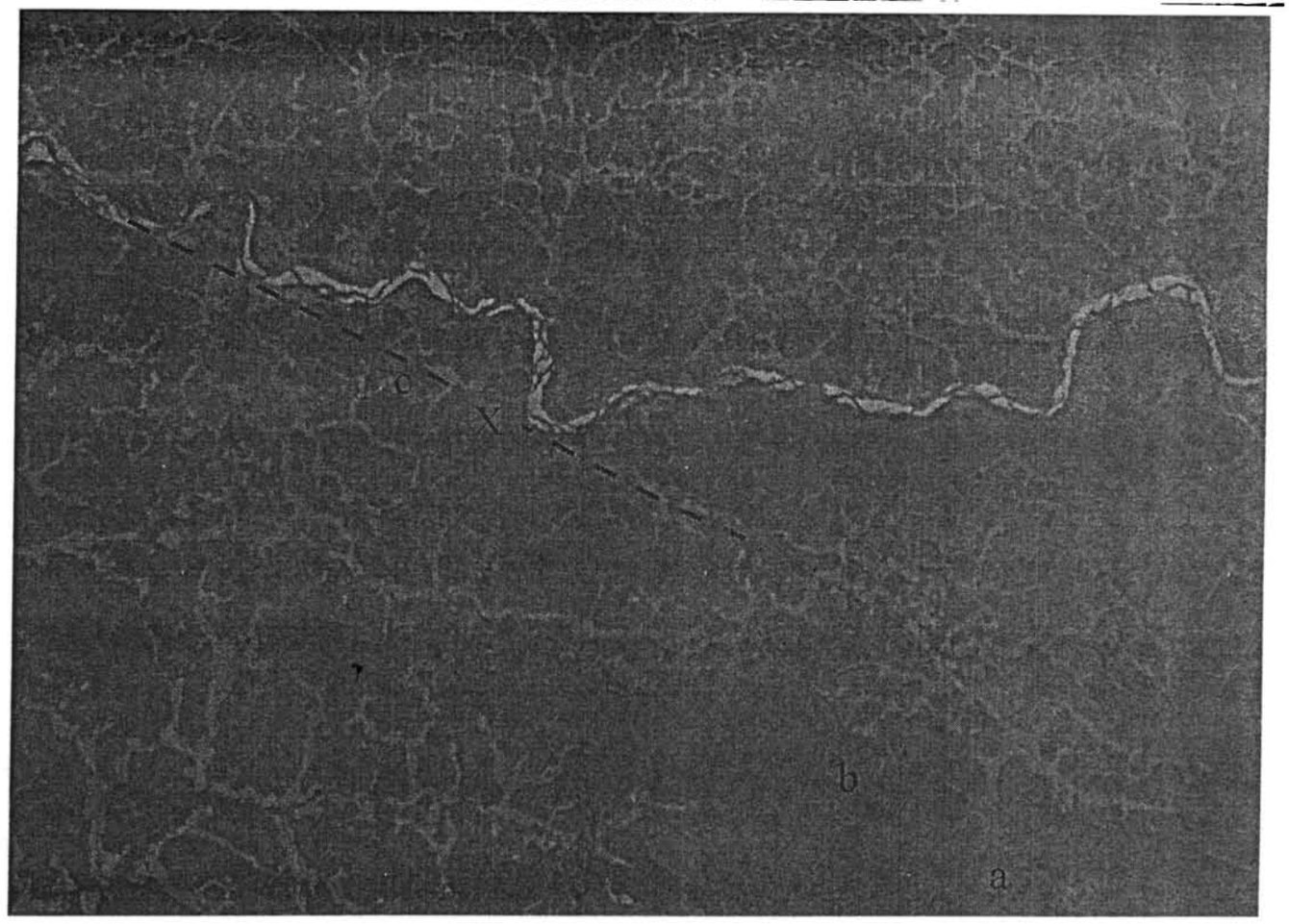

Fig. 5.4b. Satellite image of the epicentral area of the 1994 Wadakkancheri Earthquake (band 4). The prominent WNW-ESE lineament is marked in dashed lines. The hillocks a, b and c are calculated for mountain front sinuosity (Table 5. 3); X is the location of waterfall (rapid) and the quarry, which exposed brittle fault (described in the chapter 6).

Factor (AF) is defined as $AF=100(^{Ar}/_{At})$, where A_r in the area of the basin to the right (facing down stream) of the trunk stream and A_t is defined as the total area of the drainage basin. The AF is calculated for five drainage basins (see Fig. 5.5 and Table 5.2).

The transverse Topographic Symmetry Factor (T) is defined as $T=(D_a/D_d)$, where D_a is the distance from the stream channel to the middle of its drainage basin (measured perpendicular to the median line of the basin), and D_d is the distance from the midline to the basin divide; 'T' is also calculated for five drainage basins (see Fig. 5.5 and Table 5.2).

Table 5.2 Drainage basin asymmetries calculated for five basins around the epicentral area of the 1994 Wadakkancheri earthquake. The drainage basin calculated for the basin asymmetries are marked in the Fig. 5.5.

Drainage basin No in Fig.5.8	Total basin area (km^2)	Asymmetry factor	Transverse Topographic Symmetry factor
1	115.75	0.4558	0.2
2	58.631	0.4587	0.4
3	61.631	0.454	0.3
4	57.58	0.376	0.5
5	27.04	0.5586	0.6

The analysis shows that the drainage basin asymmetry values are somewhat anomalous and slightly off the normal trends. This may be due to the structurally controlled nature of the terrain. For a stream network that formed and continues to flow in a stable setting, AF should be equal to about 50, whereas unstable setting would give a deflection from normal value either <50 or >50. As for the low transverse topographic

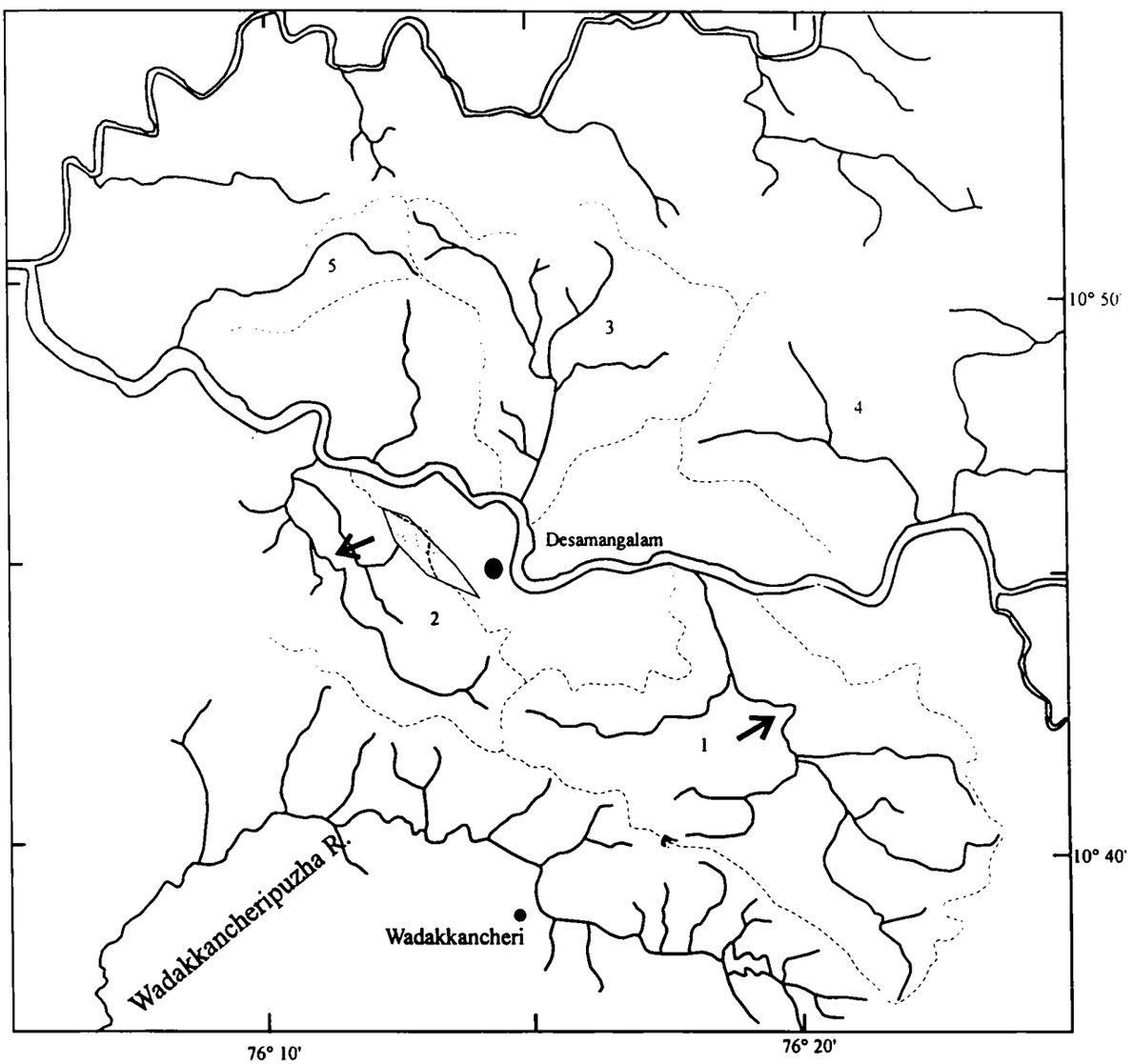

Fig. 5.5. Sketch showing the drainage network of the epicentral area of the 1994 earthquake. The basins are divided and numbered for easy reference in Table 5.2. The linear hillock (shaded patch) is associated with WNW-ESE lineament. Arrows indicate the shift in the main trunk of the drainage and dotted lines show the basin boundaries.

symmetry factor for this region, it is probably because the main channel has shifted toward the centre of the basin from its original course (Fig. 5.5).

b) Mountain front sinuosity

The morphology of fault generated mountain fronts and escarpments may provide clue for relative tectonic activity (Mayer, 1986). The sinuosity of a mountain front is related to the time elapsed since active faulting ceased (Bull and McFgdden, 1977). The mountain front sinuosity is an index that reflects the balance between erosional forces that tend to cut embayment into a mountain front and tectonic forces that tend to produce a straight mountain front coincident with an active range-bounding fault. The mountain front sinuosity is defined as follows: $S_{mf} = L_{mf}/L_s$, where S_{mf} is the mountain front sinuosity; Lmf is the length of the mountain front along the foot of the mountain at the prominent break in the slop; and L_s is the straight-line length of the mountain front.

Table 5.3 Mountain front sinuosity calculated for three elongated hillocks within the vicinity of epicentral area of the 1994 Wadakkancheri earthquake (hills- a, b and c are shown in Fig 5.4b).

Mountain number	Length of mountain front	Straight-line length of mountain front.	Mountain front sinuosity
a	5.24	4.02	1.3034
b	6.01	4.45	1.3505
c	3.25	2.75	1.1818

The mountain fronts associated with active tectonics and uplift are generally linear and with low values of S_{mf}. Three hillocks are identified in the study area for calculation of S_{mf} in the area (Fig. 5.4b). Interestingly, the one hillock, which is located close to the river shift at Desamangalam, shows a low value.

c) Ratio of valley floor width to valley height

The ratio of valley floor width to valley height (V_f) may be expressed as $V_f = 2V_w / (E_{ld}-E_{sc})+ (E_{rd}-E_{sc})$, where V_f is the valley floor width to height ratio; V_{fw} is the width of valley floor; E_{ld} and E_{rd} are elevations of the left and right valley divides, respectively, and E_{sc} is the elevations of the valley floor. This index differentiates between broad-floored valleys that show relatively high values of V_f, and 'V' shaped valleys with relatively low values. High values of V_f are associated with low uplift rates, so that streams cut broad valley floors. Low values of V_f reflect deep valleys with streams that are actively incising, commonly associated with uplift.

The V_f is calculated for the main trunk and few tributaries of the Bharathapuzha River. The V_f along Aliar and Gayatripuzha Rivers are also calculated for comparison of the values obtained for the Desamanglam region. As shown in Table 5.4, a very low value of V_f for the Desamangalam segment of the Bharathapuzha in comparison with E-W segment and other two tributaries probably suggests the influence of tectonism.

Table 5.4 Ratio of valley-floor width to valley height calculated for the major trunk and tributaries of Bharathapuzha River. Locations 5 and 6 are in the E-W segment and 7 and 8 are in the WNW-ESE segment of the Bharathapuzha River.

	Location	Height of left bank	Height of right bank	Valley height	Valley width	Index
1	Bharathapuzha 10° 41'N and 76° 47'E	165	150	130	850	17
2	Bharathapuzha 10° 47'N and 76° 33'E	90	240	60	2000	9.52
3	Gayatripuzha 10° 37'N and 76° 38'E	160	220	80	4000	18.43
4	Gayatripuzha 10° 37'N and 76° 38'E	365	135	80	4600	13.52
5	Bharathapuzha 10° 45'N and 76°20'E	100	160	60	1200	8.571
6	Bharathapuzha 10° 45'N and 76°17'E	125	160	60	4000	24.24
7	Bharathapuzha 10° 46'N and 76° 14'E	100	140	40	1200	7.5
8	Bharathapuzha 10° 47'N and 76° 12'E	100	170	20	1750	7.543

5.6 PALEOCHANNELS AND NEOTECTONISM

Our analyses also indicate shifting of channels in the region from their original courses (Fig. 5.6a). As shown in the Figure 5.6a, the channels A and C are the present courses of the Bharathapuzha and Wadakkancheri Rivers, whereas channels B and D are two paleochannels of the region. Among these channels, it may be noted that the channel

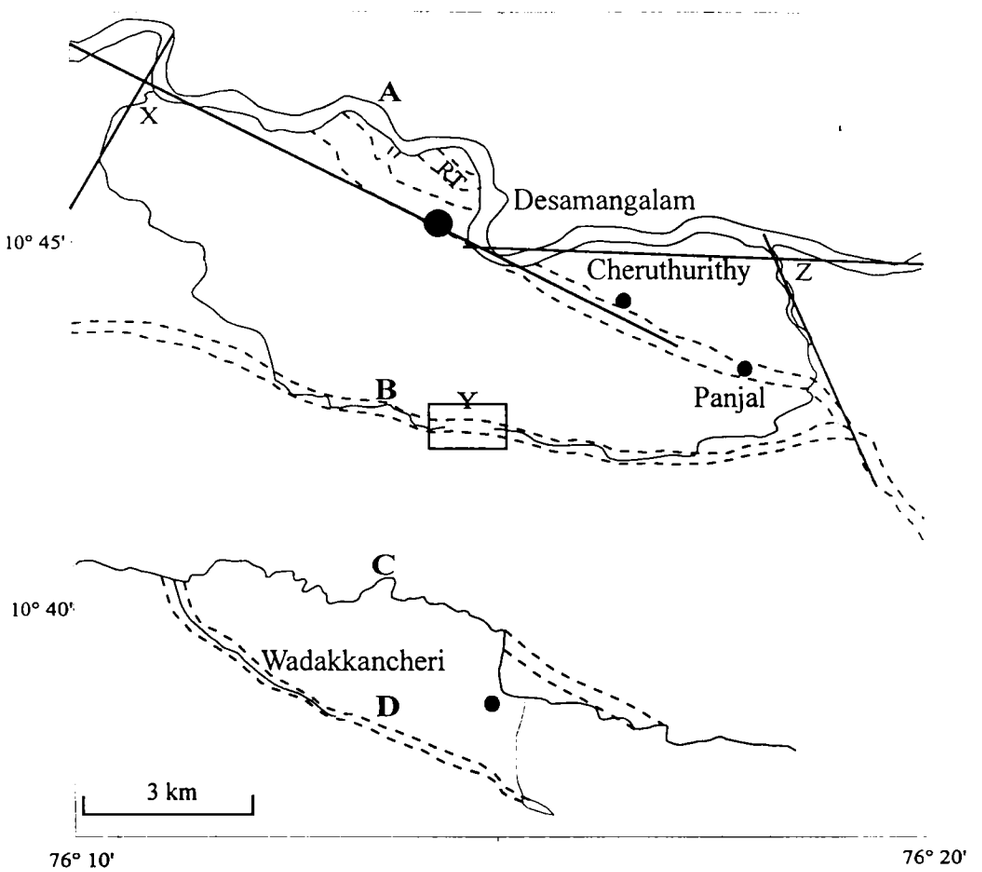

Fig. 5.6a. Locations of suspected neotectonic activity around WNW-ESE fault. RT denotes the river terraces created by the northward shift of the river. Panjal is another location of buried channel. 'XYZ' are the locations along which the profile generated in Fig. 5.9b. Dashed lines are the paleochannels

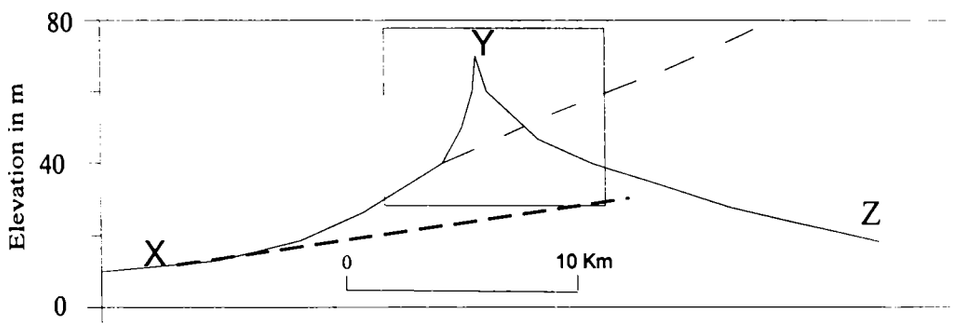

Fig. 5.6b Profile along XYZ of Fig. 5.9a. The doted lines are the projections of the slope.

'A' makes an abrupt northward turn at Desamangalam. Some anomalies are also noted for thechannel B. As shown in Fig. 5.6a, a profile taken along the channel 'B' starting from "X to Z along Y" reveals an anomalous 'dome shaped' divide in the middle of the profile, designated as 'Y' in the Figure 5.6a. As for the channel 'C', it shows a southward shift in its course around the middle portion. Whereas in the channel 'D', the original flow direction appears to have been blocked and tends to deviate towards north leaving a ponding effect in the catchment area (Fig. 5.6a).

Evidence of river shift and river piracy recorded in the form of paleochannels can be possibly attributed to the neotectonic activity along the WNW-ESE lineament, if other nontectonic geologic influences and anthropogenic disturbances can be ruled out for observed anomalies.

5.7 BASEMENT STRUCTURES

As mentioned earlier rocks of this region underwent polyphase deformation. The geological map of the area is shown in the Fig. 5.4, which also show folding in gneissic rocks. Charnockite, the major rock type in this region, shows well-developed foliation, which generally trends in WNW-ESE with a southward dip. A systematic joint set developed at many places along the hillock trending WNW-ESE (Fig. 5.7a). Well-developed mica rich foliation serves as the weaker planes in the development of these joints. Few exposures are marked by 3-5cm thick mica schist patches, which again are parallel to the regional foliation direction. Few quartzo-feldspathic veins are also occurring both parallel and perpendicular to foliation. Numerous dislocations of semi-brittle nature were commonly found in the epicentral region (Fig. 5.7b). Most of them are oriented perpendicular to the foliation (WNW-ESE) and showing strike-slip movement.

Fig. 5.7a. Photograph of a quarry section showing systematic joints developed in the hillock. These joints are parallel to the foliation direction.

Fig. 5.7b. Photograph showing left lateral strike slip fault. Note the pegmatite intrusion along the plane of fault.

Fig. 5.7c. Photograph showing fractures of multiple generations (in horizontal plane); one fracture in the middle of the photograph shows a right lateral displacement.

However, it is difficult to determine the amount of movement if occurred along the foliation planes at many places brittle minor faults are also noticed. One of such fault showed in Fig. 5.7c exhibit a 3 cm right lateral strike-slip movement.

The locations of the above mentioned minor faults (Fig. 5.7b and 5.7c) are confined to the north of the WNW-ESE trending hillock, probably the due to the deformation associated with the shear zone, whereas the systematic joint development (Fig. 5.7a) within the hillock 'c' of Fig. 5.4b is a significant observation here.

CHAPTER 6

FIELD INVESTIGATION AT WADAKKANCHERI

6.1 INTRODUCTION

In this section, we describe our efforts to characterize the fault zone, exposed in a quarry at Desamangalam, the epicentre of the 1994 earthquake. The fault zone consists of a main fault plane and two parallel fractures; the main fault plane is characterized by small-scale displacement, striations/mineral lineations, secondary mineralization, Reidel and tension fractures. Breccia and gouge (consolidated and unconsolidated form) also occur along the fault plane. The detailed evaluation of textural, structural and mineralogical characteristics of the fault zone is given in this chapter. We also describe how the episodic nature of faulting can be inferred from the textural and mineralogical changes within the gouge zone.

6.2 DESCRIPTION OF THE FAULT ZONE

The fault zone in this study is exposed in a quarry at Desamangalam, which spatially coincides with the elongation of the isoseismal of the 1994 M 4.3 earthquake. This also aligns with a 10-km-long WNW-SSE trending hill scarp, a part of the prominent lineament, which is associated with many active tectonic elements (discussed in the earlier chapters) including a rapid (Fig. 6.1a and 6.1b). The fault zone is 6 m wide and coincides with the foliation that strikes WNW-ESE with a dip of 45°S (Fig. 6.2a, 6.2b and 6.3). The zone comprises a main fault 'F2' and two sub parallel fractures 'F1 and F3' (see Fig. 6.3), and can be divisible into three zones viz., 1) a fault core, 2) damage zone, and 3) protolith or host rock.

Fig. 6.1a. Waterfall created by the rock ridge (artificial dam constructed over the ridge can also be seen). Location shown in Fig. 5.4.

Fig. 6.1b. Photograph showing both the natural dam created by rapids. The quarry discussed in the text is in the foreground. Location of the quarry is in Fig. 5.4b.

Fig. 6.2a. Photograph showing the quarry in which the fault is identified. The zone comprises a fault 'F2' and two sub parallel fractures 'F1 and F3', as represented in Fig. 6.3.

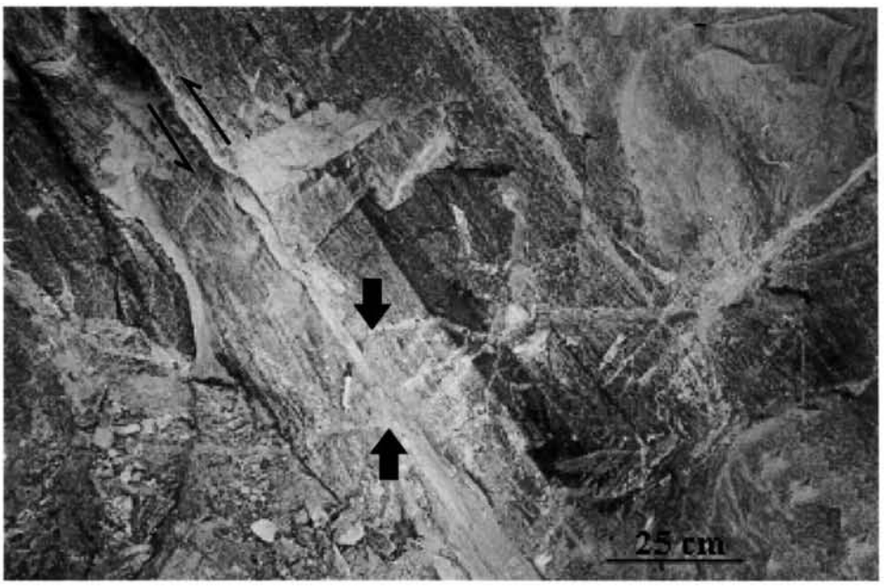

Fig. 6.2b. Photograph showing movement of the fault represented here as the dislocation of the vein (V1 of Fig. 6.3)marked by arrows; coupled arrow represents the movement along the fault.

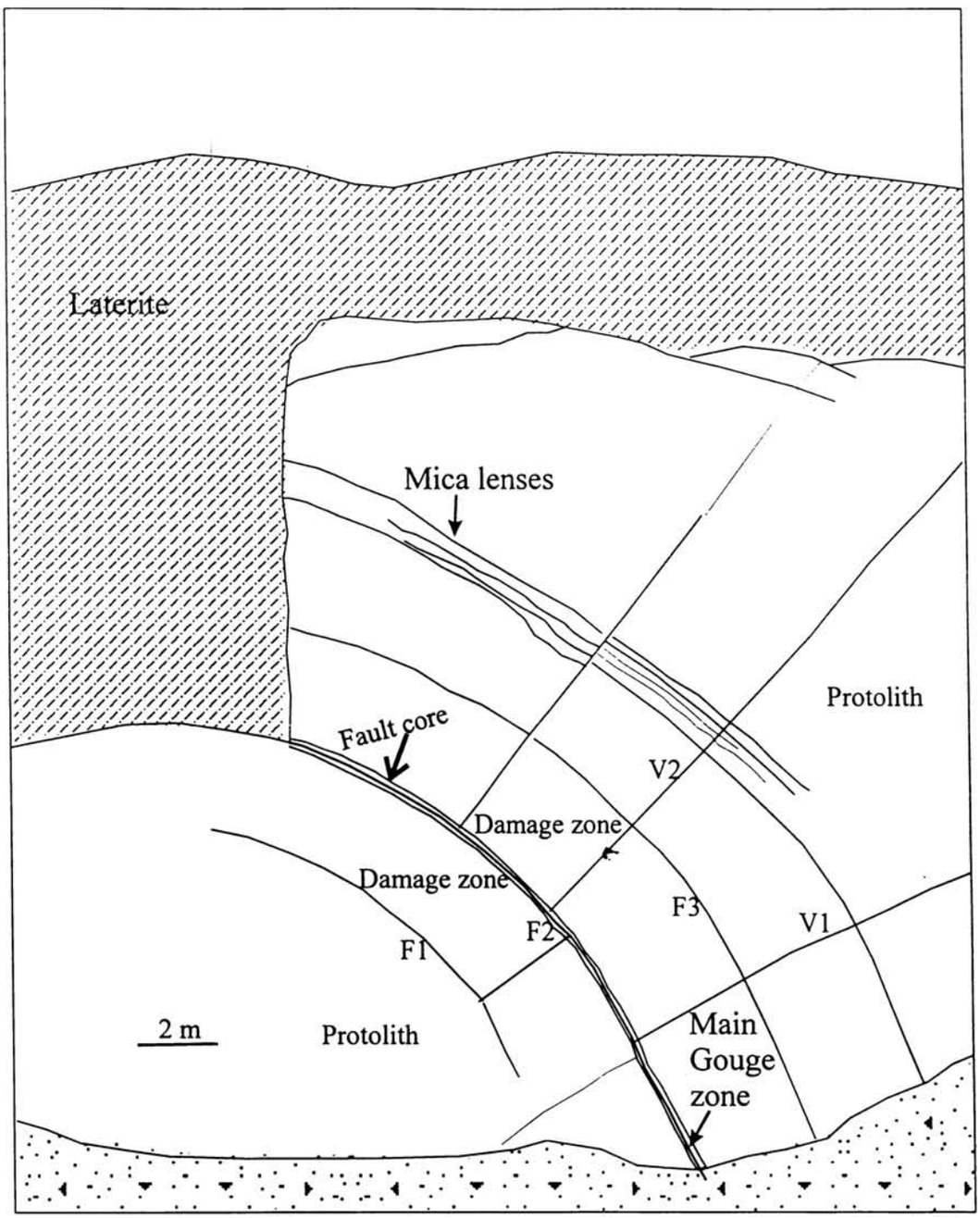

Fig. 6.3. Schematic diagram representing the fault zone in Fig. 6.2a. F1 and F2 are fractures; F2 is the main fault; V1 and V2 are the veins running across the fault showing displacement. The fault zone is demarcated as fault core, damaged zone and protolith, based on the damage characteristics.

6.2.1 Terminology

Some of the commonly used geologic terms that are employed in characterizing the fault zone are given below:

Fault zone- this term is used to refer a tabular structure with evidence of slip such as slickensides, breccia, gouge and recognizable offset (e.g. Dawers and Seeber, 1991).

Cataclasis- rock deformation accomplished by fracture and rotation of mineral grains or aggregates. The process necessarily involves dilatancy, and is therefore pressure sensitive.

Breccia- rock composed of angular to rounded fragments, formed by crushing or grinding along a fault; most fragments are large enough to be visible to the naked eye (Higgins, 1971).

Fault core- fault core is the structural, lithologic, and morphologic portion of a fault zone where most of the displacement is accommodated (Caine, 1996). Commonly, faults can be divided into two distinct zones viz., the fault core and damaged zone (Chester and Logan, 1986).

Damage zone- damage zone is the network of fault related subsidiary structures that bound the fault core. Fault related subsidiary structures in damaged zone include small faults, veins, fractures and cleavages (Bruhn et al., 1994).

Protolith- is the undeformed host rock surrounding fault rock and damaged zone.

Fault rock- Fault rock is a collective term used for the distinctive rock types found in zones of shear dislocation at both high and low crustal levels whose textures are thought to arise at least in part from shearing process (Sibson, 1977).

6.2.2 Host rock (Protolith)

Charnockite forms the predominant host rock in the region, and the constituent minerals include hypersthene, microcline and quartz. Strong foliation is observed at many outcrops and quartzo-feldspathic veins have developed in all directions including those that are parallel to foliation planes. The present fault zone seems to have been initiated along one of such quartzo-feldspathic vein of granitic composition.

6.2.3 Damage zone

As mentioned earlier, the fault is bounded by two fractures, denoted as F1 and F3 (Fig. 6.3). The fracture F1, however, does not show appreciable displacement and passes though a zone of high concentration of mica minerals, showing schistocity. Some fractures with no preferred orientation ('anastomosing') have developed in the mica zones, and a close observation shows that a few of them also bear lineation and striations, indicative of frictional movement. The fracture F3 was recognized at the upper part of the hanging wall, which has developed along an ~4-cm-thick-mica layer. The slickensides along this plane indicate a northward oblique reverse sense of movement.

Damaged zone is characterized by fractures of varying orientations. The minerals close to the gouge zone within the host rock tend to align along with the gouge zone as evident from the rotation of the mineral grains. This alignment becomes weaker within 3 cm away from the gouge zone. Within undisturbed host rock numerous 'anastomosing' fractures have developed. More details of the deformation features from the damage zone are described later in the section on fault rocks.

6.2.4 Fault core

The fault core consists of the zone demarcated as 'F2', as shown in Fig. 6.2b, which bears clear-cut evidence of slip and gouge formation (detailed description of the gouge zone will be made later in the text). The sense of movement along the fracture F2 is assessed on the basis of the offset between two veins V1 and V2, as shown in Fig. 6.3. Although, it was difficult to calculate the actual amount of slip, as it was not possible to measure the orientation of the marker vein V1, an apparent offset of 25 cm could be observed (Fig. 6.2b). Within the principal slip plane, the host rock appears to have been pulverized, and the original bulk fabrics completely disrupted, generating gouge. The faulting has created a 2-7 cm-thick gouge zone, consisting of both consolidated and unconsolidated forms. Some distinct textural and colour changes can be seen within the consolidated part of the gouge.

6.3 FAULT ROCKS

The movement along the fault obviously generated fractures of various directions in the damaged zone. Most of the fractures are in sealed conditions due to secondary mineralization. Detailed macroscopic examination of fracture fills reveals that there are three types of fractures. The first and the most easily identifiable features are chlorite filled fractures (Fig6.4a and 6.4b). Another category of fractures is filled with the white mineral, clinoptilolite. The third types of fractures are not in sealed conditions and they probably facilitate fluid transport in the fault zone (see Fig 6.5b). The percolation of water along these fractures leave the transported gouge material loosely adhered to the wall. A further distinction can be made in hand specimens for the first type of chlorite bearing fractures. One set shows a dark green colour for the intra-fracture material and are mostly sub parallel to the fault (Fig 6.4b). Whereas the second set consists of a light

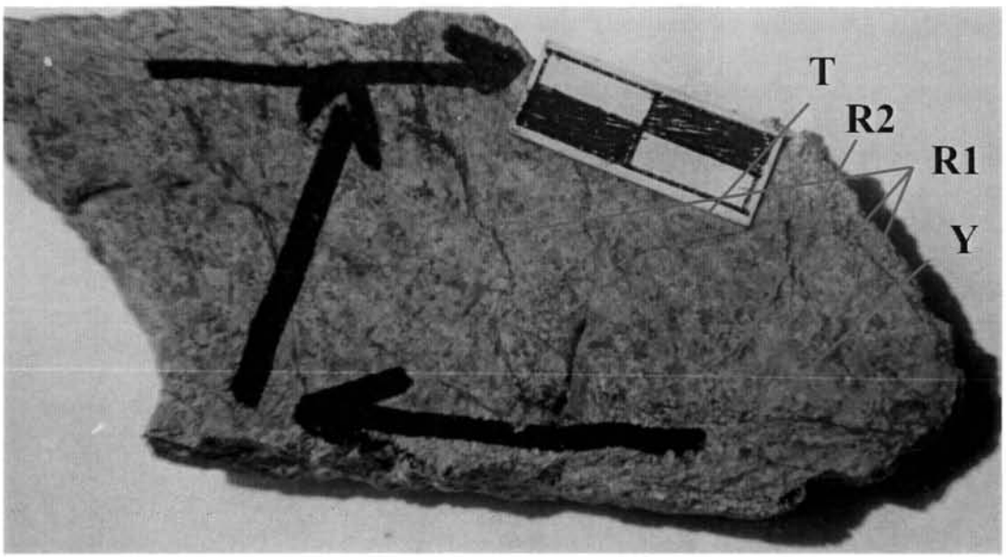

Fig. 6.4a. Photograph showing fractures with the breccia. Most of these fractures (R1, R2 and Y) are filled with light green coloured material. Another fracture 'T' cuts across the formerly mentioned fractures.

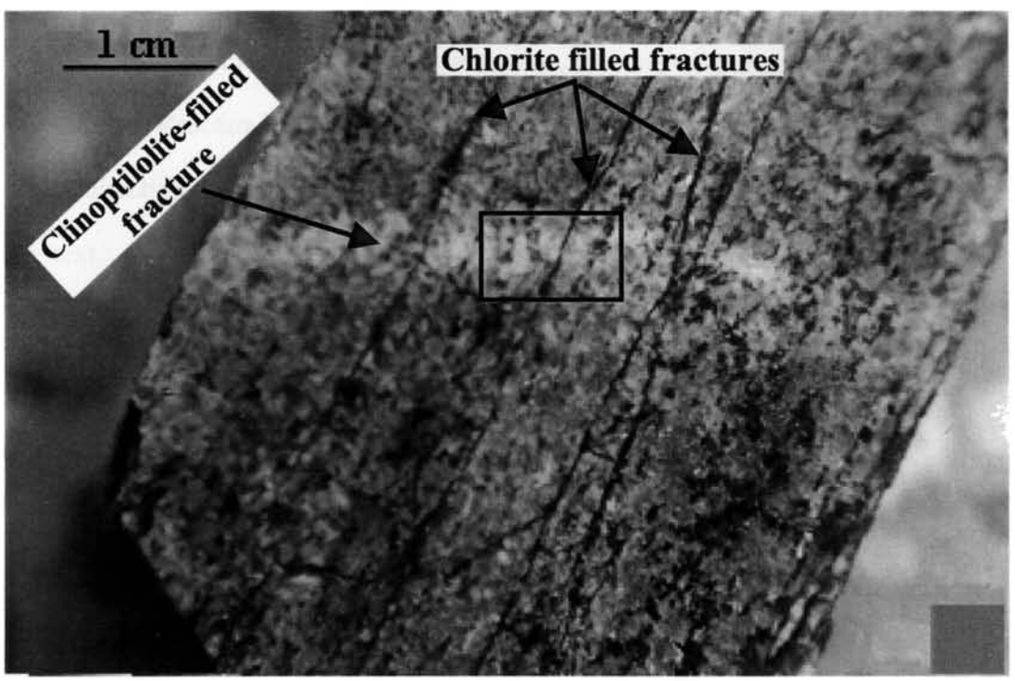

Fig. 6.4b. Photograph showing sub parallel fractures to the fault occurring within the damaged zone. Most of these fractures are filled with dark green coloured material (chlorite). Another set of fractures cutting across them is filled with clinoptilolite.

principal slip plane, the host rock appears to have comminuted and the original bulk fabrics completely disturbed, thus generating the gouge material.

In many environments, gouge is altered to clay obliterating the relation between chemical and mechanical processes, but in others the mineralogy of the source rock is preserved as such (e.g. Wu et al., 1975; Anderson et al., 1980) and offers the hope of distinguishing the physical and chemical changes that gouge undergoes as it is created and recycled each time. Detailed macroscopic examination of the gouge layer in the fault zone under study shows that there are four zones of gouge based on the mineralogical and textural characters. The zone adjacent to host rock shows rotated and crushed grains of quartz, mica and feldspar (denoted as G1 in Fig 6.5a). The second zone is a mixture of crushed and rotated grains of quartz feldspar and mica along with greenish material (chlorite) (denoted as G2 in Fig 6.5b). The greenish material has also developed layering, within the zone (denoted as Gf in Fig 6.5a), and may be due to a later deformation. The third zone (denoted as G3 in Fig. 6.5b) is separated from the second by a sharp but irregular boundary (G2 in Fig 6.5b). Finally, the loose gouge corresponds to the fourth zone. These zones can be attributed to different episodes of deformation, which is discussed later.

Another significant observation is the injected gouge within the damaged zone. The injection is 2 mm thick and can be traced back to the parent gouge zone (Fig. 6.5c). The contact between the injection veins and host cataclastic rocks are generally sharp. It appears that the gouge present in the fault was injected into the cavity and fracture space generated during seismic slip. Such gouge injections associated with faulting have been reported from other areas, as well. For example, Lin (1996) has reported such type of gouge veins in Iida-Matsukawa fault, central Japan. The other geologic examples of

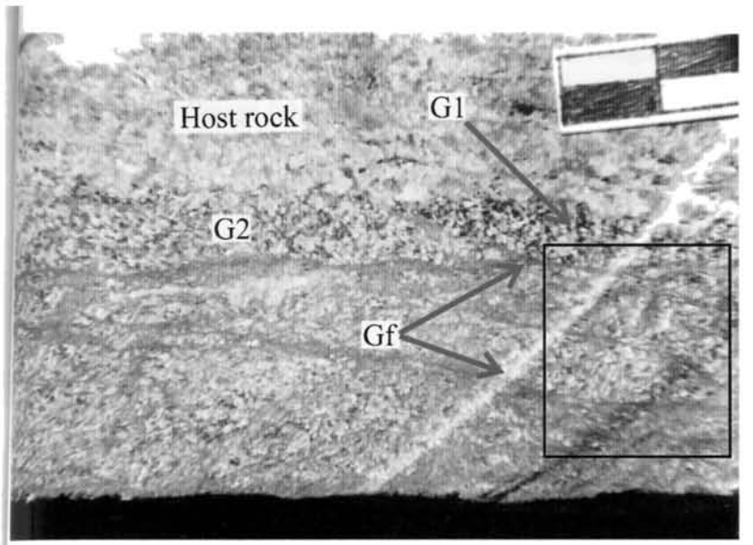

Fig. 6.5a. Photograph showing consolidated part of gouge showing shear bands. Three distinct zones can be identified with in the gouge zone (G1, G2 and Gf). The shear planes similar to R1, R2 and P, as shown in Fig. 5.4c, can be observed in the portion marked in rectangle.

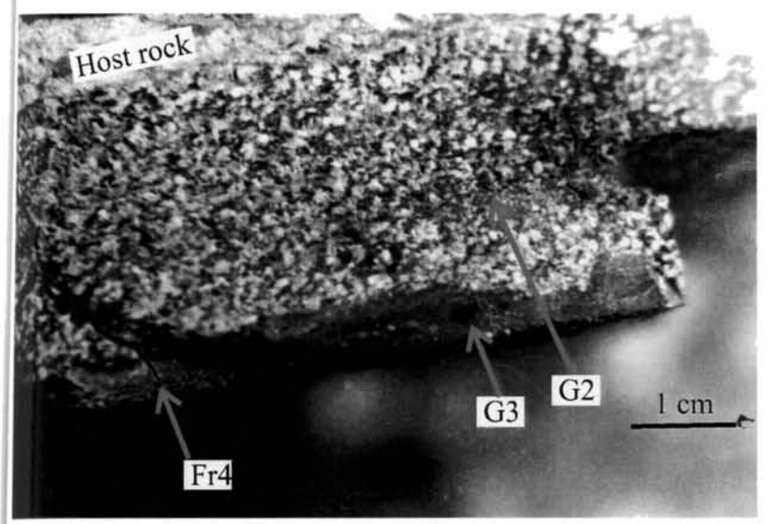

Fig. 6.5b. Photograph showing consolidated part of gouge showing two distinct regions (G2 and G3); the fracture Fr4 cutting both the gouge zones shows no secondary mineralization.

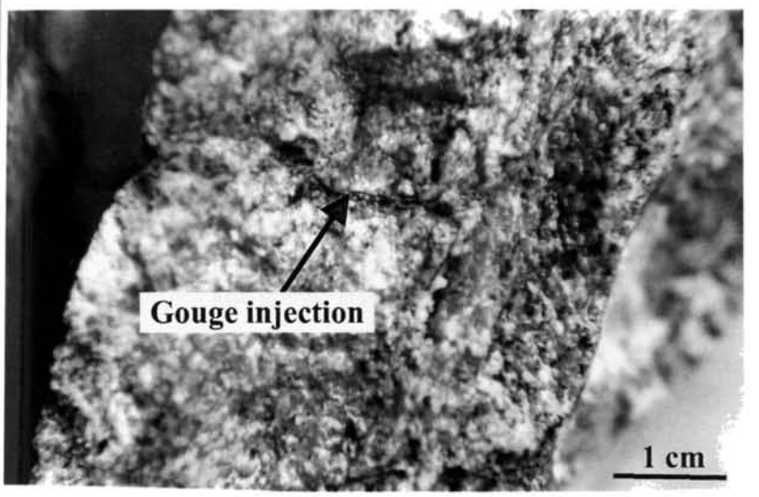

Fig. 6.6c. Photograph showing gouge injection into the damaged zone.

intrusives associated with seismic faulting are pseudotachylyte veins and liquefaction veins formed during large earthquakes, although associated mechanisms are different.

6.3.2 Gouge fabric

The gouge zone can be distinguished from the host rock on the basis of texture and colour. It is typically 6 cm wide, but varies from 2 to 7 cm. The entire gouge zone is indurated except for a thin layer of loose gouge. The unconsolidated part of the gouge seems easily erodable. The mineral constituents of gouge at Desamangalam are given in Table 6.1. The boundary between the gouge and the host rock is not sharp as it is a zone of bulk crushing of quartz feldspar and mica. But a major part of the gouge zone is found as pale green on fresh surface, and most part of it is indurated and very fine grained. The variation in color, indurations and texture define a crude layering that is approximately parallel to the fault surface (Fig 6.5a).

The term foliated gouge used widely for such planar fabrics within the gouge (Chester, et. al, 1987). The compositional layering and preferred alignment of clay grains and porphyroblasts in the gouge define approximately coplanar textural and compositional foliation that is generally oriented subparallel to the shear direction of the fault. Development of such locally strong fabric within the gouge or cataclasite has been observed in experimental studies and also observed in the field exposures (Chester and Logan, 1987; Marone and Scholz, 1989). These studies showed that the shear bands developed in the matrix shears smaller grains more, compared to larger ones. Whereas, Logan and Rauenzahn (1987) explained that steady- state sliding would create shear localization, leading to foliation development. Concentrated shear within the fault core is also produced by the reorientation and destruction of primary structures.

The gouge-layer at the Desamangalam site seems to be a product of multiple slip events. Fault gouge can be extremely fine grained and the energy involved in its creation

can be a significant part of earthquake energy budget. Both grain size and degree of sorting tend to increase with increasing displacement. The thickness of the gouge-breccia zone generally increases with displacement. The rate of thickening depends on the level of effective normal stress. Many previous studies have established the fact that the increment in gouge thickness is related to amount of shear displacement. During each sliding episode, the thickness of the gouge increases when asperities are sheared or crushed, and get incorporated into the gouge, leading to increase in its thickness. According to Engelder (1974), the shear displacement is eight times to the thickness of the gouge (D=8t). Scholz (1990) inferred that the thickness of the gouge is proportional to the displacement and the proportionality constant is 10^{-2}, whereas, Beeler, et al. (1996) observed the thickness of the gouge depends on the sliding velocity.

6.4 MINERALOGY OF FAULT ROCKS

The primary (pre-cataclasis) mineralogy of all samples includes quartz, plagioclase feldspar, alkali feldspar, phlogopite etc. Cataclasis has greatly changed the mineralogy although associated alteration has produced a variety of secondary minerals like chlorite, serusite, montmorillorite and clinoptilolite. The XRD of the different samples are shown in Table 6.1.

6.4.1. Primary minerals

Quartz, feldspar and mica are common both in the host rock and the fault rocks (Table 6.1). The clay minerals are relatively abundant in fault rock, while secondary minerals are absent in host rock (Table 6.1). Quartz appears to be abundant as it is the most resistant mineral to alteration. Within the gouge zone, the bigger quartz grains are more angular along with altered feldspar and some porphyroclasts. Smaller quartz grains

appear to be more rounded. Characteristic signatures of strain shown by quartz in the protolith region are fractures within the grains and undulose extension.

Table 6.1 Mineralogy of the host rock and gouges (Desamangalam) of successive generation based on XRD data

Minerals	Host rock	Consolidated Gouge				Loose gouge
		G1	G2	Foliated	G3	
Quartz	Abundant	Abundant	Abundant	Abundant	Abundant	Common
Microcline	Abundant	Common	Trace	Common	Nil	Nil
Plagioclase	Abundant	Abundant	Trace	Trace	Nil	Nil
Phlogopite	Common	Common	Trace	Trace	Nil	Nil
Chlorite	Nil	Small	Minor	Common	Common	Common
Muscovite	Nil	Nil	Trace	Trace	Trace	Trace
Montmorillonite	Nil	Nil	Nil	Nil	Trace	Common
Clinoptilolite	Nil	Nil	Nil	Nil	Nil	Abundant

The two feldspar, microcline and albite, are found in protolith to fault core, but its quantity decreases toward the fault. The deformation behavior of plagioclase and K-feldspar is rather similar. Laboratory experiments and observation of naturally deformed feldspars have shown that feldspar deformation is strongly depended on metamorphic conditions. Feldspars deforms mainly by brittle fracturing and cataclastic flow, below 300° C (Chester and Logan, 1987; Evans, 1988). The grain fragments show strong intercrystalline deformation including grain scale faults and bend cleavage planes. Patchy undulose extinction and sub grains with vague boundaries are common.

Phlogopite is the mica mineral present in the host rock. Phlogopite is not stable in the calaclasic rocks, and is commonly deformed and partially or fully chloritized. Micas

deform relatively easily by grain boundary sliding, cleavage plane slip, and dislocation glides in the (001) plane (Bell and Wilson, 1981). Micas generally show abundant evidence for accommodation mechanics such as pressure solution and fracturing undulose extinction, kinking and folding (e.g. Mares and Kronenberg, 1993).

6.4.2 Secondary minerals

Chemical reactions in fault-zones are generally fluid induced and are commonly suggested to result in changes in fault rock rheology. Water is a potentially powerful chemical agent and reactions between aqueous fluids and minerals in active fault zones are widely known. Phyllosilicates are common in fault zones especially within the depths of penetration of meteoric water (Kerrich and Kamineni, 1988). Clay minerals are generated in large part by weathering of aluminous silicates, but they may be formed also in the environment of sedimentation or in the post-burial environment. Some are also product of hydrothermal processes. Clay minerals are therefore indicators of reacting environments (Keller, 1970).

Quantification of clay minerals remains the most challenging aspect of quantitative mineral analysis because of their particle size, plate shape and chemical and structural variability. Moreover, aggregates commonly contain more than one clay mineral, but are so fine grained that the individual crystals can rarely be discriminated with petrographic microscope. Thus different clay minerals usually are identified by X-ray diffraction. The XRD analyses reveal that the secondary minerals associated with fault zone at the Desamangalam quarry are chlorite, montmorillonite, muscovite and clinoptilolite. To develop such a suite of clay minerals, the fault deformation should have promoted water-rock interaction along the fault plane.

Based on the mineralogical association the consolidated gouge can be distinguished as three zones. The first zone is the unaltered mixture of quartz, feldspar and mica minerals (G1 in Table 6.1). Chlorite also occurs as the only appreciable secondary mineral in this zone. The second zone is characterized by the enrichment of chlorite and presence of sericite (G2 in Table 6.1). The third zone is marked by montmorillonitic clay (G3 in Table 6.1). Foliated gouge seems to be marked by the same composition, as that of G2, however, it is more enriched in chlorite. The clay content of the loose gouge is characterized by the presence of clinoptilolite (Table 6.1).

Clay minerals could be expected to form rapidly as an alteration of the pulverized rocks due to leaching by percolating fluids (either meteoric or hypogene). With increase in depth, the rate of clay formation increases 3-4 fold with each 10°C increase in temperature (Millot, 1970). The nature of hypogene solutions is a crucial factor in the formation of various clay minerals since the clay mineral developed would depend on the pH and the composition of solutions. The types of clay minerals that can form depend upon: 1) the composition of country rocks, 2) the composition of solutions, and 3) the temperature and pressure. Below the depth of 12 km, under normal geothermal gradient, clay minerals start to become unstable. The fault zones, as well as the repeatedly strained rocks near the fault zone, form a natural conduit for migrating solutions. Fracturing and fluid flow is episodic because hydrothermal processes destroy permeability that is generated either during the faulting or between the faulting episodes.

Muscovite (sericite): We observed fine grained muscovite within the fault zone in Desamangalam. These minerals constitute some of the most important secondary minerals in the fault zones. At lower greenschist facies conditions, usually feldspar breaks down to white mica. The break down reactions of albite and orthoclase to fine grained muscovite may represent by the following equation (Hemley et al., 1980).

$$3KaAlSi_3O_8 + 2H^+ \rightarrow KAl_3Si_3O_{10}(OH)_2 + 6SiO_2 + 2K^+$$

Orthoclase Muscovote

$$3NaAlSi_3O_8 + K^+ + 2H^+ \rightarrow KAl_3Si_3O_{10}(OH)_2 + 6SiO_2 + 3Na^+$$

Albite Muscovote

Optical microscopic observations indicate that the reactions of feldspar to muscovite took place along feldspar grain boundaries, intra-granular fractures and more rarely on a pervasive intra-granular alteration (eg: sericitization). Given the protolith mineralogy and the inferred conditions at which deformation took place, the development of the muscovite most likely proceeded according to the reaction mentioned above.

Chlorite- Chlorite is another common secondary phase and occur both as a replacement of other mafic silicates and as new crystals growing at the interface between porphyroclasts and matrix. The formation of chlorite in fault zone may be represented by the following equation (Wintsch, et al., 1995)

$$2KMg_3AlSi_3O_{10}(OH)_2 + 4H \rightarrow Mg_5Al_2Si_3O_{10}(OH)_8 + 3SiO_2 + Mg^{++} + 2K^+$$

Phlogopite Chlorite

$$KAl\ Si_3O_8 + 5Mg + 8H2O \rightarrow Mg_5Al_2Si_3O_{10}(OH)_8 + 3SiO_2 + 2K^+ + 8H^+$$

Microcline Chlorite

Chlorite in thin section can be identified by its low birefringence and refractive index, which is above those of the mounting medium, and usually shows a faint greenish colour in plain light.

Montmorillonite ($Al_2Si_4O_{10}(OH)_2.xH_2O$)- Montmorillonite generally forms by the alteration of aluminium silicate. The composition of montmorillonite is always deviates from the ideal formula through substitution in the structure, such as Mg for Al and Al for Si. In montmorillonite, the three-layer units are loosely held together in the c-direction with water and cations between them. The amount of water varies so that the c-dimension ranges from 9.6 to 21.4 A° units. Thus this mineral is said to have expanding lattice. The presence of montmorellonite generally weakens a fault zone.

Clinoptilolite $(Na, K, Ca)_{2-3}\ Al_3\ (Al, Si)_2\ Si1_3\ O_{36}\ .12H_20$)- Clinoptilolite is a high silica member heulendite group of zeolite family (Mumpton, 1960) and crystallizes in monoclinic systems (Merkle and Slanghter, 1968). Zeolites are found in geological formations of all ages ranging from newly erupted basalt to those of the 1.3Ga old basalt (Jakobsson, 1978, Karlsson, 1988). It forms fine-grained euhedral crystals usually less than 45μm long (Kastner and Stonecipher, 1978). The occurrence of clinoptilolite was reported in fault zones like Punchbowl fault (Chester and Chester, 1998).

6.5 FRACTURES AND FRACTURE FILLINGS

As mentioned earlier, numerous subparallel fractures were observed in the hanging wall side of the slip plane (Fig 6.4a). These fractures occur up ~30 cm on either side of the gouge zone. Thin section studies reveal the crosscutting relations of fracture development. The two distinct chlorite filled fractures observed in Figs. 6.4a and 6.4b shows a cross-cutting relations in which the fractures having dark green coloured chlorite was cut across a fracture having green coloured material, both the materials appear to be chlorite (Fig 6.6a). Crosscutting relationships between clinoptilolite and chlorite can also observed in hand specimen (Fig. 6.4a and 6.4b) as well as in the thin section (Fig 6.6b).

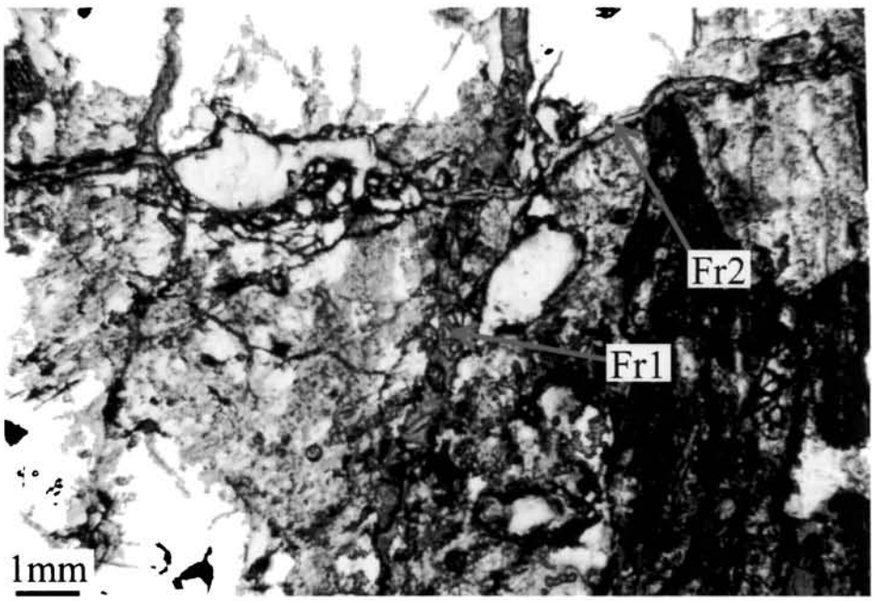

Fig. 6.6a. Photomicrograph showing two generations of fractures (Fr1 and Fr2) in plane polarized light. Both the fractures are filled with chlorite, but in hand specimen the older fracture (Fr1) shows a dark green whereas the younger fracture (Fr2) shows a light green colour.

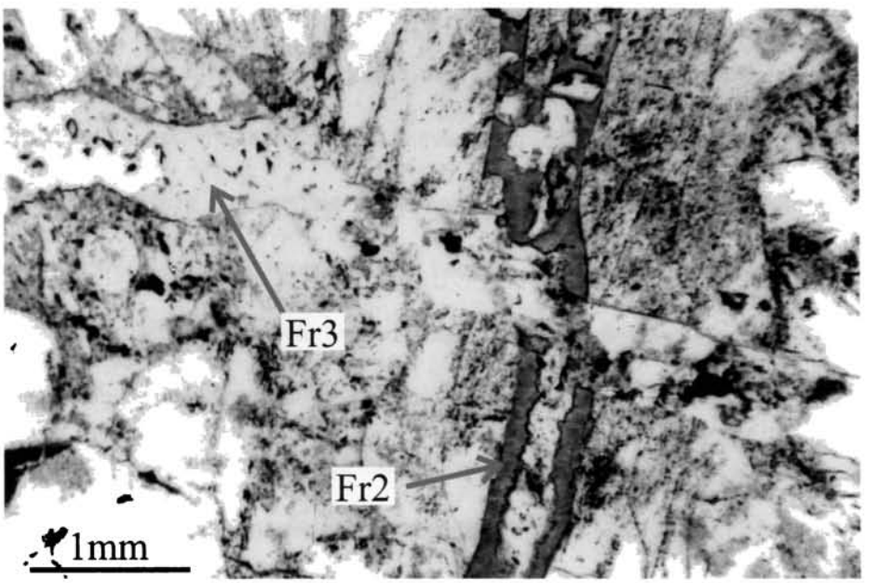

Fig. 6.6b. Photomicrograph showing two generations of fractures (Fr2 and Fr3) in plane polarized light. Fr2 is filled with chlorite and in hand specimen it shows a dark green colour. Fr2 is filled with a white mineral clinoptilolite. This section is made from the sample shown in the Fig. 6.4b and is marked in square. It should be noted that the fracture bearing chlorite further opened up during the development of the next set of fractures facilitating the deposition of clinoptilolite.

Table 6.2 Mineralogy of intra-fracture materials from different generations of fractures deduced form thin section studies and XRD Data.

	Fracture (Fr1)	Fracture (Fr2)	Fracture (Fr3)	Fracture (Fr4)
Minerals	Mainly chlorite	Mainly chlorite	Only clinoptilolite	montmorillonite quartz microcline chlorite clinoptilolite

6.6 SENSE OF MOTION

Slickensides are non-penetrative smoothened or polished surfaces normally developed in planes of movement (eg: Power and Tullis, 1989; Doblas, et al., 1997). The deduction of sense of shear on fault surfaces from slickensides has been a usual procedure in structural geology for many years, particularly within the brittle field. Slickensides and related features have been used to infer the history of surface interaction as they may pertain to the earthquake cycle (eg. Engelder, 1974; Power and Tullis, 1989). In this respect it has become evident that slickensides may undergo numerous modifications via various seismic and interseismic events. Doblas (1998) distinguished 61 kinematic indicators subdivided into eleven groups. Some of the indicators observed in the field might show mixed characteritics. Many fault surfaces display several lineations resulting from different movement in more than one direction. If several movements occur on a single slip plane it introduces a series of complications.

The fractures F1 and F2 bear slickensides at their fracture surfaces, but in F2, slickensides are developed mainly in subsidiary planes. Two directions of movement are revealed from slickensides viz., one, a perfect reverse movement and two, an oblique reverse movement.

6.7. DEFORMATION MECHANISMS

Fault rocks from different depths in the crust will record different deformation mechanisms depending on pressure temperature and fluid composition. They generally exhibit a complex overprinting of structures, which records changes in deformation mechanisms during progressive deformation or deformation during exhumation. However, inferring the process responsible for the textural characteristics visible in hand specimen or a thin section of a fault rock is always difficult.

Cataclasis involves the brittle fragmentation of mineral grains with rotation of grain fragments accompanied by frictional grain boundary sliding and dilatancy. There are three modes of rock fragmentation in a fault zone viz., 1) bulk crushing occurring at locations distant from the fault, 2) Surface grinding of fractures occurring at locations close to the fault, and 3) polishing, replacing, and crushing of fragments in the fault gouge itself (Hattori and Yamamato, 1999).

Factors that determine which deformation mechanism will dominant in a fault zone are temperature, total stress, differential stress, fluid pressure, composition, grain size, texture and strain rate. Even though the frictional heat generation is significant in a fault zone, studies in San Gabrial fault, California (a text book example) shows that the temperature near the fault has never exceeded 380°C while the fault was active (d'Alessio, et. al., 2003). In such an environment, cataclastic type of deformation is expected to dominate, which mainly concentrate rock mass along movement surfaces,

noncohesively. Cataclasis occurred mainly at low temperature within a few kilometers of the surface and results from brittle failure. The material that forms out of this deformation includes breccias and gouge, along with structural features like fractures and faults.

The microstructures documented from the fault zone at Desamangalam show progression in deformation towards the fault core from intragranular fracture, cataclasis, slip along layer silicate, cleavage, phyllosilicate cataclasis, development of foliation and the development of very fine grained fault core material. Toward the fault core, measured fracture density and mineralogic alteration also tend to increase, dramatically.

6.8 EPISODIC NATURE OF FAULTING

The different textural elements in the fault zone and overprinting of structures allow us to develop up a scenario of sequential development of fault-rocks at Desamangalm. Although, the repeated frictional sliding could result in disruption of earlier generation of deformational signatures, based on the above referenced cross cutting relations and distinct difference in deformation characters, a minimum of four episodes of fracturing/faulting and gouge development and secondary mineralization can be recognized (Fig. 6.7). Sequential development of fault rocks is represented in Figure 6.8 a-g.

The first episode of faulting presumed from the fault rocks may be responsible for producing the major part of cataclasts and gouge along the slip plane. This deformation may have produced subsidiary fractures with varied orientations. The XRD data shows that apart from the host rock minerals, traces of chlorite development can also be observed in this particular fossil gouge zone. The infiltrating surface water may

have facilitated the formation of chlorite, thus giving greenish in color to gouge. The occurrence of chlorite within the first generation fractures confirms this observation.

Events	I	II	III	IV
Deformation Mode	Chronology			
Fracuting / Faulting	1	5	9	13
Gouge/Breccia formation	2	6	10	
Gouge induration	3	7	11	
Secondary fracture filling	4	8	12	

Fig. 6.7. Schematic diagram showing the sequential development of fault rocks.

Second episode of faulting might have increased the thickness of the gouge and can be easily distinguished from an enrichment of chlorite content. However, the distinction between the first episode and second episode of faulting is recognized by the enrichment of chlorite in the consolidated part of gouge zone, by the crosscutting relationship shown by two chlorite filled fractures.

Third episode of faulting, fracturing and gouge formation produced the intersecting zones of secondary cataclasists, followed by hydrothermal deposition of clinoptilolite. During this episode, the earlier formed gouge is further pulverized to form a distinctly visible zone (Fig. 6.5b). The well-developed cataclastic foliation within the gouge signifies high shear strain. The fractures in this episode have varying orientations and are marked by the presence of clinoptilolite. Some of the earlier fractures may have opened up during this phase with the onset of secondary mineralization.

The next, presumably the last and final episode of faulting in the development of fault rock fabric involved the formation of new fractures that are devoid of any intrafracture mineralisation, but the fractures seem to be act as path ways of infiltration of water and as a result, the fine grained gouge material are found adhered to the fracture

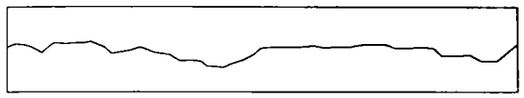

a. Early fracture or fault

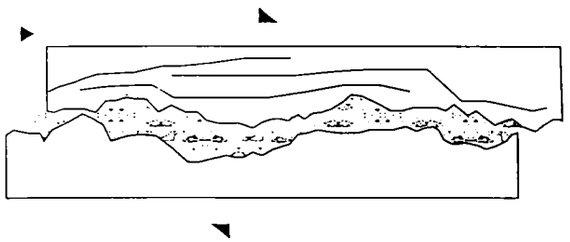

b. First episode of displacement: high strain rate, high velocity slip, cataclasists and dilation

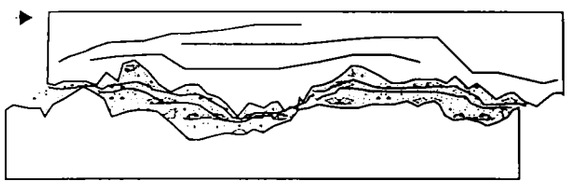

c. Period of stress accumulation

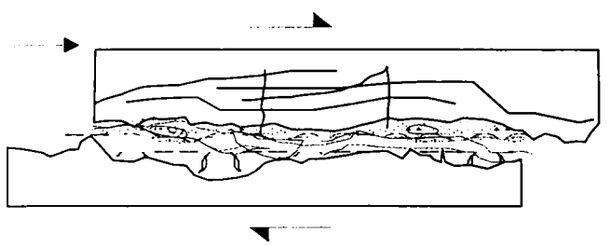

d. Second episode of movement: high strain rate subsidiary fractures and increase in thickness of gouge

Fig. 6.8. Schematic diagrams (a-d) illustrating sequential development of fault rocks. Single arrow represents stress towards north direction; coupled arrow represents movement.

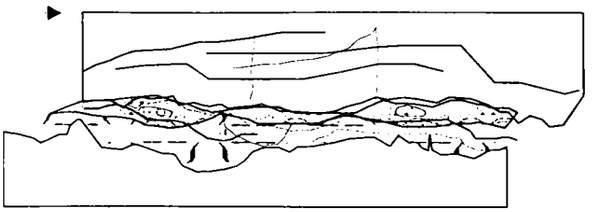

e. Period of stress accumulation secondary mineralization

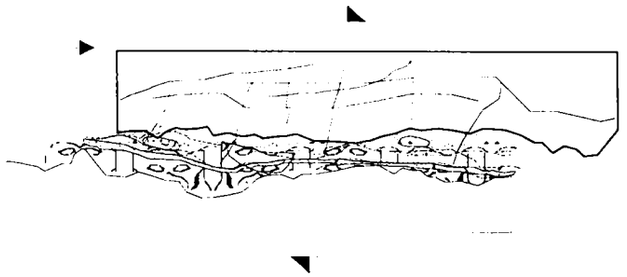

f. Third episode of movement: Foliated gouge formation and associated fractures

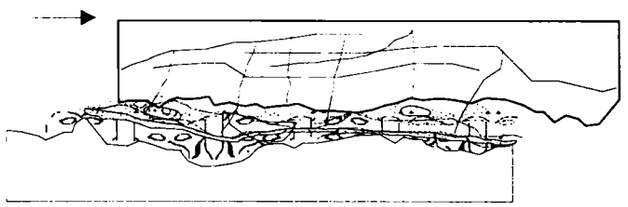

g. Period of stress accumulation secondary mineralization

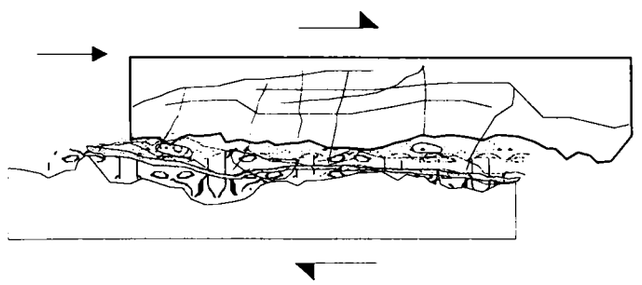

h. Last episode of movement: high strain rate gouge formation and associated fractures

Fig. 6.8. (contd.) Schematic diagrams (e-h) illustrating sequential development of fault rocks.

walls. These fractures show cross-cutting relations with the earlier ones. Generation of the unconsolidated gouge is the significant observation of this episode. Some of these fractures are parallel and others oblique or perpendicular to the fault plane. Finally, the fault will be in the stage of sealing, which will remain so, until the fault completely seals and achieves critical stress conditions for the next failure.

6.9 PRESENCE OF FLUID

In brittle fault zones, the presence of aqueous fluids at the time of deformation has been confirmed by the minerals precipitated as veins and as cements in gouge and breccia and/or by hyderothermal alteration. Fluids are intimately linked to a variety of faulting processes like long term structural and compositional evolution of fault zones, fault creep, and the nucleation propagation, arrest and recurrence of earthquake ruptures (Hickman, et al., 1995 and reference therein). Potential sources of fluids in brittle faults and shear zone include metamorphic fluid generated by hydration of minerals during prograde metamorphism (including shear heating), fluids trapped in pore spaces and meteoric water carried out downward by circulation (Kerrich, et al., 1984). Coseismically dilatant fractures that were charged with fluids and post-seismically filled with secondary materials (Chester et al., 1993). Alteration of gouge, with the composition of participating wall rocks, to that of clay suggests a hydrothermal alteration.

Relatively shallow parts of fault may be influenced by shallow groundwater flow and its geochemical signature whereas deep circulation could produce volume loss and enrichment of immobile elements, and complex geochemical signatures due to higher fluid temperatures (Evans and Chester, 1995). Both fluid assisted mechanisms and the

presence of fluid swelling clays in the ultracataclasite may reduce frictional strength of a fault (Logan and Rauenzahn, 1987, Chester and Higgs, 1992).

6.10 DATING THE SEISMIC EVENTS

With a view to improve the interpretation for earthquake hazard, the loose gouge from the study site was dated using ESR technique. The ESR (electron spin resonance) experiments on the quartz isolated from the unconsolidated gouge revealed significant signals from Al and Ti centers, which normally recorded at 100° K and E′ centers for different grain-size showed consistent decrease in age (Rao, et al., 2002). Preliminary results of ESR dating of this material yielded a mid-Quaternary date of 430±43 ka for the last event, which affected the quartz grains within the unconsolidated gouge (Rao et al., 2002; see appendix for full paper). However one should not forget the fact that the resetting of quartz grains in fault rocks needs a normal stress. Schwarcz and Lee (2000) found that for zeroing to occur, normal stress acting on the fault plane during faulting must be >2MPa. Other methods like K-Ar and Rb-Sr may also have the potential to date the fault rocks (Tanaka et al., 1995; Karlsson, 2001; Gundogon, et.al., 1989).

CHAPTER 7

SYNTHESIS AND CONCLUSIONS

7.1 INTRODUCTION

The purpose of the present study is to understand the surface deformation associated with the Killari and Wadakkancheri earthquakes and to examine if there are any evidence of occurrence of paleo-earthquakes in this region or its vicinity. The present study identified features indicative of previous seismic activities at both these sites. The Killari site in Maharashtra exposed ample evidence of earlier generated earthquake related deformation that could be compared with the recent coseismic structures. The evidence obtained from this site mostly consists of tilted thrust sheets of Deccan trap layers. The other site in Kerala near Wadakkancheri features brittle displacement encompassing generations of fault rocks that is exposed in an exhumed crystalline outcrop. The last major movement at this site is dated at 430 ± 30 BP.

The results indicate that the Killari and Wadakkancheri sites show typical characteristics of mid-cratonic (unrifted SCR crust) tectonic processes. The low strain rate is evident from the subdued topography, long interval between the earthquakes and little background seismicity. These sites can be called as passive seismic sources as they are located far from the influence of plate boundaries, and as such, the seismic cycle may be poorly defined. The study further highlights the feasibility of geological studies to help to recognize such discrete potential seismic sources. The study concludes that the earthquakes in the shield area are mostly associated with discrete faults that are developed in association with the preexisting shear zones or structurally weak zones.

7.2 Results from Killari

The observations gathered in the epicentral area of Killari earthquake suggest that the 1993 event is not the first to occur here, and it may be part of an episodic activity, with long intervals separating each event. Initial observations by various workers from

shallow trenches in the 1993 rupture zone have been equivocal in regard to the existence of an older fault in the region. Their assumption was based on the apparent lack of signatures of past deformation such as slickensides, concentrated weathering, and mineralization. It was further suggested that a new fault might have propagated into an area of more intensely weathered and fractured basalt, following the path of least resistance. The apparent absence of pre-1993 Cenozoic warping and related tilting was thus considered indicative of relative tectonic stability.

The data presented in this thesis, however, shows the presence of a WNW-ESE trending regional structure around the epicentral area of Killari. This structure was initially identified through remote sensing data. The fault plane solution of the main shock and the spatial coincidence of aftershocks show that the present activity may be associated with this structure. Historic seismicity of the region, though sparse, further indicates potential preexisting structures in this area. Further, an exhumed fossil deformation zone, east of the epicentre of the 1993 earthquake may be indicative of the preexisting structures in the region.

Deeper trench excavations indicate repeated thrusting prior to the recent movement. The pattern of near-surface deformation associated with the earthquake indicates that the basalt layers on the southwest side of the rupture zone moved in a northeast direction over the footwall, conformable with the regional stress field. The older structures showed a similar sense of movement but displayed a higher degree of crushing and weathering. Many outcrops that were also located within and outside the currently active zone bear signatures of multiple deformations. These observations are strongly supportive of the reactivation hypothesis. Based on the development of soil profile, it can be roughly estimated that the causative structure of Killari earthquake might have been producing events at very longer intervals (>20 ka). Lack of better age

constraints at Killari is a major impediment in developing earthquake chronology.

Our experience shows that the presence of "offset" or lack of it should not be the only criterion on which the "deformation rates" in the SCR locates are based. It has been demonstrated that even in the active regions characterized by repeated thrusting, there may not be much of a displacement on the surface. The lack of geomorphic features in the stable continental regions should in fact be no surprise, considering that these earthquakes produce very little surface deformation to begin with and that the interseismic periods are too long compared to the active erosional processes.

In shield regions under compression where fault slip is obscured by thick overburden, coseismic folding may accommodate much of the shortening. Because the layered structure of the basalt flows at Killari, near-surface deformation must have assumed the invariable form of bedding plane thrusts. Thus, in the given situation, recognition of older thrusts may be the best bet to understand the recurrence pattern of active faulting in Killari.

The subdued nature of geomorphic features and displacements from prior earthquakes may arise not only from reasons discussed above but also due to the deformation characteristics of midplate regions in general. Most midcrust deformation occurs on reverse faults and their true displacements may be difficult to assess because of the structural complexities of the upper crust. Deeper mid-continental faults may terminate near the surface forming splays or terminate into folds, and displacement along the main fault may be almost undetectable at the surface. Thus, the displacement records in the compressive regimes may be incomplete and may not be the true reflection of processes at depth.

For the geometry of fault movement at Killari, the footwall block should occur at a higher elevation, but in reality in gives a perception of being at a lower elevation. The

question is how to reconcile this inverted topography with the actual tectonic movement. Presumably, repeated thrusting should have left the hanging wall block on the southwest side a higher elevation, but the present morphology must have evolved by active weathering and erosional processes. In other words, the inverted topography at Killari interpreted to be the result of relatively slower rates of deformation, as compared to deformation.

The digital satellite image of the area defines two contrasting blocks separated by the northwest flowing Tirna River. The 1993 earthquake occurred close to this contact of these blocks, which may be corresponding to the surface trace of the fault. The focal mechanism of the main event indicates the involvement of a northwest oriented fault in the faulting process. This is compatible with the regional stress field in Indian shield with Sh_{max} oriented in the northeast direction. That there is also a regional structure, striking northwest and measuring about 400 km long, is evident from the distribution of historical earthquakes. Geophysical studies further indicate a prominent northwest trending gravity low in the region (Kailasam, 1975). Our data on relocated aftershocks of A and B quality at hand suggest that a large number of earthquakes occurred at hypocentral depths between 5 km and 7 km that show a spatial trend in the NW direction. Studies at Killari suggest how a variety of data can lead to a better appreciation of regional seismogenic structures even in areas where field exposures are not quite imposing.

7.3 Results from Wadakkancheri

The epicentral area of 1994 Wadakkancheri (Desamangalam) earthquake (M 4.3) is within the Palghat–Cauvery shear zone. The evidence of brittle faulting was obtained from a quarry section exposed at Desamangalam. The field data show the faulting at this site took place under brittle conditions ie., shallow crustal levels. This brittle fault zone

developed by the progressive incorporation and amalgamation of newly formed and preexisting subsidiary shears and extension fractures of varying size and orientation. The fault rocks from this exhumed fault represents cumulative deformation produced during different episodes of fault activity. Continued slip on the newly formed principal slip surface is associated with various wear processes that produces layers of breccia, calaclasite and gouge bounded by tabular zones of damaged rocks. Subsequent slip could modify the internal structure of a fault zone in a number of ways.

The texture in the fault record several episodes of deformation followed by cementation. The difference in composition between the main gouge zone and the host rock coincides with an abrupt change in rock texture and mineralogy at the gouge host contact. This suggests that the mineral alteration may have occurred in the presence of fluid. The occurrence of fault gouge in the subsidiary fractures as veins suggest that these are related to dynamic rupture propagation and slip during incremental coseismic displacement. Occurrence of repeated earthquakes on an existing principal slip surface implies that the surface re-strengthened during interseismic periods. The problem of how faults regain strength between earthquakes is crucial for our understanding of the seismic cycle. During earthquake the accumulated stress is released and the fault strength drops. Between earthquakes, fault stress and strength recovers through slip- and time-dependent healing. At this site, the last faulting may have occurred at 430±30 ka, a constraint obtained from the fault gouge using ESR techniques.

The neotectonic activity in this area could be discerned also from the geomorphic anomalies. The drainage system of the area is also structurally controlled viz., E-W, NNE-SSW and WNW-ESE. The geomorphic analyses indicate that the WNW-ESE trending lineament is associated with greater anomalies. This lineament defined by a linearity of hills was marked by paleochannels associated with river shift, sub basin

symmetries, low valley floor valley height ratio, straight hillock with low mountain front sinuosity and a cascade. Spatially these anomalies coincide with the fault zone identified on the basis of outcrop studies. Thus the present study underlines the fact that the combined use of outcrop studies together with geomorphic analyses can be a successful exploration tool in locating active faults within the exhumed zones of Precambrian shear zones.

REFERENCES

Adams, J. Percival, J.A., Wetmiller, R.J., Drysdale, J.A., Robertson, P.B., 1992. Geological controls on the 1989 Ungava surface rupture: a preliminary interpretation, *Geological Sur. Canada,* 92-1c, P. 147-155.

Anderson, J.L., Osborne, R.H. and Palmer, D.F., 1980. Petrogenesis of cataclastic rocks within the San Andreas system, California, *Tectonophysics*, Vol. 295, P. 199-221.

Basu, K.L., 1964. A note on Coimbatore Earthquake of 8 February 1900. *Indian J. Meteorol. Geophys.,* Vol.15, P. 281-286.

Baumbach, M., Grosser, H., Schmidt, H.G., Paulat, A., Rietbrock, A, Rao, C.V., Raju, P., Sarkar, D., and Mohan, I., 1994. Study of the foreshocks and aftershocks of the intraplate Latur earthquake of September 30, 1993, India, *In: Mem. Geol. Soc. India*, No. 35, P. 33-63.

Beeler, N.M., Tullis, T.E., Blanpied, M.L and Weeks, J.D., 1996. Frictional behavior of large displacement experimental faults. *J. Geophys. Res.* Vol. 101, P. 8697-8715.

Bell, I.A. and Wilson, C.J.L., 1981. Deformation of biotite and muscovite: TEM microstructure and deformation model, *Tectonophysics*, Vol. 78, P. 201-228.

Bhattacharya, S.N. and Dattatrayam, R.S., 2002. Earthquake sequence in Kerala during December 2000 and January 2001, *Current Science*, Vol. 82, P. 1275-1278.

Bilgrami, S.Z., 1999. A geological map of the eastern part of the Deccan traps (Bidar-Nagpur). *Mem. Geol. Sur. India*, No. 43, P. 219-232.

Bruhn, R.L., Parry, W.T., Yonkee, W.A. and Thomson, T., 1994. Fracturing and hydrothermal alteration in normal fault zones, *Pure Appl. Geophys.*, Vol. 142, P. 609-644.

Bull, W.B., and McFadden, L.D., 1977. Tectonic geomorphology north and south of the Garlock fault, California, *In: D.O. Doehring (ed.), Geomorphology in Arid Regions,* Proceedings of the Eighth Annual Geomorphology Symposium, State University of Yew York at Binghamton, Bringhamton, NY.

Caine, J.S., Evans, J.P., and Forstes, C.B., 1996. Fault zone architecture and permeability structure, *Geology*, Vol. 24, P. 1025-1028.

CESS, 1996. Report on the investigations of the tremor in Trichur area on 6 October, 1996. 10p.

Chandra, U., 1977. Earthquakes of peninsular India- a seismotectonic study, *Bull. Seismol. Soc. Am.,* Vol. 67, P. 1387-1413.

Chester, F.M. and Chester, J.S., 1998. Ultracataclastic structure and friction processes of the Punchbowl fault, San Andreas System, California, *Tectonophysics*, Vol. 295, P. 199-221.

Chester, F.M. and Higgs, N.G., 1992. Multimechanism friction constructive model for ultrafine quartz gouge at hypocentral conditions, *J. Geophys. Res.*, Vol. 97, P. 1859-1870.

Chester, F.M., Evans, J.P., Biegel, R.L., 1993. Internal structure and weakening mechanisms of the San Andreas Fault, *J. Geophys. Res.*, Vol. 98, P. 771-786.

Chester, P.M. and Logan, J.M., 1986. Implications for Mechanical properties of Brittle faults from observations of the Punchbowl fault zone, California, *Pure Appl. Geophys.,*. Vol. 124, P. 79-106.

Chester, P.M. and Logan, J.M., 1987. Composite planar fabric of gouge from the Punchbowl Fault, California, *J. Struct. Geol.*, Vol. 9, P. 621-634.

Chetty, T.R.K. and Rao, M.N., 1994. Latur earthquake of September 30, 1993: Surface deformation and lineament pattern, *Mem. Geol. Soc. India*, No.35, P. 65-73.

Crone, A.J., Machette, M.N. and Bowman, J.R. 1997. Episodic nature of earthquake activity instable continental region revealed by paleoseismicity studies of Australian and North American Quaternary faults, *Aust. Jour. Earth. Sciences*, Vol. 44, P. 203-214.

d'Alessio, M.A., Blythe, A.E. and Burgmann, R., 2003. No frictional heat along the San Gabriel fault, California: Evidence from fission-track thermochronology, *Geology*, Vol. 31, P. 514-544.

Dawers, N.H. and Seeber, L., 1991. Intraplate fault revealed in crystalline bedrock in the 1983 Goodnow and 1985 Ardsley epicentral area. New York, *Tectonophysics*, Vol. 186, P. 115-131.

Doblas, M., 1998. Slickenside kinematics indicators, *Tectonophysics*, Vol. 295, P 187-197.

Doblas, M., Faulkner, D., Maheecha, V., Aparicio, A., Lopez-Ruiz, J., Hoyos, M., 1997. Morphologically ductile criteria for the sense of movement on slickensides from an extensional detachment fault in southern Spain, *J. Struct. Geol.*, Vol. 19, P.1045-4054.

Drury, S.A, Harris, N.B.W., Holt, R.W., Reeves-Smith, G.J, and Wightman, R.T., 1984. Precambrian tectonics and crustal evolution of south India, *J. Geology*, Vol. 92, P. 3-20.

Drury, S.A. and Holt, R.W., 1980. The tectonic framework of the South Indian craton: a reconnaissance involving LANDSAT imagery, *Tectonophysics,* Vol.65, T1-T15.

Engelder, J.T., 1974. Microscopic wear grooves on slickensides: Indicators of paleoseismicity, *J. Geophys. Res.*, Vol. 76, P. 4387-4392.

Evans, J.P. and Chester, F.M., 1995. Fluid-rock interaction in faults of the San Andreas system: Inferences from San Gabriel fault rock geometry and microstructures, *J. Geophys. Res.*, Vol. 100, P. 13,007- 13,020.

Evans, J.P., 1988. Deformation mechanisms in granite rocks at shallow crustal levels, *J. Struct. Geol.*, Vol. 10, P. 437-443.

Gahalat, V.K., Kalpana, Raju, P.S., 2003. Rupture mechanism of the 1993 Killari earthquake, India: constraints from aftershocks and static stress change, Tectonophysics, Vol. 369, P. 71-78.

Goud, T.N., Srirama Rao, S.V. and Gour, V.K., 1992. Tectonic stress field in the Indian subcontinent. J. Geophys. Res. Vol. 97 P. 11,879-11,888.

Grady, J.L., 1971. Deep Main Faults in South India, *J. Geol. Soc. of India,* Vol.12, P. 56-62.

GSI, 1992. Quadrangle Geological map 58B.

Gundogdu, M.N., Bonnot-Courtois, C. and Clauer, R., 1989. Isotope and chemical signatures of sedimentary smectite and diagenic clinoptilolite of lacustrine Neogene basin near Bigadie, western Turkey, *Appl. Geochem.*, Vol. 4, P. 635-644.

Gunnel, Y. and Fleitont, L., 1998. Shoulder uplift of the Western Ghats Passive Margin, India: A Denudational Model. *Earth Surf. Processes and Ldfms.*, Vol. 23, P. 391-404.

Gupta, H. K. and Diwivedy, K. K., 1996. Drilling at Latur earthquake region exposes a peninsular gneiss basement, *Jour. Geol. Soc. India,* Vol. 47, P. 129-131.

Gupta, H.K., 1994. Latur earthquakes, *Geol.Soc. India.Mem.*, No.35, 149 p.

Gupta, H.K., Rao, R.U.M., Srinivasan, R., Rao, G.V., Dwivedy, K.K., Banerjee, D.C., Mohanty, R and Satyasaradhi, Y.R., 1999. Anatomy of surface rupture zones of two stable continental region earthquakes, 1967 Koyna and 1993 Latur India, *Geophys. Res. Lett.*, Vol. 26, P. 1985-1988.

Gupta, H.K., Rastogi, B.K., Indra Mohan, Rao, C.V.R.K., Sarma, S.V.S., Rao, R.U.M. 1998. An investigation of the Latur earthquake of September 29, 1993 in southern India, *Tectonophysics*, Vol. 287, P. 299-318.

Gupta, H.K., Rastogi, B.K., Mohan, I., Rao, C.V.R., Mishra, D.C., Rao, G.V., Rao, R.V.M., Rao, M.N., Chetty, T.R.K., Sarkar, D., Subramanyam, K., Singh, V.S., Sarma, S.V.S. and Raju, P.S., 1995. Investigation of Latur earthquake of September 30, 1993, *GSI Spl. Publ.*, No. 27, P. 17-40.

Gupta, H.K., Srinivasan, R., Rao, R.U.M., Rao, G.V., Reddy, G.K., Roy, S., Jafri, S.H., Dayal, A.M., Zacharia, J., Parthasarathy, G., Poornachandra Rao, G.V.S., Gowd, T.N., Srirama Rao, S.V., Dwivedy, K. K., Banerjee, D.C., Mohanty, R., Sathyasaradi, Y.R., Katti, V.J., Prasad, A.R., Ramanujam, C.G.K., Reddy, P.R. and Shukla, M., 2003. Borehole investigations in the surface rupture zone of the 1993 Latur SCR earthquake, Maharashtra, India: Overview of results, *Mem. Geol. Soc. India*, No. 54, P. 1-22.

Harris, N.B.W., Santosh, M. and Tayler, P. N., 1994. Crustal evolution in south India: constraints from Nd isotopes, *J. Geol.*, Vol. 102, P. 139-150.

Hattori, I. and Yamamoto, H., 1999. Rock fragmentation and particle size in crushed zones by faulting, *J. Geology*, Vol. 107, P. 209-222.

Hemley, J.J., Montaya, J.W., Marinenko, J.W. and Luce, R.W., 1980. Equilibria in the system Al_2O_3-SiO_2-H_2O and some General implications for Alterization/Mineralization processes, *Economic Geology*, Vol. 75, P. 210-228.

Hickman, S., Sibson, R.H. and Bruhn, R., 1995. Introduction to special section: Mechanical involvement of fluids in faulting. *J. Geophys. Res.*, Vol. 100. P. 12,831- 12,840.

Higgins, M.W., 1971. Cataclastic rocks, *U.S. Geol. Surv. Profess. Pap.*, No.687, 97 p.

IMD, 1995. Report on microearthquake survey in Trichur District, Kerala, 18 p.

Jakobsson, S.J., 1978. Environmental factors controlling the palagonitization of the Surtsey Tetra Iceland, *Bull. Geol. Soc. Denmark*, Vol. 27, P. 91-105.

Johnston, A.C. and Kanter, L.R., 1990. Earthquakes in stable continental crust, *Scientific American,* 262, P. 68-75.

Johnston, A.C.,1989. The seismicity of stable continental interiors. *In: S.Gregersen and P.W.Basham (eds) Earthquakes at North Atlantic passive margins: neotectonics and post glacial rebound Kluwer, Dordrecht.* P 582-599.

Jones, V.T. and Drozel, R.J., 1993. Prediction of oil or gas potential by near surface geochemistry, *Am. Asso. Petrol. Geology*, Vol. 67, P. 932-952.

Kailasam, L. N., 1993. Geophysical and Geodynamical aspects of the Maharastra earthquake of September 30,1993, *Current Science*, Vol. 65, No.10, P. 736-738.

Karlsson, H.R., 1988. Oxygen and hydrogen isotope geochemistry of zeolites; Ph.D Dissertation, University. Chicago, Chicago, Illinois, 288 p.

Karlsson, H.R., 2001. Isotope geochemistry of zeolites. *In: Natural zeolites: occurance, properties, application. Rev. in Minerlogic and Geochemistry*, Vol. 45, P 163-205.

Kastner, M. and Stonecipher, S.A., 1978. Zeolites in pelagic sediments of the Atlantic, Pacific and Indian Oceans, *In. Natural Zeolites: Occurance properties, use* C.B. Sand FA Mumpton (eds) Pergomon Press Elmsford, New York, P. 199-220.

Keller, E.A, and Pinter, N., 1996. *Active Tectonics Earthquakes, Uplift and Landscape*, Prentice Hall- Inc.337p.

Keller, E.A., 1986. Investigation of active tectonics: use of surficial earth processes, In *Active tectonics*. National Academy Press, P.136-147.

Keller, W.D., 1970. Environmental aspects of clay minerals, *J. Sed. Petrology*, Vol. 40, P. 788-854.

Kerrich, R. and Kamineni, D.C., 1988. Characteristics and chronology of fracture – fluid infiltration in Archean Eye Dashwa Lakes pluto, Superior Province: Evidence from H,C,O- Isotopes and fluid inclusions, *Contrib. Mineral. Petrol.*, Vol. 99, P. 430-435.

Kerrich, R., La Toue, T.E. and Willmore, L., 1984. Fluid participation in deep fault zones: Evidence from geological, geochemical, and $^{18}O/^{16}O$ relations, *J. Geophys. Res.*, Vol. 89, P. 4331- 4343.

Kesavamoni, M., and Bose, R.N., 1979. Evolution of Palghat Gap- Geophysical Appraisal: *In: Proceedings of Third workshop on Status, Problems and Programmes in Indian Peninsular Shield*, Institute of Peninsular Geology, P. 178-185.

KrishnaBrahmam, N. and Negi, J.G., 1973. Rift valleys beneath Deccan Traps (India), *Geophys. Res. Bull.*, Vol. 11, P. 207-237.

Krishnan, M.S., 1968. *Geology of India and Burma*, Higgin Bothams (P) Ltd., Madras, 536 p.

Krishnaswami, V.S., 1981. The Deccan volcanic episode; related volcanism and Geothermal manifestations. *In: K.V. Subbarao and R.N. Sukheswala, (eds) Deccan volcanism*. GSI Mem. 3. P. 1-7.

Lin, A., 1996. Injection veins of crusting - originated pseudotactylite and fault gouge formed during seismic faulting, *Engineering Geology*, Vol. 43, P. 213-224.

Logan, J.M. and Rauenzahn, K.A., 1987. Frictional dependence of gouge mixture of Quartz and Motmorillonite on velocity, compaction and fabric, *Tectonophysics*, Vol. 144, P. 87-108.

Machette, M.N., Crone, A.J. and Bowman, J.R., 1993. Geologic investigations of the 1986 Marryat Creek, Australia earthquake - implications for paleoseismicity in stable continental regions, *US. Geol. Surv. Bull.*, 2032-B, 29 p.

Mares, V.M. and Kronenberg, A.K., 1993. Experimental deformation of Muscovite, *J. Struct. Geol.*, Vol. 15, P 1061-1075.

Marone, C. and Scholz, C.H., 1989. Particle-size distribution and microstructures within stimulated fault gouge, *J. Struct. Geol.*, Vol. 11, P. 799-814.

Mayer, L., 1986. Tectonic geomorphology of escarpments and mountain fronts, *In Active tectonics*. National Academy Press, P.125-135.

McCalpin, J.P. (Ed.) 1996. *Paleoseismology*, Academic Press, London, 588p.

Merkle, A.B. and Slangher, M., 1968. Determination and refinement of the structure of henlendite, *American Mineral*, Vol. 52, P. 1120-1138.

Millot, G., 1970. *Geology of clays*, Chapman and Hall New York, 429 p.

Mishra, D.C., Tiwari, V.M., Gupta, S.B. and Rao, V.M.B.S., 1998. Anomalous mass distribution in the epicentral area of Latur Earthquake, *Current Science*, Vol. 70, P. 385-390.

Misra, D.C., 1988. Geophysical evidence for a thick crust south Palghat Tiruchi gap in the high grade terrain of south India, *Jour. Geol. Soc. India*, Vol. 33, P. 79-81.

Mitchell, C and Widdowson, M., 1991. A geological map of southern Deccan traps, India and its structural implications, *Jour. Geol. Soc. London*, Vol. 148, P. 495-505.

Mumpton, F.A., 1960. Clinoptilolite redefined, *American Mineral*, Vol. 48, P. 351-369.

Nair, M.M., 1990. Structural trend line patterns and lineaments of the Western Gnats, south of 13° latitude, *Jour. Geol. Soc. India*, Vol. 35, P. 99-105.

Narula, P.L., Kayal, J.R., Pande, P., Gupta, S.K., Venkataraman, N.V., Maran, N. and Harendranath, 1996. Geotectonic setting and siesmicity of the area in Killari earthquake, 30 September 1993, *GSI, Spl. Publ.*, No. 37, P. 5-14.

Negi, J.G., Agarwal, P.K. and Pande, O.P., 1996. Pre-earthquake Deccan Trap thickness estimation by Aeromagnetics in Latur earthquake zone, *J. Geol. Soc. India*, Vol. 48, P. 353-356.

Noller, J. S., Sowers, J.M. and Lettis, W.R., 2000. Quaternary Geochronology Methods and applications. *AGU Reference shelf* 4. 581p.

Pande, P., Gupta, S.K., Venkataraman, N.V. and Venkataraman, B., 1995. Terrain changes consequent to the Killari earthquake of 30th September, 1993, *GSI, Spl. Pub.*, No.27, P. 215-220.

Power, W.L. and Tullis, T.E., 1989. The relationship between slickenside surfaces in fine-grained quartz and the seismic cycle, *J. Struct. Geol.*, Vol. 11, P. 879-893.

Rajendran, C. P. and Rajendran, K., 1996. Low- moderate seismicity in the vicinity of Palghat gap, South India and its implications, *Current Science*, Vol.70, P. 304-307.

Rajendran, C.P. and Rajendran, K., 1999. Geological investigations at Killari and Ter, central India and implications for Paleoseismicity in the shield region, *Tectonophysis*, Vol. 308, P. 67-81.

Rajendran, C.P. and Rajendran, K., 2003. Earthquake recurrence in Peninsular India: Status and Prospects, *Gond. Geol. Magz. Spl.*, Vol. 5, P. 107-124.

Rajendran, C.P., Rajendran, K. and Biju John, 1996. The 1993 Killari (Latur), Central India earthquake: An example of fault reactivation in the Precambrian crust, *Geology,* Vol. 24, P. 651- 654.

Rajendran, C.P., Rajendran, K. and Biju John, 1998. Paleoseismological studies of the 1993 Killari (Latur) Earthquake: implications for intraplate seismicity, *Project Report Sponsored by DST*, 46 p.

Rajendran, K and Rajendran, C.P., 1995. A report on the December 2, 1994 Earthquake, *Technical Report,* Centre for Earth Science Studies, 34 P.

Ramachandran, C., 1992. P-wave velocity in granulites from South India: implications for the continental crust, *Tectonophysics.* Vol. 201, P.187-198.

Rao, T.K.G., Rajendran, C.P., Mathew, G. and Biju John, 2002. Electron spin resonance dating of fault gouge from Desamangalam, Kerala: Evidence for Quaternary movement in Palghat gap shear zone, *Proc. Indian Acad. of Sciences (Earth and Planetary sciences),* Vol.111, P. 103-113.

Rastogi, K.K., Chanda, R.K., and Sarma, C.S.S., 1995. Investigation of June7, 1988 earthquake of magnitude 4.5 near Idukki dam, India, *Pure Appl. Geophys.*, Vol. 145, P. 109-122.

Ravindra Kumar, G.R. and Chacko, T., 1994. Geothermnobarometry of mafic granulites and metapelite from the Palghat Gap; South India: Petrological evidence for isothermal uplift and rapid cooling, *J. Metamorphic Geol.*, Vol. 1, P 479-492.

Ravishanker, 1993. Structural and Geomorphological evolution of 'SONATA' rift zone in central India in response to Himalayan uplift. *J. Palaeon. Soc. India*, Vol. 38, P. 17-30.

Reddy, G.K., Rao, G.C., Rao, R.U.M and Gopalan, K., 1994. Surface rupture of Latur earthquake: The soil-gas Helium signature, *Mem. Geol.Soc. India*, No. 35, P. 83-99.

Scholz, C.H., 1990. *The mechanics of earthquakes and faulting*, Cambridge university press, 439 p.

Schwarcz, H.P. and Lee, H.K., 2000. Electron Spin Resonance dating of fault rocks, *In: Noller, J.S., Sowers, J.M. and Lettis, W.R (eds) Quaternary geochronology*, AGU reference shelf-4, P. 177-186.

Schwartz, D.P and Coppersmith, K.J., 1986. Seismic hazards: New trends in analysis using geologic data. In: Active tectonics: Studies in geophysics (R.E. Wallace, Chairman), Natl. Acaa. Press, Washington, D.C., 215-230.

Seeber, L., Goran Ekstrom, Jain, S.K., Murty, C.V.R., Chandak, N and Armbruster, J.G., 1996. The 1993 Killari earthquake in central India: A new fault in Mesozoic basalt flow? *J. Geophy. Res.*, Vol. 101, P. 8543-8560.

Seeber, L., Jain, S.K., Murthy, C.V.R., and Chandak, N., 1994. Surface rupture and damage patterns in the Ms = 6.4m, September 29, 1993 Killari (Latur) earthquake in central India, *Nat. Center for Earthquake Eng. Res. Bull.17*, 12 p.

Sibson, R.H., 1977. Fault rocks and fault mechanics. *J. Geol. Soc. London*, Vol. 133, P. 191-213.

Sieh, K.E., 1978. Prehistoric large earthquakes produced by slip on the San Andreas fault at Pallet Creek, California, *J.Geophys. Res.*, Vol. 83, P. 3907-3939.

Singh, H.N. and Raghavan, V., 1989. A note on earth tremor of September 2, 1988 in Trivandrum district, Kerala, *J. Geol. Soc. India*, Vol.36. P. 323-325.

Singh, H.N. and Santosh, M., 1993. Report on the investigations of the tremors in Chavakkad and Trichur area during 25-26 February, 1993, in relation to the seismicity of Kerala region, CESS report, 25P.

Snow, D. T., 1982. Hydrogeology of induced seismicity and tectonism: Case histories of Kariba and Koyna. *Geol.Soc.Am.Bull.*, Vol. 189, P. 317-360.

Subrahmanyam, C. and Verma, R.K., 1986. Gravity fields, structure and tectonics of the Eastern Ghats, *Tectonophysics*, Vol. 126, P. 195-212.

Sudo, T., 1954. Clay mineralogical aspects of the alteration of volcanic glass in Japan, *Clay Min. Bull.*, Vol. 2., P. 96-106.

Sykes, L.R., 1978. Intraplate seismicity, reactivation of preexisting zones of weakness, alkaline magmatism and other tectonism postdating continental fragmentation. *Rev. Geophys. Physics*, Vol. 16, P.621-628.

Talwani, P., 1999. Fault geometry and earthquakes in continental interiors, *Tectonophysics*, Vol. 305, P. 371-379.

Tanaka, N., Vehara, N, and Itaya, T., 1995. Timing of the cataclastic deformation along the Akaishi Tectonic line, Central Japan, *Contrib. Mineral Petrol.*, Vol. 120, P. 150-158.

U.S.G.S., 1996, *GTOPO30 global digital elevation model*, Sioux Falls, South Dekota, EROS Data center.

Wintsch, R.P., Christoffersen, R. and Kronenberg, A.K., 1995. Fluid rock reaction weakening of fault zones, *J. Geophys. Res.*, Vol. 100, P. 13,021-13,032.

Wu, F.T., Blatter, L., Roberson, H., 1975. Clay gouges in the San Andreas Fault System and this possible implications, *Pure Applied Geophysics*, Vol. 113, P. 87-95.

Yeats, R.S., Sieh, K. and Alien, CR., 1997. The Geology of Earthquakes. Oxford University Press, New York. 568p.

Yoshida, M. and Santosh, M., 1996. Southernmost Indian Peninsula and the Gondwana land. *Gondwana Research Group Memmoir*-3, P. 15-24.